University of New Mexico
UNM Digital Repository

Electrical and Computer Engineering ETDs | Engineering ETDs

2-7-2008

Analysis and design of reconfigurable multi-band stacked microstrip patch antennas (MSAs) for wireless applications

Mahmoud Alayesh

Follow this and additional works at: https://digitalrepository.unm.edu/ece_etds

Recommended Citation
Alayesh, Mahmoud. "Analysis and design of reconfigurable multi-band stacked microstrip patch antennas (MSAs) for wireless applications." (2008). https://digitalrepository.unm.edu/ece_etds/10

This Thesis is brought to you for free and open access by the Engineering ETDs at UNM Digital Repository. It has been accepted for inclusion in Electrical and Computer Engineering ETDs by an authorized administrator of UNM Digital Repository. For more information, please contact disc@unm.edu.

Mahmoud Ayesh Alayesh

Candidate

Electrical & Computer Engineering Department

Department

This thesis is approved, and it is acceptable in quality and form for publication on microfilm:

Approved by the Thesis Committee:

Prof. Christos Christodoulou,
Chairperson

Prof. Edl Schamiloglu

Prof. Mark Gilmore

Prof. Yasamin Mostofi

Accepted:

Dean, Graduate School

Date

Analysis and Design of Reconfigurable Multi-Band Stacked Microstrip Patch Antennas (MSAs) for Wireless Applications

by

Mahmoud Ayesh Alayesh

B.S., Electrical Engineering, Mu'tah University, 2003

THESIS

Submitted in Partial Fulfillment of the
Requirements for the Degree of

Master of Science
Electrical Engineering

The University of New Mexico

Albuquerque, New Mexico

December, 2007

©2007, Mahmoud Ayesh Alayesh

Dedication

To my parents, Ayesh and Seham Khodeir, sisters and brothers for their support, love and patience.

Acknowledgments

First of all I would like to express my sincere thanks and gratitude towards Prof. Christos Christodoulou, my advisor and thesis chair, for continuous encourage, guidance and support through a beautiful year of academic coursework, writing and doing experiments of this thesis. Prof Christos patiently went over the drafts suggesting and numerous improvements.

Thanks go to other committee members, Prof. Edl Schamiloglu, Prof. Mark Gilmore, and Prof. Yasamin Mostofi, for their valuable recommendations pertaining to this study and assistance in my professional development.

Deep gratitude goes to my beloved family; parents, brothers and sisters, for their constant encouragement, support, love and patience they have bestowed upon me. Your encouragement is greatly appreciated.

Finally, I wish to thank my friends in Jordan, United States and elsewhere for their kindness, love, support, crucial assistance and fruitful suggestions they gave all the time. Special thanks go to Ahmad Ababneh and Eyad Zuraiqi for good time we spent together.

Analysis and Design of Reconfigurable Multi-Band Stacked Microstrip Patch Antennas (MSAs) for Wireless Applications

by

Mahmoud Ayesh Alayesh

ABSTRACT OF THESIS

Submitted in Partial Fulfillment of the
Requirements for the Degree of

Master of Science
Electrical Engineering

The University of New Mexico

Albuquerque, New Mexico

December, 2007

Analysis and Design of Reconfigurable Multi-Band Stacked Microstrip Patch Antennas (MSAs) for Wireless Applications

by

Mahmoud Ayesh Alayesh

B.S., Electrical Engineering, Mu'tah University, 2003

M.S., Electrical Engineering, The University of New Mexico, 2007

Abstract

There is an increasing demand for smaller low-cost reconfigurable antennas that can be easily integrated with packaging structures. Reconfigurable Microstrip Patch Antennas (MSAs) received great attention in wireless communication systems due to their capability to vary their operating frequency, pattern and polarization. Reconfigurability enables us to accommodate more than one service using the same antenna.

This thesis presents the analysis and design of new reconfigurable stacked (MSAs) of operating frequencies in the range of (2-5) GHz. The first new antenna is composed of two layers. The bottom layer is a MSA with two slots designed on each side that can be controlled via switches. By adjusting the statuses of the switches (that optimally fixed along the slots) we can vary the resonance frequencies, thus achieving frequency reconfigurability. In order to increase the number of resonance frequencies and to enhance the bandwidth and gain of the overall MSA, another patch is placed on top of the first antenna. The two patches are separated with a dielectric layer optimized to yield the maximum number of resonance frequencies, bandwidth and gain. The second antenna is the same as the first one but with switching top and bottom patches. Several results are included to verify the validity of the newly designed antennas.

Table of Contents

List of Figures

List of Tables

Chapter 1

An Introduction to Reconfigurable Microstrip Patch Antennas (MSAs)

1.1 Introduction

In modern mobile, satellite and wireless communication systems, there is an increasing demand for smaller low-cost reconfigurable antennas that can be easily integrated with packaging structures. Reconfigurable Microstrip Patch Antennas (MSAs) received great attention in wireless communication systems due to their selectivity for operating frequency, pattern and polarization [1]. Many wireless products started to be designed to operate in more than one frequency. This technique is cost effective because it is more convenient for a certain design to operate with a single antenna than multiple antennas. Reconfigurability enables to accommodate more than one service in the same antenna. In general reconfigurable antennas have similar radiation patterns for all designed frequency bands and enable efficient use of electromagnetic spectrum and frequency selectivity which is useful for reducing the adverse effect of co-site interference and jamming, also reconfigurability can add advantages of frequency reuse for tripling the system capability and frequency diversity for good performance of reception and transmission or to integrate the receiving and transmitting functions into one antenna. The resonance frequency can be adjusted by changing the shape of the radiating element. For example, by modifying the position of the feeding point we can adjust the resonance frequency.

It is well known that planar antennas such as MSAs have a significant number of advantages over conventional antennas, such as low profile, lightweight, conformability,

low production cost and easy fabrication properties [2], [3]. A number of techniques such as shorting walls and shorting pins have been proposed to reduce the physical size of a conventional half-wave to $\lambda_0/4$ or even further [4]. The most straightforward approach in designing MSAs is to use a high dielectric constant substrate, but it leads to poor efficiency and narrow bandwidth [5].

Diversity in general refers to transmitting multiple replicas of certain information independently, where the probability of error in received signal (bits) is reduced. This is achieved by sending the same information in different methods.

There are four kinds of diversities;

- Frequency diversity: repeating information over multiple frequencies.
- Time diversity: repeating information over different time slots.
- Space diversity: repeating information over separate spaces.
- Polarization diversity: repeating information over differently polarized antennas.

In this work, the efforts will be dedicated to design antennas that perform frequency diversity.

A single patch antenna has a low gain (5-8 dBi) and a narrow bandwidth. It is well known that a multi-layer structure is a useful method to improve these problems as well as increasing the number of resonance frequencies. To increase the bandwidth of a MSA, additional parasitic radiators (patches), placed in the same or in different layers with a relative permittivity larger than one, are used [6].

The charactenstics of the stacked MSA depend on the distance between the feeding patch and the parasitic patch, where if the parasitic patch is very close to the feeding patch, stacked MSA will have wide bandwidth. On the other hand, spacing the parasitic patch about a half wavelength from the feeding patch enhances the gain of stacked MSA.

1.2 Objectives and Work Scope

The objective of this thesis is to design, analyze and fabricate two different reconfigurable MSAs with rectangular patches and operating frequencies in the range (2-5) GHz. This would be accomplished by using two substrate layers; the first (bottom)

layer is a Duroid 5880 substrate with dielectric constant $\varepsilon_r = 2.2$ and almost 1.6 mm thick. The second (top) layer is a 1.6 mm thick of any material that has dielectric constant $\varepsilon_r = 1.44$ and FR4 Epoxy of dielectric constant $\varepsilon_r = 4.4$

The first antenna has a bottom rectangular patch that has two slots on the top of the Duroid 5880 layer, where the slots are added to achieve more resonance frequencies. A 1.6 mm thick layer of dielectric constant $\varepsilon_r = 1.44$ and $\varepsilon_r = 4.4$ with a conventional rectangular top patch is stacked over the bottom patch to add more resonance frequencies to that ones achieved from the bottom patch alone. In order to get reconfigurability in frequency, two switches are added to the slots in such away that gives a good performance. In the second antenna, the top and bottom patches in the first antenna are switched.

A coaxial probe excites both antennas by feeding a point on the bottom patch, where the location of the feeding point is at the distance (x_0) away from the leading radiating edge of the patch. However, there is no direct connection between the bottom and top patches. To improve performance of both antennas, the size of the bottom patch is made a little bit smaller than the top patch.

The designed antennas are simulated using CST Microwave Studio [CST MWS] and fabricated using a new model of LPKF laser and electronic company called ProtoMat S62. Network Analyzer is used to measure the antennas characteristics where both simulated and measured data are compared and contrasted and results are agreed well.

1.3 Literature Review on Reconfigurable MSAs

In order to attain frequency or polarization selective functions, improve bandwidth and gain, several researches for a patch antenna have been studied. In [1] a novel reconfigurable MSA having frequency and polarization diversities simultaneously was proposed. A U-slot is incorporated into the square patch, where the frequency diversity characteristic of the antenna is realized by switching a PIN diode on a U-slot of a MSA ON and OFF. The polarization diversity is also obtained by turning three PIN diodes on the slot and the truncating corners of a square patch ON and OFF. The proposed antenna

is designed to operate at 2415 MHz in wireless local area network (WLAN) systems or at 2650 MHz in digital multimedia broadcasting (DMB) systems.

The novel kind of the MSA suggested in [7] has a patch antenna with switchable slots (PASS). The antenna can work at dual frequencies with a linear polarization (LP) characteristic. The slot is incorporated into the patch and a PIN diode is utilized to switch the slot ON and OFF.

In [8] the switchable dual-band patch antenna with a small and flexible frequency ratio and almost the same polarization was proposed, the polarization was circular polarization (CP).

The antenna presented in [9] operated with right-hand circular polarization (RHCP) or left-hand circular polarization (LHCP) using the same feeding probe. To achieve CP diversity, two orthogonal slots are incorporated into the patch and two PIN diodes are utilized to switch the slots ON and OFF.

In [10], the slot antenna having polarization diversity capability between RHCP and LHCP or between LP and CP was introduced. The antenna has a slot-ring with perturbations that are switched ON and OFF using PIN diodes.

The reconfigurable MSA proposed in [11] consists of a corner-truncated square-radiating patch, four small triangular conductors a microstrip line feed. The antenna is capable of making polarization diversity among LP, RHCP, and LHCP using independently biased PIN diodes on the patch.

In [12] a corner-truncated square patch approach is used to realize CP characteristics. This patch has a pair of a triangular shape truncated corners and four slits. This approach has an antenna-size reduction of about 36% as compared to the conventional corner-truncated square microstrip antenna at a given operating frequency.

A novel reconfigurable MSA with a switchable slot (PASS) has been proposed in [13] to realize various functionalities such as dual frequency operation, dual band CP performance and polarization diversity with only one patch and a single feeding point.

The PASS concept is used in [14] to design a compact dual band circularly polarized antenna at the UHF band for a future Mars rover mission. Here a switch is fixed at the center of a slot that is incorporated into the patch of a MSA. By changing the switch ON and OFF, the patch will resonate at two different frequencies.

In [15], electrically small MSAs incorporating shorting posts are thoroughly investigated. The radius of the circular patch was reduced by a factor of three, making the antenna size very suited for handset terminals used in mobile communications where limited antenna size is a premium. Techniques to enhance the bandwidth of these antennas are presented and performance trends are established.

In [16]–[17] shorting posts were used in different arrangements to reduce the overall size of the printed antenna. As shown in [4], the maximum reduction in physical size can be achieved if a single shorting post is used.

It is well known that a multi-layer structure is a useful method to improve problems of bandwidth and gain [l8, 19, 20, 21]. By stacking two parasitic patches on a fed patch, the antenna with high gain and wide bandwidth can be realized. The behavior mechanism for both the wide bandwidth and the high gain performances of the 3-element stacked MSA is explained in [22]. The upper parasitic patch of the 3-element stacked MSA increases the gain. When the patch distance is approximately half a wavelength, the standing wave contributing to the radiation is excited in the cavity between the patches. The space between the patches forms a leaky resonant cavity, and the gain becomes higher by the interaction with the fed patch cavity.

In [6] different layers are used to improve the bandwidth and the gain, where the radiators (patches) as well as feed lines (in aperture-coupled antennas) are etched on different dielectric substrates with a relative permittivity larger than one.

1.4 Outline of the Thesis

The thesis comprises of four chapters and the overview of all the chapters are as follows:

Chapter 1: This chapter provides the introduction, objective and work scope and includes the literature review on reconfigurable MSA.

Chapter 2: Presents the basic theory of MSAs, including the basic geometries and characteristics of the MSA, the advantages and disadvantages of MSAs,

impedance matching, shorting techniques, the methods of analysis used for the MSA design and finally theory of stacked MSAs.

Chapter 3: The calculations needed to find the dimensions of the conventional MSA using transmission line model are presented in this chapter. Using CST Microwave studio software, simulations of stacked MSAs with two slots and two switches being added to the rectangular patches of either the top or bottom layers are implemented for different dielectric constants and different dielectric substrates thicknesses. Results are shown and comparison between reflection coefficients curves before and after adding the top layers of the stacked MSAs are presented in this chapter.

Chapter 4: This chapter contains practical experiments to antennas simulated in chapter three with brief summary about the tools used in fabricating staked MSAs. The measured results agreed well with the simulated results with accepted range of error due to the nature of fabrication. Finally the conclusion of the thesis and suggestions for future work are presented.

Chapter 2

Theory of Microstrip Patch Antenna (MSA)

2.1 Introduction

MSAs became very popular in 1970*s* for space borne application [1]. Since then a massive amount of research and development efforts have been put into it. They are considered to be low profile, conformable to planner and non-planer surfaces, simple and inexpensive to fabric using modern printed-circuit technology, very versatile in terms of resonance frequency, polarization pattern and impedance. We can find MSAs on the surfaces of high-performance aircraft, spacecraft, satellites, missiles, cars and new held mobile telephone, where size, weight, cost, performance and ease of installation are important factors.

2.2 Basic MSA Shapes and Geometries

A conventional MSA consists basically of a radiating metallic patch on one side of a dielectric substrate, and has ground plane on the other side. Figure 2.1 shows top and side views of a conventional MSA.

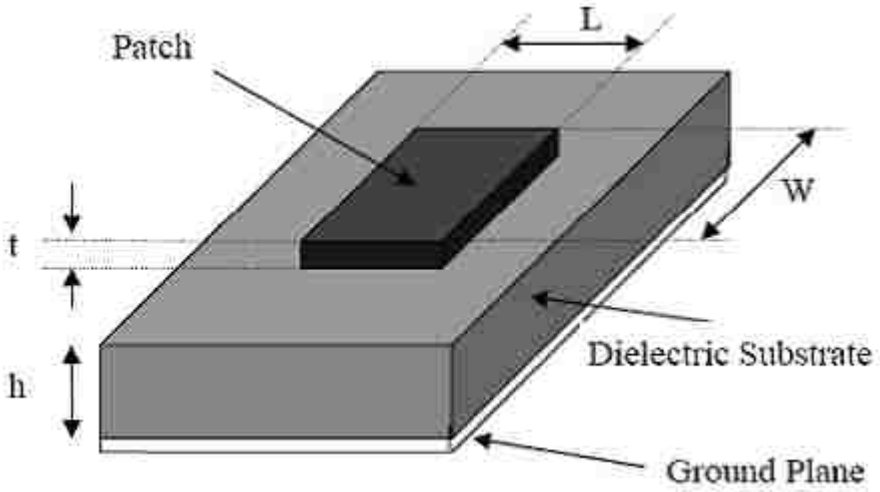

(a) top view

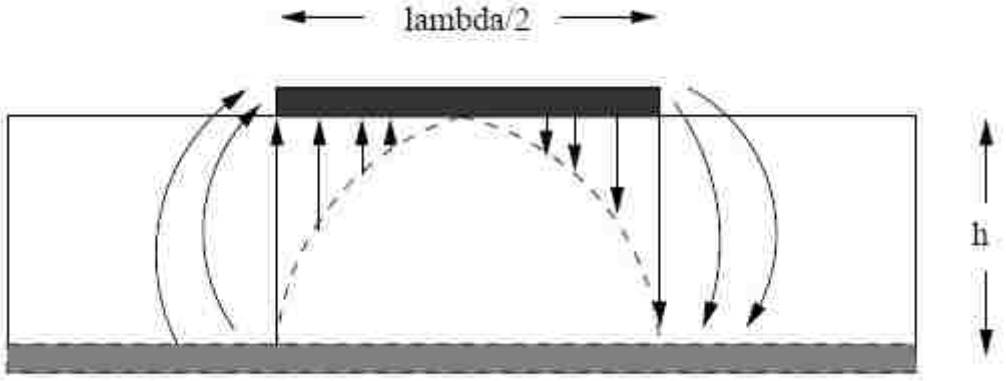

(b) side view

Figure 2.1: Structure of a conventional rectangular MSA: (a) top view, (b) side view.

The metallic patch can generally be made of conducting material such as copper or gold, and it can take many different configurations such as square, rectangular, dipole, circular, elliptical, triangular, disk sector, circular ring, and ring sector as shown in Figure 2.2. However, the conventional square, rectangular and circular MSAs are the most popular because of simple fabrication, performance prediction and analysis, besides their attractive radiation characteristics such as low cross-polarization radiation.

Rectangular patches are probably the most utilized patch geometry. It has the largest impedance bandwidth compared to other types of geometries.

Circular and elliptical shapes are slightly smaller than of rectangular patches. Thus it will have smaller bandwidth and gain. This circular geometry patches were difficult to analyze due to its inherent geometry.

Triangular patch is even smaller than both rectangular and circular geometries. However, this will produce even lower gain and smaller bandwidth. It will also produce higher cross-polarization due to its unsymmetrical geometry. Dual polarized patch could be generated from these geometries.

Circular ring patches has relatively the smallest conductor size, but at the expense of bandwidth and gain. Furthermore, for this geometry, it will not be easy to excite lower order modes and obtain a good impedance match for resonance. Non-contacting forms of excitation are normally turned to for this shape.

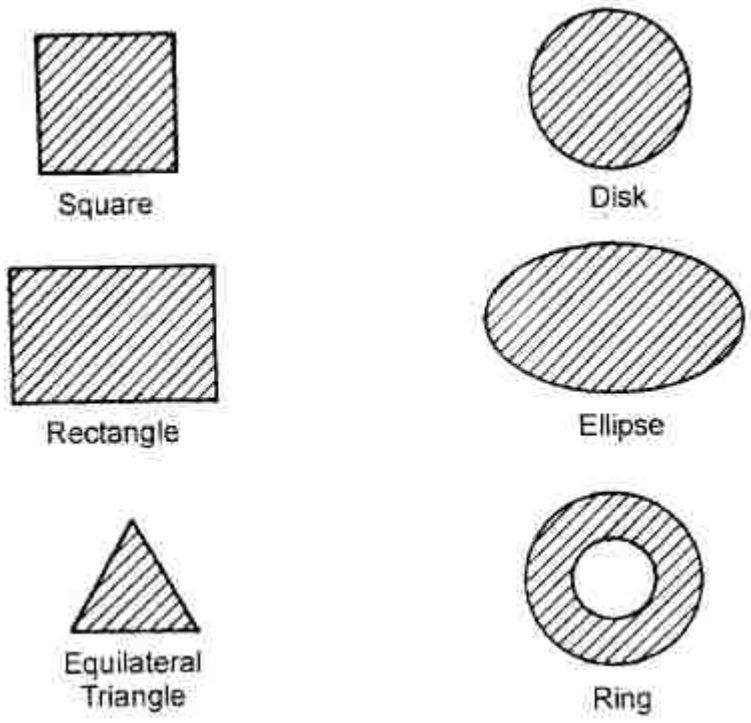

Figure 2.2: Common shapes of patch elements used in MSAs.

2.3 Advantages of MSAs

MSAs have several advantages compared to conventional microwave antennas, and therefore many applications cover the broad frequency range from ~ 100 MHz to ~ 100

GHz. Some of the principal advantages of MSAs compared to conventional microwave antennas are [3]:

- Lightweight, low volume, low profile planar configurations, which can be made conformal to host surfaces and ease the process of incorporating into any package.
- Ease fabrication and low cost; readily amenable to mass production.
- Can be made thin hence they do no perturb the aerodynamics of host aerospace vehicles.
- Can be easily mounted on missiles, rockets and satellites without major alterations.
- The antennas have low scattering cross section.
- Linear, circular (left hand or right hand) polarizations are possible with simple changes in feed position.
- Capable of dual and triple frequency operations and provides flexibility to be constructed in any shape.
- No cavity backing required.
- MSAs are compatible with modular designs (solid state devices such as oscillators, amplifiers, variable attenuators, switches, modulators, mixers, phase shifters etc., can be added directly to the antenna substrate board). Also it can be easily integrated with microwave integrated circuits (MICs).
- Feed lines and matching networks are fabricated simultaneously with antenna structure.
- Mechanically robust when mounted on rigid surfaces.

2.4 Disadvantages of MSAs

MSAs also have some drawbacks compared to conventional microwave antennas including [3]:

- Narrow bandwidth, which typically is from a fraction of a percent to a few percent depending on the substrate dielectric constant and thickness (Commonly 2.5% for single layer; 30% for multi-layer).
- High Losses resulting from surface wave excitation and conductor and dielectric losses, hence lower gain and inherently low directivity.
- Most MSAs radiate into a half plane.

- Practical limitations on the maximum gain (20 dB).
- Poor end fire radiation performance.
- Poor isolation between the feed and the radiating elements.
- Possibility of excitation of surface waves.
- Lower power handling capability.
- Difficult to analyze - Typically a full-wave computationally intensive numerical analysis is required.

Narrow bandwidth is the most limiting factor for MSA to widespread in different applications. Fortunately the bandwidth could be increased using a thick substrate with a low dielectric constant. MSAs brought to the front, because personal mobile communications requires smaller and low profile antennas where it is used in ultra high frequencies (UHF) to millimeter wave frequencies band.

There are many applications for MSAs like radars that use small arrays of microstrip radiators, missiles, aircraft related applications and satellite imaging systems. Also it used in pagers, the global systems for mobile communications (GSM) and global positioning system (GPS).

There are ways to minimize the effect of some of these limitations. For example, bandwidth can be increased to more than 60% by using special techniques; lower gain and lower power handling limitations can be overcome thorough an array configuration. Surface wave associated limitations such as poor efficiency, increased mutual coupling, reduced gain and radiation pattern degradation can be overcome by the use of photonic band gap structures.

2.5 Basic MSAs Characteristics

An antenna is a device that converts a guided electromagnetic wave on a transmission line to a plane wave propagating in free space as shown in Figure 2.3. Thus, one side of an antenna appears as an electrical circuit element, while the other side provides an interface with a propagating plane wave. Antennas are inherently bi-directional, they can be used for both transmit and receive functions.

Generally, MSA as shown in Figure 2.1 consists of a very thin metallic strip (radiating patch) t placed a small fraction of a wavelength ($t<<\lambda_0$, where λ_0 is the free space wavelength) placed on one side of a dielectric substrate with thickness h ($h<<\lambda_0$, usually $0.003\lambda_0 \leq h \leq 0.05\lambda_0$) that locates above a grounded plane and bellow the strip. There are many kinds of substrates, which have different dielectric constants in the range of $2.2 \leq \varepsilon_r \leq 12$, that we can use for designing MSAs [5]. For good antenna performance, thick dielectric substrates having dielectric constants in the lower end of the range mentioned above is desirable to get better radiation efficiency, larger bandwidth, offers lowest losses and loosely bound fields for radiation into space. This is besides enhancing the fringing fields which is account for radiation. However, such a configuration leads to a larger antenna size. Besides, higher ε_r results in smaller elements which boarder radiation pattern. However, very thick MSAs in spite of giving better bandwidth, it cases probe inductance that prevents patch impedance matching to the input connector, the probe inductance can be tuned out with a capacitive gap.

In MSA the radiating patch and the feed lines are usually photo etched on the dielectric substrate, it radiates primarily because of the fringing fields between the patch edge and the ground plane as shown in Figure 2.4.

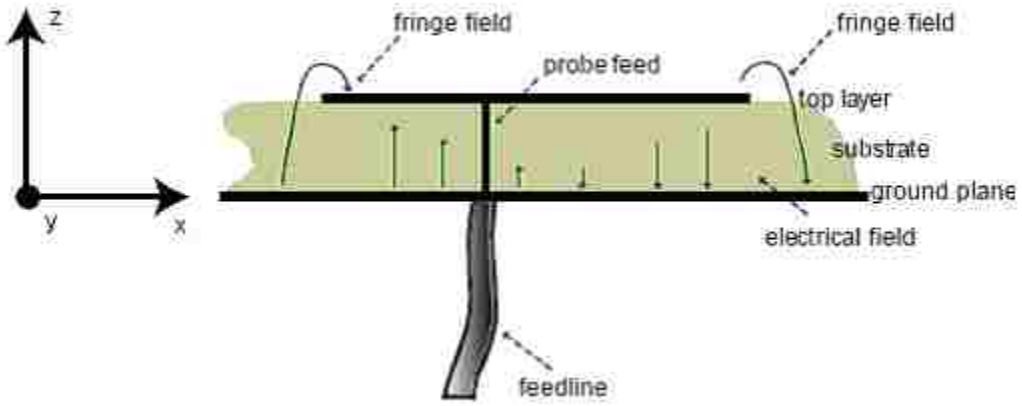

Figure 2.3: Microstrip feeding and fringing field lines.

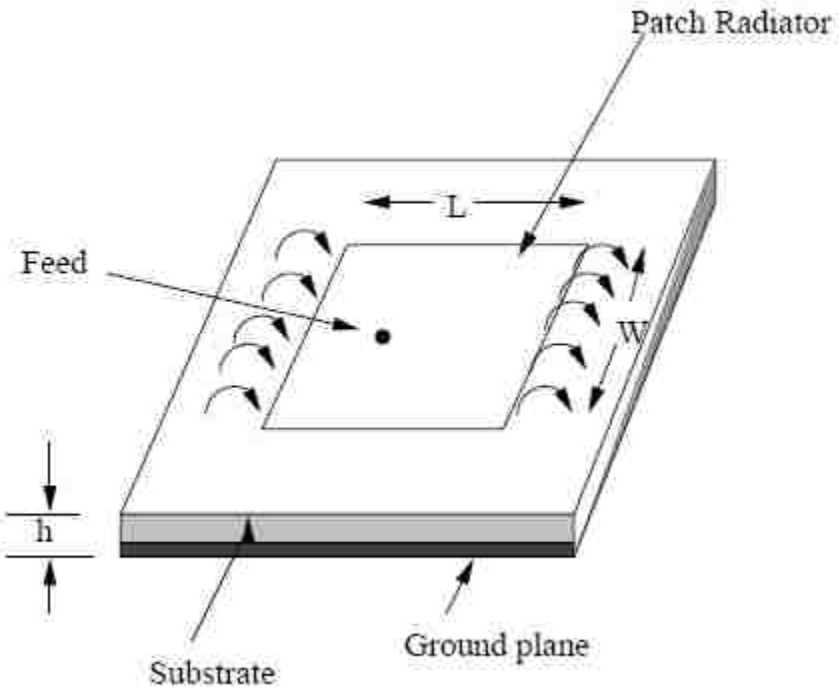

Figure 2.4: Microstrip fringing field lines.

2.6 Feeding Techniques

Power can be coupled into or out of the antenna by a variety of methods that can be broadly classified into contacting and non-contacting feeding [20], [21] and [27].

Contacting feeds involve the direct connection of a transmission line (coax or microstrip line to the patch antenna). The input impedance depends on the location of the connection with the patch boundaries, which provides a commonly used means of impedance matching. Non-contacting feeds use electromagnetic coupling to transfer power between the feed line and the radiating patch, it has more degree of freedom than contacting feeds, hence, they are harder to be designed but provides greater flexibility.

There are many configurations used to feed MSA. The four most popular techniques are the coaxial probe, microstrip line (both contacting schemes), aperture coupling and proximity coupling (both non-contacting schemes).

2.7 Impedance Matching

Figure 2.5 shows the current (magnetic filed) and voltage (electric filed) variation along the patch. The current is maximum at the center and minimum near the right and left edges, while the voltage (electrical filed) is zero in the center and maximum near the left edge and minimum near the right edge.

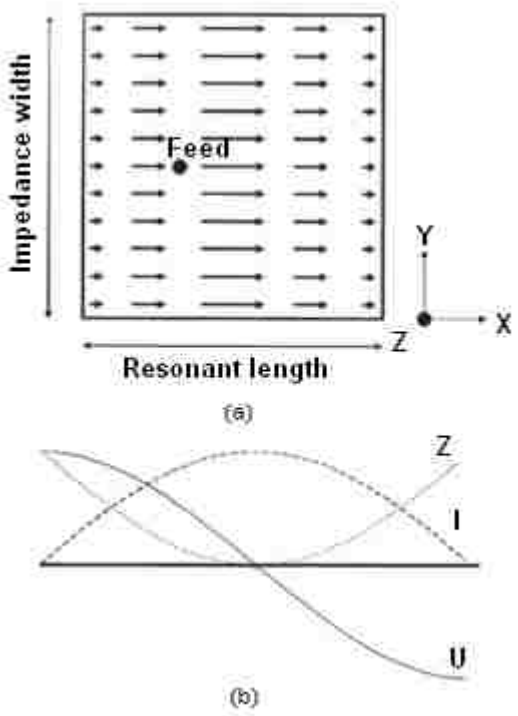

Figure 2.5: (a) Current distribution on the patch surface. (b) Voltage (U), current (I) and impedance (|Z|) distribution along the patch's resonant length.

From the magnitude of the current and voltage, we can predict that the impedance is minimum (theoretically zero Ω) in the middle of the patch and maximum (typically around 200 Ω) near the edges. Hence, the electric filed is zero at the center of the patch, maximum (positive) at one side and minimum (negative) on the opposite side. The maximum and minimum continuously change side according to the instantaneous phase of the applied signal. Somewhere Along the resonant length, there is a point where the impedance is 50 Ω. This point is use to couple electromagnetic in and /or out of the patch, which is called the feeding point.

The electric filed does not stop abruptly at the patch's periphery as in a cavity, the electric filed extend the outer periphery to some degree. These field extensions are known as fringing fields and cause the patch to radiate.

Fringing fields between the periphery of the patch and the ground plane generates radiation from the MSA. To enhance the fringing fields from the patch, the width of the patch is increased, ε_r is decreased or the substrate thickness h is increased. In general h is taken to be greater or equal to 0,159 cm. [1]

2.8 Shorting Techniques in MSAs

Size miniaturization of MSAs is increasingly essential in many practical applications, such as mobile cellular handsets, cordless phones, direct broadcast satellites (DBS), wireless local area networks (WLAN), global position satellites (GPS) and other next-generation wireless terminals [18], [22], [23].

Applications in present-day mobile communication systems usually require smaller antenna size in order to meet the miniaturization requirements of mobile units. Thus, size reduction is becoming major design considerations for practical applications of MSAs. For this reason, studies to achieve compact MSAs have greatly increased. Much significant progress in the design of compact MSAs has been reported over the past several years.

The antenna physical sizes are an important factor in the design process owing to the miniaturization of the modern mobile terminals. Any technique to miniaturize the sizes of the MSAs has received much attention. Electrical requirements for these mobile antennas are sufficient bandwidth, high efficiency, impedance matching, omni-directional radiation patterns, and minimum degradation by the presence of near objects.

In general, the size miniaturization of the normal MSA has been accomplished by loading, which can take various forms such as [23];

- Using high dielectric constant substrates.
- Modification of the basic patch shapes.
- Using short circuits, shorting-pins or shorting-posts.
- A combination of the above techniques.

Employing high dielectric constant substrates is the simplest solution, but it exhibits narrow bandwidth, high loss and poor efficiency due to surface wave excitation [23]. Modification of the basic patch shapes allows substantial size reduction; however, some of these shapes will cause the inefficient use of the available areas. In contrast, shorting posts, which were regarded as a more efficient technique, were used in different arrangements to reduce the overall dimensions of the MSA.

In order to achieve a small size MSA, different shorting techniques are used. The advantages of using these methods are that the required patch sizes are smaller for a given frequency. Following is a brief about these techniques;

2.8.1 Shorting Wall Method

The resonance frequency for a MSA of half-wavelength structures ($\lambda_o/2$) operating at the fundamental resonant mode TM_{01} or TM_{10}, is given by (valid for a rectangular MSA with a thin microwave substrate);

$$f \cong \frac{c}{2L\sqrt{\varepsilon_r}} \tag{2.1}$$

Where c is the speed of light in free space, L is the length of the patch and ε_r is the relative permittivity of the patch rectangular MSA.

When a shorting wall is used as shown in Figure 2.6, the first resonance frequency occurs close to or at about $0.5 \times f$.

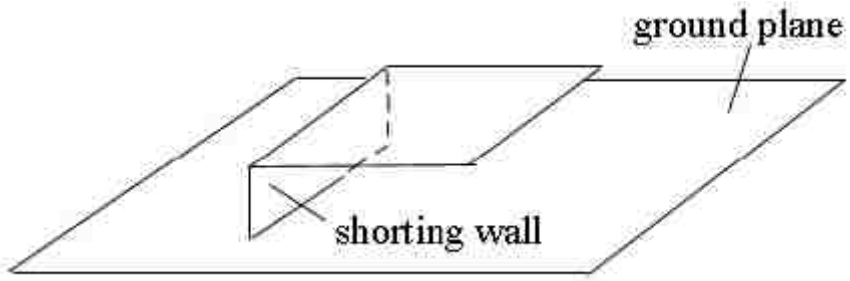

Figure 2.6: A rectangular patch with a shorting wall.

2.8.2 Shorting Pin Method

The antenna's fundamental resonance frequency can be further lowered and hence further size reduction can be obtained when a shorting pin is used instead of a shorting wall. Here the dimensions of a shorting-pin-loaded a rectangular MSA are shortened to one-third of that of the corresponding MSA without a shorting pin at the same operating frequency results in an antenna size reduction of about 89%.

When there is a shorting pin placed at x = -L/2, y = 0 (center of the patch edge) and the fed position is chosen on the center line (x axis) as shown in Figure 2.7, the first resonance frequency occurs at about $0.38 \times f$ [23].

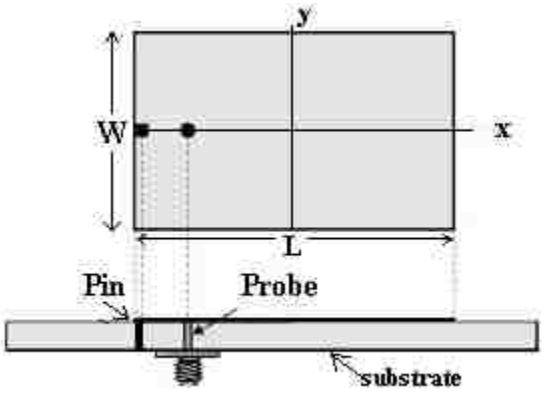

Figure 2.7: Geometries of compact rectangular MSA with shorting pin loading.

With the shorting pin loading technique, the antenna size reduction is mainly due to the shifting of the null-voltage point at the center of the rectangular patch (excited at the TM_{01} mode), to their respective edges, which makes the shorted patches resonate at a much lower frequency. Thus, at a given operating frequency, the required patch dimensions can be significantly reduced and the reduction in the patch size is limited by the distance between the null-voltage point in the patch and the patch edge [18].

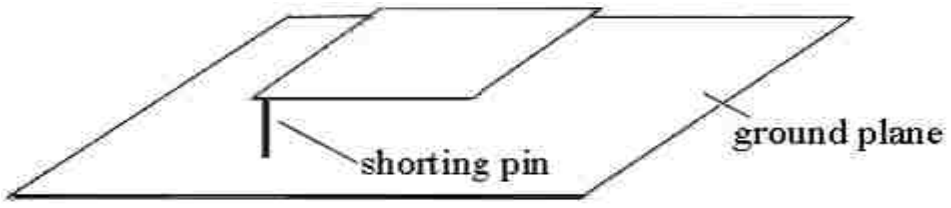

Figure 2.8: A rectangular patch with a shorting pin.

The conventional shorted MSA is constructed by short-circuiting the entire width of the zero potential plane of a regular antenna, or what is popularly called a Quarter wavelength antenna. We can construct a partially shorted MSA, by shorting only a portion or few portions of the zero potential plane. The total width of the shorted sections controls the resonance frequency and the input impedance of the shorted MSA. Reducing the width of the shorted edge proportionally increases the loading inductance of the antenna and hence, decreases the resonance frequency. As fabricating short circuit portions in these kind of partially shorted antennas are relatively difficult task, shorting pins are generally used. The antennas made by using shorting pins have been experimentally and numerically studied. As shown in [22], [23], [28], [31] and [32]. The maximum reduction in physical size can be achieved if a single shorting post is used.

The patch dimensions are reduced by a factor of three or four, making the antenna size well suited for portable handsets. When the shorting pin located close to the feed point results in a significant reduction in overall patch size. The principle behind this can be easily explained in terms of simple circuit theory. For more details see [22].

As suggested in [17,19 and 20], development of a stronger shorting plane results in an improved matching and an increased bandwidth. There are two methods by which a stronger shorting plane can be developed. One method is to increase the thickness of the shorting pin and the other is to increase the number of shorting pins employed. To get maximum reduction, the shorting pins have to be placed very close to the patch edge. In order to reduce the inductive loading the shorting pins have to be close to the feeding point. It has to be observed that many different positions of the feeding and shorting pins are possible and a fair degree of freedom exists in this kind of a design. The better antenna performance is, however achieved at the expense of a larger patch area compared to a single shorting-pin patch design, but its merits outweighs the disadvantages and therefore this design is followed.

Shorted patch antennas can achieve dual band operations with a large frequency ratio. Also the position of the shorting pin has a critical effect on the antenna characteristics. Due to the cavity nature, the Q factor of the patch is high, so the impedance bandwidth is inversely proportional to Q factor, results in a narrow bandwidth.

2.10 Methods of Analysis

The most popular models for the analysis of MSAs are the transmission line model, cavity model, and full wave model (which include primarily integral equations / Moment Method) [1]. The transmission line model is the simplest of all and it gives good physical insight but it is less accurate. The cavity model is more accurate and gives good physical insight but is complex in nature. The full wave models are extremely accurate, versatile and can treat single elements, finite and infinite arrays, stacked elements, arbitrary shaped elements and coupling. These give less insight as compared to the two models mentioned above and are far more complex in nature. The cavity model and the full wave models are out of my scope in this thesis, for more information see [1]

2.10.1 Transmission Line Model

Transmission line model is the easiest of all but it yields the least accurate results and it lakes the versatility [4], [5], [20], [23]. However it does shed some physical insight. As shown in Figure 2.9, we can represent a rectangular patch antenna with two narrow radiating apertures (slots), each slot of width W and height h and separated by a low-impedance transmission line with a length equal to that of the patch antenna L and with characteristic impedance Z_{01}, where $Z_{01} = \frac{1}{Y_{01}}$. ($Y_{01}$ is the characteristic admittance).

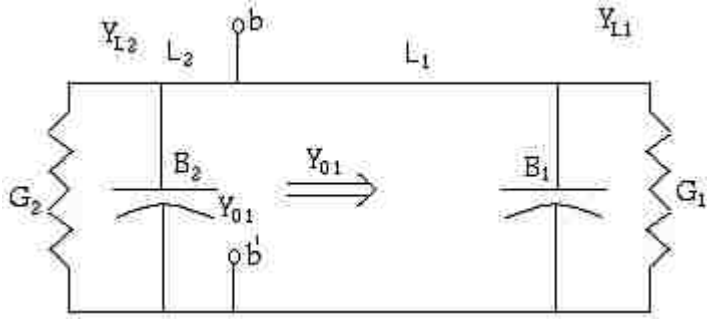

Figure 2.9: Transmission line model for rectangular MSA.

In this model Y_{L1} and Y_{L2} represents the radiating apertures on the edges of the patch antenna, and because they are identical, we get

$$Y_{L1} = G_1 + jB_1 = Y_{L2} = G_2 + jB_2 \Rightarrow B_1 = B_2, G_1 = G_2 \tag{2.2}$$

Where G_1, G_2 are the aperture conductances and B_1, B_2 are the aperture susceptances. Approximate values of G_1, G_2 and B_1, B_2 can be computed using [29]

$$G_1 = G_2 = 0.00836\frac{W}{\lambda_0}$$

and $$B_1 = B_2 = 0.01668\frac{\Delta L}{h}\frac{W}{\lambda_0}\varepsilon_{reff}$$

Where W is the width of a rectangular MSA, ΔL is the length extension, h is the thickness (height) of the dielectric substrate, ε_{reff} is the effective dielectric constant and λ_0 is the wavelength in free space.

The input feed point for the signal must be placed in such a point along the transmission line where the input impedance match 50 Ω and the antenna reactance minimized as much as possible.

At the signal feed point, the input admittance $Y_{bb'}$ is given by:

$$Y_{bb'} = Y_{01}\left(\frac{Y_L + jY_{01}\tan(\theta_1)}{Y_{01} + jY_L\tan(\theta_1)} + \frac{Y_L + jY_{01}\tan(\theta_2)}{Y_{01} + jY_L\tan(\theta_2)}\right) \tag{2.3}$$

The optimal width of a rectangular MSA can be found as follows [5]:

$$W = \frac{1}{2f_0\sqrt{\mu_0\varepsilon_0}}\sqrt{\frac{2}{\varepsilon_r + 1}} = \frac{c}{2f_0}\sqrt{\frac{2}{\varepsilon_r + 1}} \tag{2.4}$$

Where c is the free-space velocity of light ($\approx 3\times10^8$ m/s), f_0 is the resonance (operating) frequency and ε_r is the dielectric coefficient of the substrate.

Because of fringing phenomena, where some waves travel in the substrate and some in the air as shown in Figure 2.10, the effective dielectric constant ε_{reff} is defined.

On the edges of the patch antenna, fringing electric fields affect the electrical length of the MSA. Thus, it affects the resonance frequency of the MSA, so it must be taken into account. The same applies for the width.

In fact, the patch is electrically a bit larger than it is physical dimensions due to fringing fields. The deviation between the electrical and physical size is dependent on both dielectric constant and height.

In general, fringing is a function of the ratio of the length of the patch, L to the height of the substrate h (L/h), and the dielectric coefficient of the substrate ε_r. The resonance frequency is influenced by ground plane size, dielectric height and patch (impedance) width. So we have to find the actual length that would give the same desired resonance frequency.

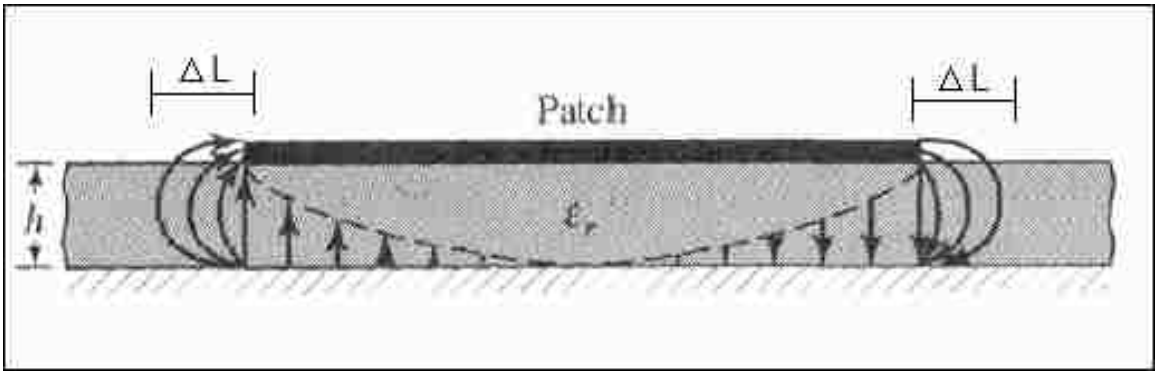

Figure 2.10: Fringing field effect in MSA.

When $W/h>1$ the ε_{reff} of the MSA could be found using [5]:

$$\varepsilon_{reff} = \frac{\varepsilon_r + 1}{2} + \frac{\varepsilon_r - 1}{2}\left[1 + 12\frac{h}{W}\right]^{-.5} \tag{2.5}$$

Where $1 < \varepsilon_{reff} < \varepsilon_r$ and ε_{reff} is a function of frequency, so when frequency of operation increases, most of the electric field lines concentrate in the substrate.

We can find the effective length using the following equation [5]:

$$L_{eff} = \frac{c}{2f_0\sqrt{\varepsilon_{reff}}} \tag{2.6}$$

To find the length extension, we use the following equation [5]:

$$\Delta L = 0.412h\frac{\left(\varepsilon_{reff} + 0.3\right)\left(\frac{W}{h} + 0.264\right)}{\left(\varepsilon_{reff} - 0.258\right)\left(\frac{W}{h} + 0.8\right)} \tag{2.7}$$

The actual length of the patch can be found using [5]:

$$L = L_{eff} - 2\times\Delta L \tag{2.8}$$

For practical considerations, it is essential to have a finite ground plane, but this is critical issue where if the ground plane width goes below a certain value, relatively very sharp variation in the impedance bandwidth would occur [29]. To calculate the ground plane dimensions (L_{ground}, W_{ground}), it has been shown that similar results for finite and infinite ground plane can be obtained if the size of the ground plane is greater than the patch dimensions by approximately six times the substrate thickness all around the periphery. Hence, for this design, the ground plane dimensions would be given as:

$$L_{ground} = 6h + L \tag{2.9}$$

$$W_{ground} = 6h + W \tag{2.10}$$

It is not practical to have W_{ground} less than 30 mm. However, increasing the width of the ground plane, the impedance bandwidth and the resonant frequency will increase. The aperture conductance G_L and the resonant input impedance are given by [5]:

$$G_1 = \frac{1}{120\pi^2}\int_0^{\pi}\left[\frac{\sin\left(\frac{k_0 W}{2}\cos\theta\right)}{\cos\theta}\right]^2 \sin^3\theta d\theta \tag{2.11}$$

$$R_{in} = \frac{1}{2G_1} \tag{2.12}$$

Where $k_0 = \omega\sqrt{\varepsilon\mu}$ is the wave number.

If we take the mutual effects between the slots into account, equation (2.12) is modified to

$$R_{in} = \frac{1}{2(G_1 \pm G_{12})} \tag{2.13}$$

The mutual conductance G_{12} is found as follows [5]:

$$G_{12} = \frac{1}{120\pi^2}\int_0^{\pi}\left[\frac{\sin\left(\frac{k_0 W}{2}\cos\theta\right)}{\cos\theta}\right]^2 J_0(k_0 L\sin\theta)\sin^3\theta d\theta \tag{2.14}$$

Where J_0 is the Bessel function of the first kind of order zero.

The (+) sign in equation (2.13) is used for modes with odd resonant voltage (filed) distributions beneath the patch and between the slots while (-) sign is used for modes with even resonant voltage distributions.

Since the desired place to fix the coaxial cable with the patch is where the impedance is 50 Ω, then we have to find the distance (x_0) between the feeding point and the leading radiating edge. This can be accomplished using [5]

$$R_{in}(x = x_0) = R_{in}(x = 0)\cos^2(\frac{\pi}{L}x_0) \tag{2.15}$$

2.11 Stacked MSA

Although a MSA has practical advantages such as low profile and lightweight, a single patch antenna has a low gain (5-8 dBi) and a narrow bandwidth, hence the need for stacked MSA had risen to increase the bandwidth by using multiple resonators [3], [29].

A stacked MSA has two or more patches on different layers of the dielectric substrates that are stacked on each other to improve the bandwidth, the gain and to increase the number of resonance frequencies. This method increases the overall height of the antenna but the size in the planer direction (surface area) remains the same as that of the single-patch antenna. Thus, it is suitable for array elements.

As shown in Figure 2.11, a stacked MSA consists of a bottom substrate (layer) that has on its top a patch, called the fed patch, and a top substrate that has on its top a patch, called the parasitic patch. The top and bottom substrates could have the same or different dielectric constants. These multilayer MSA configurations yield BW of nearly 25%-30% increase for $VSWR \leq 2$, and the variation of the radiation pattern over the impedance bandwidth is small [6], [36-40].

A transmission line or a coaxial cable can feed the bottom patch, while the parasitic (top) patch is capacitivly coupled from the bottom patch.

The bandwidth enhancement is obtained by adjusting the lengths of the two-stacked patches to be slightly different, which make it possible to excite two resonant modes at close frequencies, thereby leading to a wider impedance bandwidth formed by the two closely excited resonant modes.

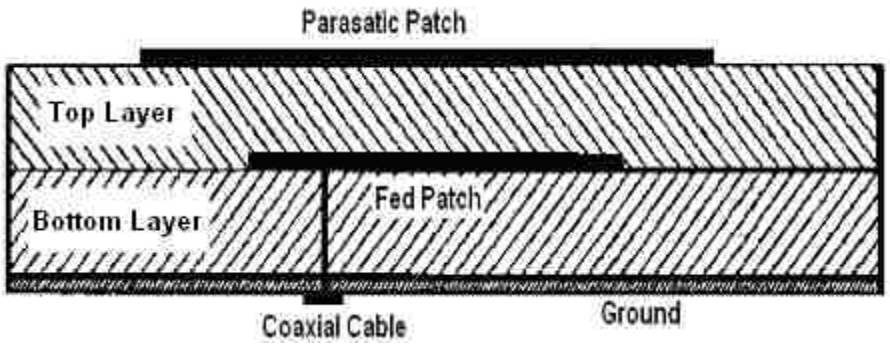

Figure 2.11: Tow layers stacked MSA.

When the parasitic patch is very close to the fed patch, the stacked MSA yields two resonant frequencies close to each other and the wide bandwidth is obtained, while when the patches distance is about a half wavelength, in the cavity between patches, the electric standing wave contributed to radiation exists and the amplitude of the electric fields becomes large which means high antenna's gain. As we will see in the next chapter, the scope of this thesis is to use stacked MSAs to increase the number of resonance frequencies.

The large number of parameters associated with stacked MSA geometry (two patches sizes, two or more substrate thicknesses, dielectric constants and feed locations) implies design freedom for optimization, but at the same time it makes such optimizations very difficult.

Chapter 3

Design and Simulations

3.1 Introduction

In order to design reconfigurable-stacked MSAs, the transmission line model is implemented to calculate the dimensions of the conventional MSA and some critical parameters related to antenna performance are discussed. The CST Microwave Studio [CST MWS] software [42] is used in modeling and analyzing the designed antennas.

More specifically, we try to met the following requirements:

- The antenna should be of the smallest dimensions as much as possible and the return loss should be minimal.
- We try to achieve as many resonance frequencies as possible in the range of (2-5) GHz.
- We should achieve a radiation pattern within the frequency range of interest.

A two layer reconfigurable-stacked MSA with different dielectric constant are simulated and results are achieved. A comparison between top layers of different dielectric constants is implemented too.

3.2 Initial Design

The resonance frequency (f_0) of the conventional MSA is needed to be around 2.4 GHz, and the dielectric material used is RT/ Duroid 5880 with dielectric constant ε_r approximately 2.2. We chose ε_r to be in the lower limit to get better efficiency and larger bandwidth.

The height of the ground plane is chosen to be 0.1 cm, the thickness of the patch (t) is 0.07 cm and the height of the substrate (h) is 0.1588 cm, where transmission line model is most accurate for thin substrates.

To design the conventional rectangular MSA that operates at frequency around 2.4 GHz, the optimal width can be found using [5]:

$$W = \frac{1}{2f_0\sqrt{\mu_0\varepsilon_0}}\sqrt{\frac{2}{\varepsilon_r+1}} = \frac{c}{2f_0}\sqrt{\frac{2}{\varepsilon_r+1}}$$

$$W = \frac{1}{2\times 2.4\times 10^9\sqrt{4\pi\times 10^{-7}\times 8.854\times 10^{-12}}}\sqrt{\frac{2}{2.2+1}} \approx 4.941 \text{ cm} = 49.41 \text{ mm}$$

To find the effective dielectric constant ε_{eff}, and when $W/h>1$, we can use [5]:

$$\varepsilon_{reff} = \frac{\varepsilon_r+1}{2} + \frac{\varepsilon_r-1}{2}\left[1+12\frac{h}{W}\right]^{-0.5}$$

For $\varepsilon_r = 2.2$, $h = 1.588$ mm, and $W = 49.38$ mm, and since $W/h = 311.15$ which is greater than 1, we get:

$$\varepsilon_{reff} = 2.1097$$

It is right to have like this value for ε_{reff}, because $1 \le \varepsilon_{reff} \le \varepsilon_r$ is valid all the time.

The effective length we can be found using [5]:

$$L_{eff} = \frac{c}{2f_0\sqrt{\varepsilon_{reff}}}$$

For $c \approx 3\times 10^8$ m/s, $\varepsilon_{reff} = 2.1097$ and $f_0 = 2.4$ GHz we get:

$$L_{eff} = 4.303 \text{ cm} = 43.03 \text{ mm}.$$

To find the length extension, we use [5]:

$$\Delta L = 0.412h\frac{\left(\varepsilon_{eff}+0.3\right)\left(\frac{W}{h}+0.264\right)}{\left(\varepsilon_{eff}-0.258\right)\left(\frac{W}{h}+0.8\right)}$$

Substituting ε_{reff} = 2.1097, h = 1.588 mm, and W = 49.41 mm we get:

$$\Delta L = 8.3711\text{e-}002 \text{ cm} = 0.83711\text{mm}.$$

The actual length of the patch can be found using [5]:

$$L = L_{eff} - 2 \times \Delta L$$

For ΔL = 0.8311mm and ε_{reff} = 2.1097 we get:

$$L = 4.136 \text{ cm} = 41.36 \text{ mm}$$

the dimensions of the ground plane can be found using equations (2.9) and (2.10) ,

$L_{ground} = 6h + L = 6(1.588) + 41.3 = 50.828$ mm.

$W_{ground} = 6.h + W = 6(1.588) + 49.38 = 58.908$ mm.

Where L is the patch resonant length, and W is the patch impedance width.

The aperture conductance G_L is given by equation [5]:

$$G_1 = \frac{1}{120\pi^2} \int_0^{\pi} \left[\frac{\sin\left(\frac{k_0 W}{2} \cos\theta \right)}{\cos\theta} \right]^2 \sin^3\theta d\theta = 0.00157$$

Using equation (2.17) we can determine the resonant input impedance by taking the mutual effects between the slots into account as follows:

$$R_{in} = \frac{1}{2(G_1 \pm G_{12})} = 2.4477 \times 10^2 \, \Omega$$

The mutual conductance G_{12} is found as follows:

$$G_{12} = \frac{1}{120\pi^2} \int_0^{\pi} \left[\frac{\sin\left(\frac{k_0 W}{2} \cos\theta \right)}{\cos\theta} \right]^2 J_0(k_0 L \sin\theta) \sin^3\theta d\theta = 4.70265 \times 10^{-4}$$

The (+) sign is used in equation (2.13) for modes with odd resonant voltage (filed) distributions beneath the patch and between the slots.

To find the desired distance (x_0) between the feeding point and the leading radiating edge to fix the coaxial cable with the patch, we use [5]:

$$R_{in}(x = x_0) = R_{in}(x = 0)\cos^2(\frac{\pi}{L}x_0)$$

Solving this equation using Matlab Program No. 1 shown in appendix A at the end of this thesis we get: x_0 = 1.45 cm = 14.5mm or x_0 = 2.685 = 26.526 mm.

3.3 Simulation Setup and Results

For design simplicity of the conventional MSA, the patch's length and width and the ground plane have been rounded off to the following values: L = 40 mm, W = 50 mm, L_g = 50 mm, W_g = 60 mm. The general dimensions for the conventional MSA that will be designed is as follow:

L_g = 50 mm.
W_g = 60 mm.
ε_r for RT/ duroid 5880 is 2.2.
h = 1.588 mm.
L = 40 mm.
W = 50 mm.
t = 0.07 mm.
The height of the ground plane is 1 mm.
Using Matlab Program No. 2 shown in appendix A we get
x_0 = 1.39 cm =13.9 mm or x_0 = 2.61 =26.1 mm.

The feeding point location is approximately (13.9 mm, W/2), and the radius of the outer ring of the coaxial cable that is adjacent to the substrate is chosen to be 3 mm and the radius of the inner ring, which is called the feeding pin is 1.2 mm.

By using CST MWS with the dimensions previously driven, the conventional MSA is simulated as shown in Figure 3.1.

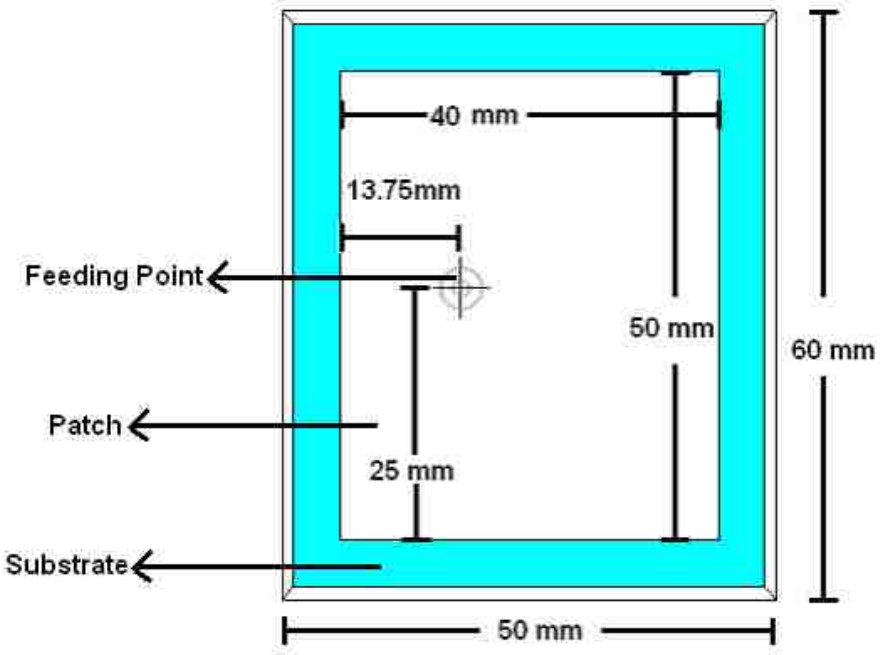

Figure 3.1: Simulated conventional rectangular MSA.

For different feeding point locations (x_0, y_0), we find the reflection coefficient curve (return loss), center frequency and *VSWR* as shown in table 3.1,where the origin of the patch coordinate (0,0) is at the lower left corner of the patch.

Table 3.1:Return losses vs. feeding location.

Feed Location (mm) (x_0, y_0)	Center Frequency (GHz)	Return Loss (*RL*) (dB)	*VSWR*
(12.50, 25)	2.4016	-15.91	1.381
(13.00, 25)	2.4008	-19.94	1.224
(13.50, 25)	2.4	-29.42	1.070
(13.65, 25)	2.4	-39.23	1.022
(13.75, 25)	2.4	-47.04	1.009
(13.85, 25)	2.4	-34.70	1.038
(14.00, 25)	2.3992	-28.12	1.082
(14.50, 25)	2.3984	-18.41	1.273
(15.00, 25)	2.3982	-13.67	1.523

At the feeding point (13.75, 25) mm, the reflection coefficient curve will be minimum when the resonance frequency equals 2.4 GHz. Figure 3.2 shows the reflection coefficient curve and Figure 3.3 shows the radiation pattern.

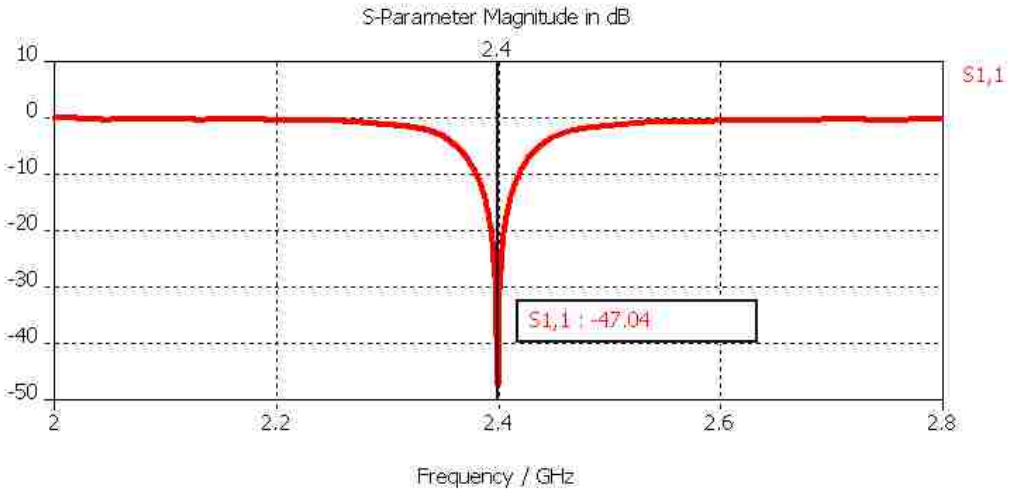

Figure 3.2: Simulated reflection coefficient in (dB) for conventional rectangular MSA.

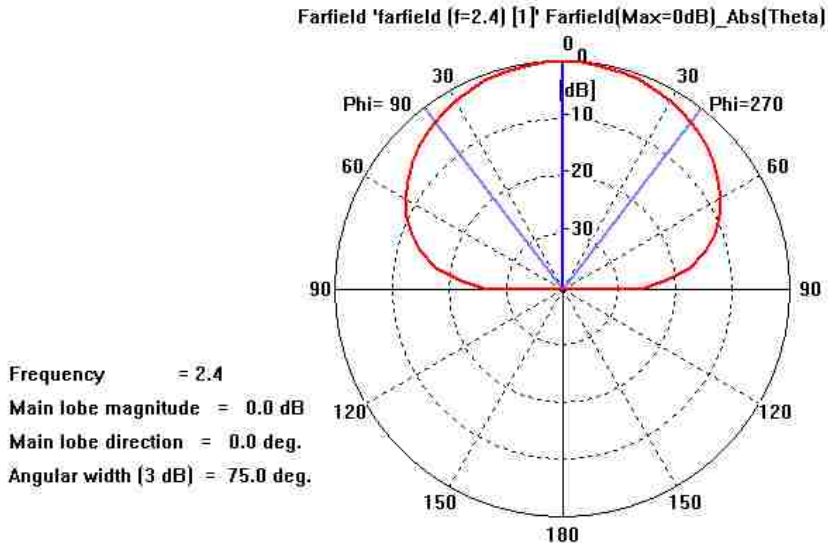

Figure 3.3. Simulated radiation pattern for conventional rectangular MSA.

In this thesis the same dimensions of the fundamental MSA are used to design a reconfigurable MSA that works at different frequencies. The design of a triple-band MSA is shown in Figure 3.4, where slot # 1 and slot # 2 are fixed in the lower left corner of the patch and upper right corner of it respectively. The length, width and locations of the slots are chosen by trial and error to get a low reflection coefficient.

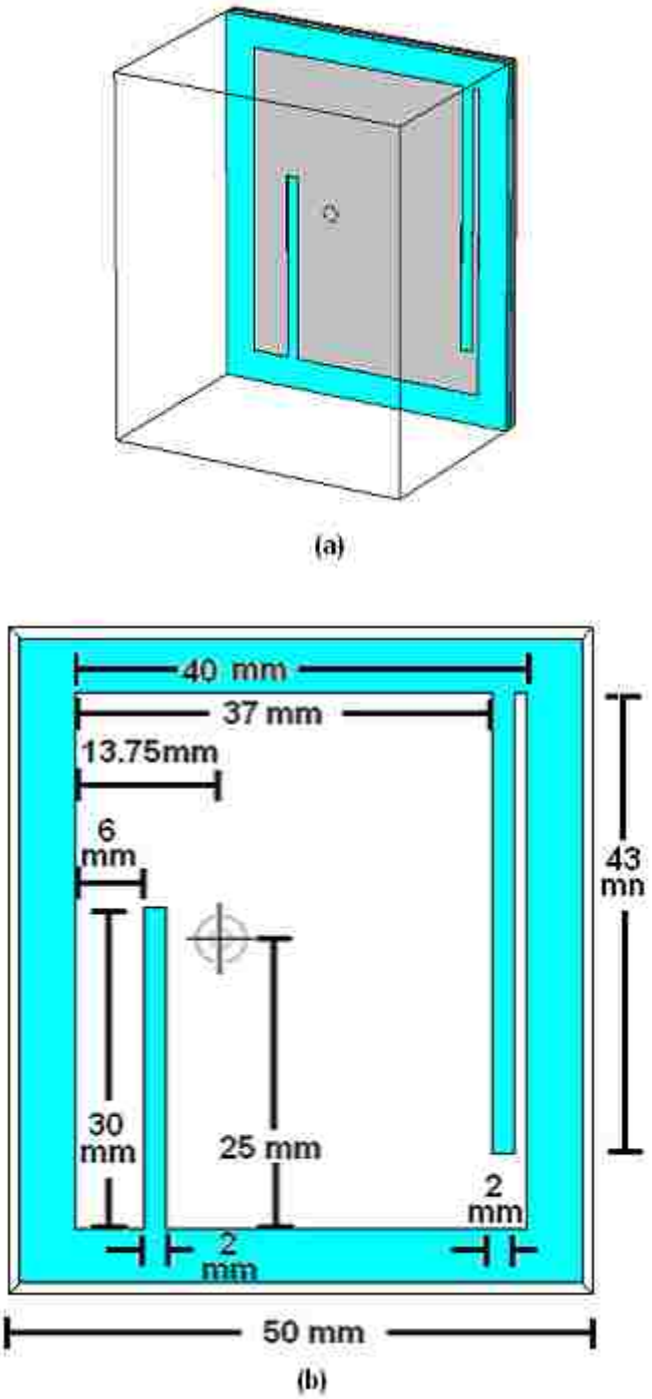

Figure 3.4: Simulated triple-band MSA (a) prospective view, (b) front view.

At the feeding point (13.75, 25) mm, the return loss is below –10 dB for the resonance frequencies are 2.906, 3.284 and 3.923 GHz as shown in Figure 3.5. The simulated radiation patterns of each operating frequency are shown in Figure 3.6.

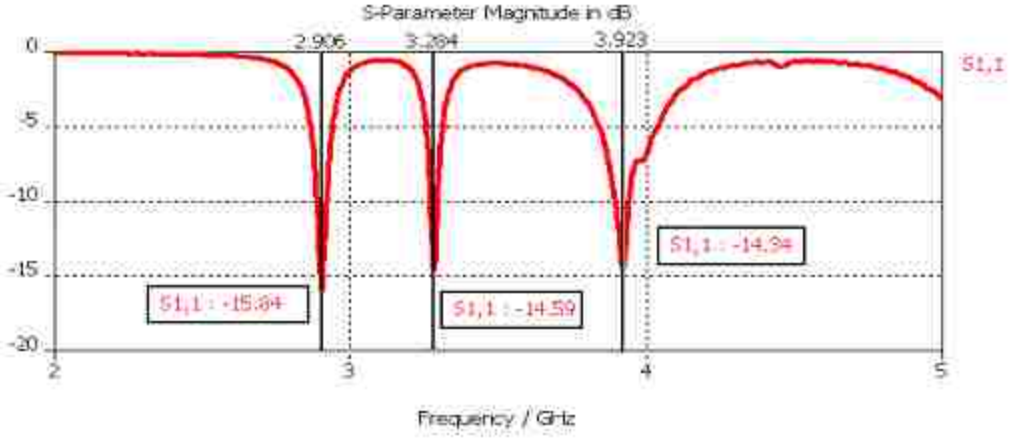

Figure 3.5: Simulated reflection coefficient in (dB) for triple-band MSA that resonates at the frequencies 2.906, 3.284 and 3.923 GHz.

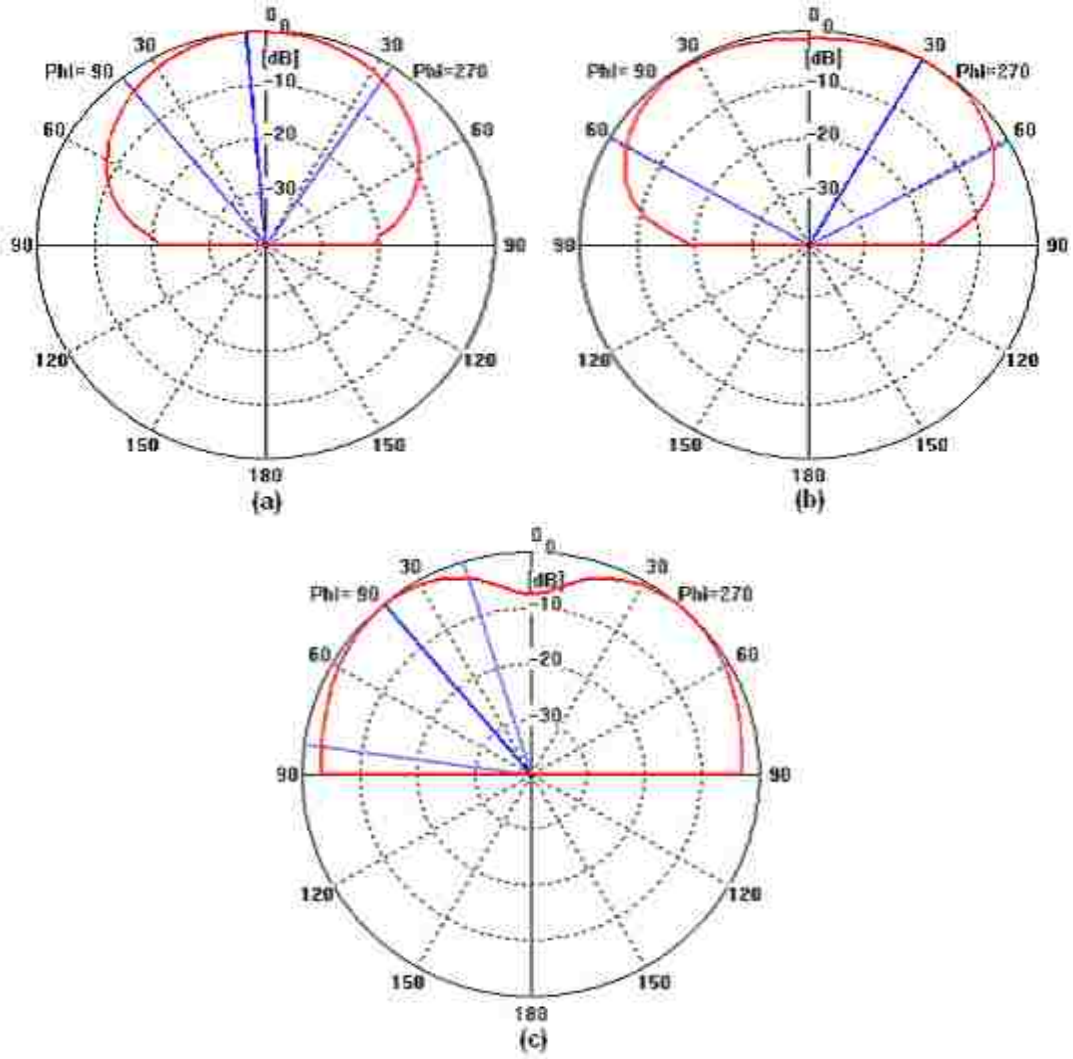

Figure 3.6: Simulated radiation patterns for triple-band MSA at the frequencies: (a) 2.906, (b) 3.284 and (c) 3.923 GHz.

Since MSAs radiate normal to its patch surface, the elevation pattern for φ = 0 and φ = 90 degrees would be important. From Figure 3.6 the backlobe radiation is sufficiently small. This low backlobe radiation is an added advantage for using this antenna in a cellular phone, since it reduces the amount of electromagnetic radiation which travels towards the users head. Radiation patterns plots shown don't contain unwanted side lobes or local minima caused by surface waves because dielectric-constant substrate is not high.

To obtain reconfigurability in this MSA, switches are added to the slots where the current paths become shorter and hence the operating frequencies move higher.

First of all, switch # 1 (SW1) of 1 mm width is added at the center of slot # 1 as shown in Figure 3.7.

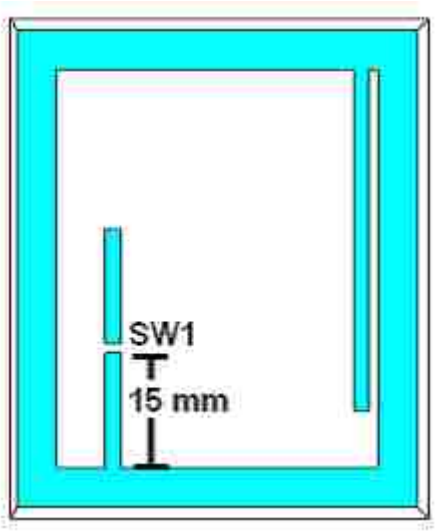

Figure 3.7: Simulated MSA with SW1 added to slot # 1.

When SW1 is at the center, we get only two resonance frequencies as shown in Figure 3.8, and the radiation patterns at the resonance frequencies are shown in Figure 3.9.

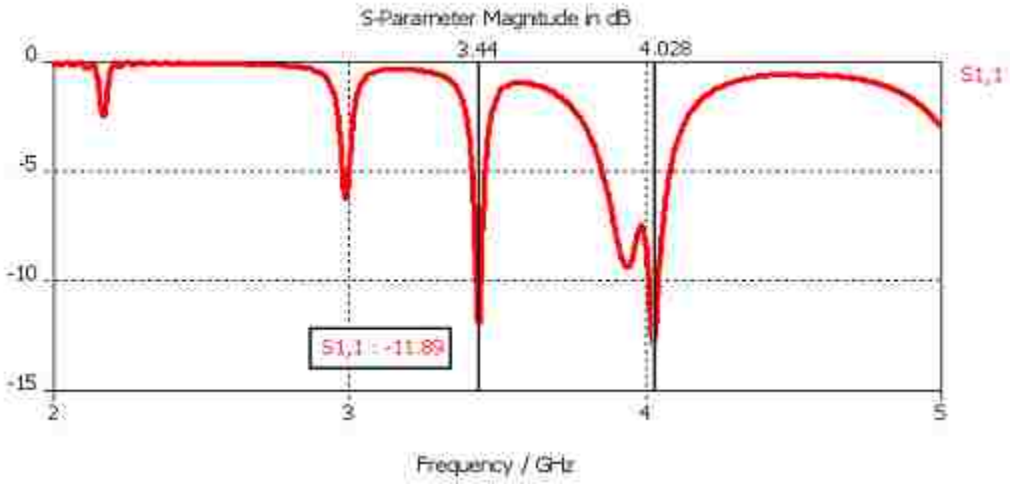

Figure 3.8: Simulated reflection coefficient in (dB) for MSA with SW1 at the center of Slot # 1 that resonates at the frequencies 3.44 and 4.028 GHz.

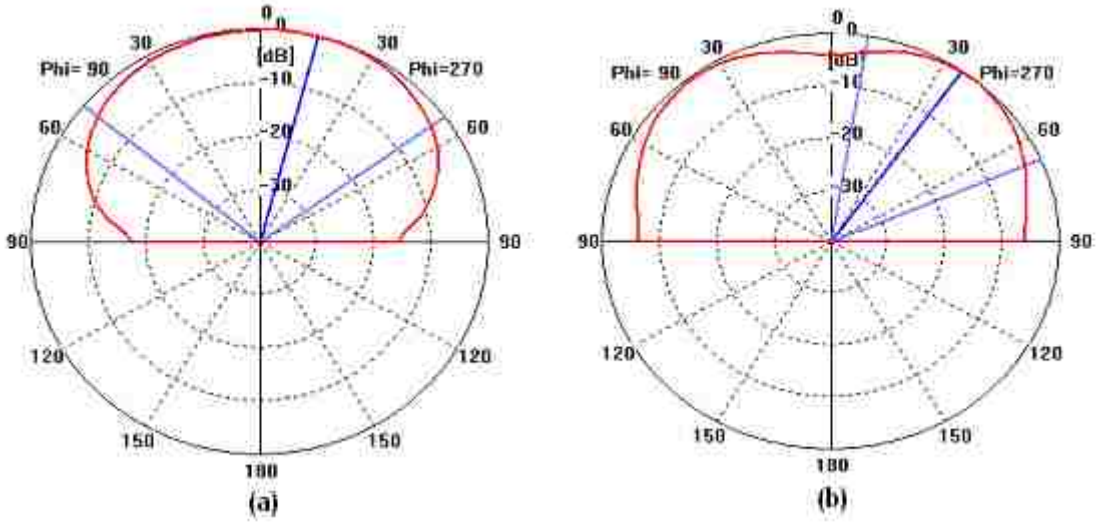

Figure 3.9: Simulated radiation patterns MSA with SW1 at the center of Slot # 1 at the frequencies : (a) 3.44 and (b) 4.028 GHz.

To get triple-band reconfigurable MSA, the position of SW1 must be changed either above or below the center of slot # 1. By changing the position of SW1 with different distances above the center of slot # 1 we get different reflection coefficient curves as shown in Figures 3.10 and 3.11.

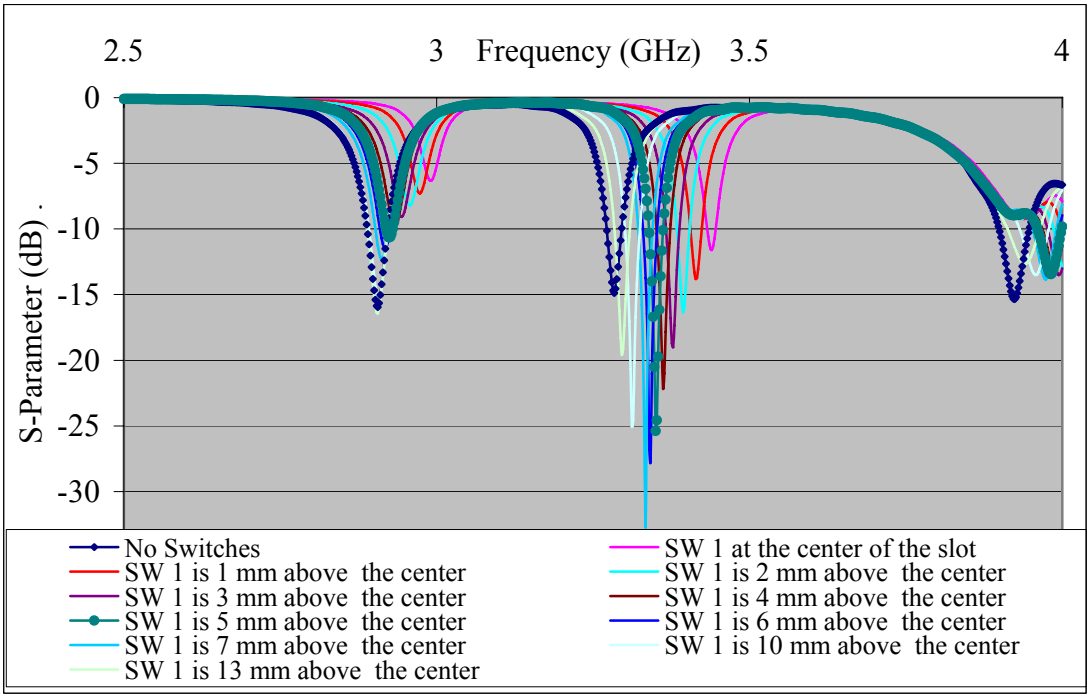

Figure 3.10: Simulated reflection coefficient curves for different positions of SW1 above the center of slot # 1.

For more detailed information, Figure 3.10 is redrawn with a lower frequency range as shown in Figure 3.11.

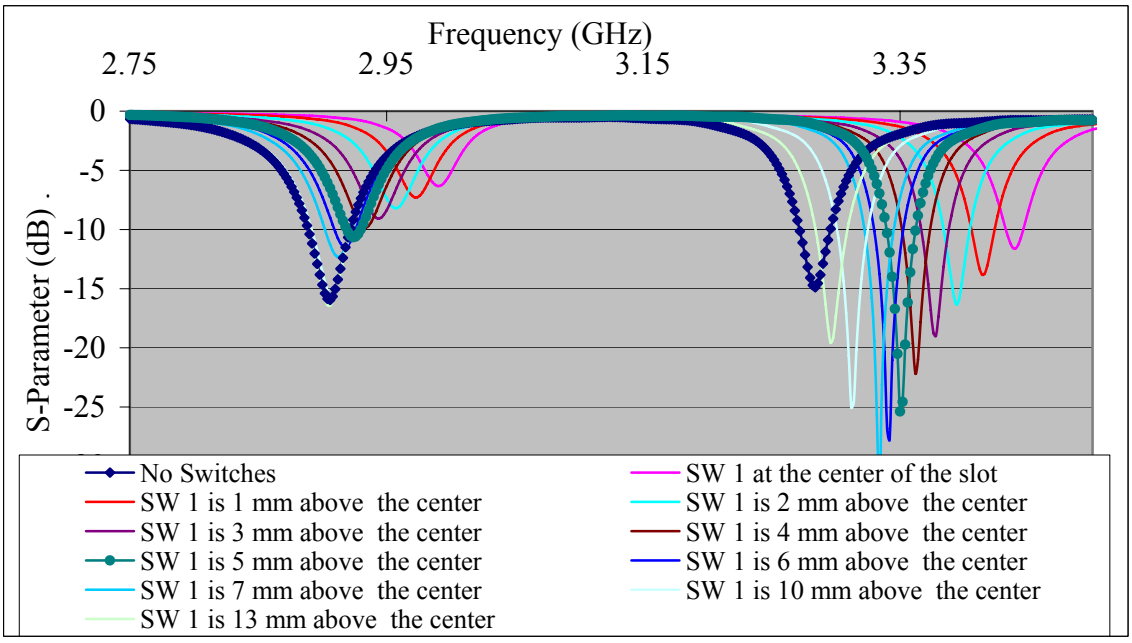

Figure 3.11: Simulated reflection coefficient curves for different positions of SW1 above the center of slot # 1.

From Figures 3.10 and 3.11, the best position to fix SW1 in order to perform the best frequency diversity is 5 mm above the center of slot # 1 as shown in Figure 3.12, where three resonance frequencies are attained as shown in Figure 3.13.

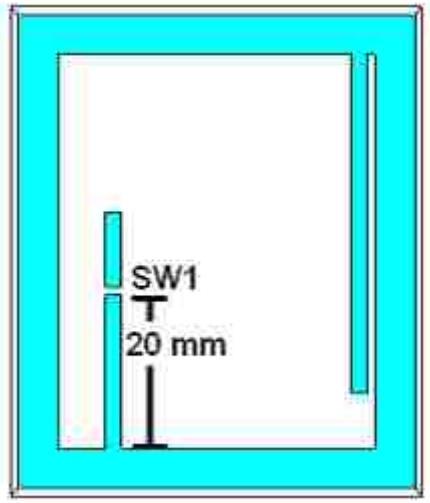

Figure 3.12: Simulated position of SW1 that gives a triple-band MSA.

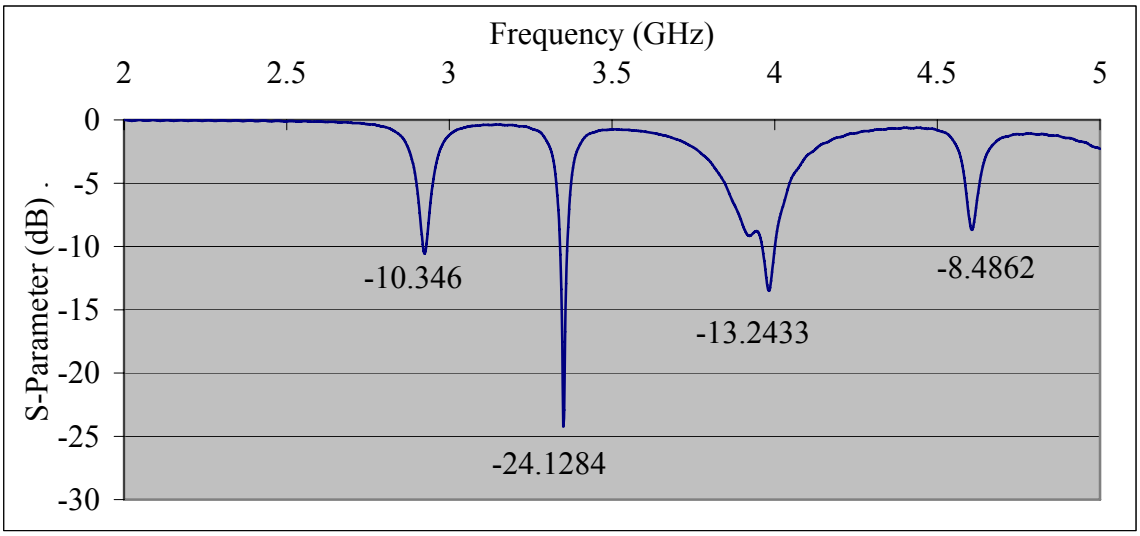

Figure 3.13: Simulated reflection coefficient curve when SW1 that fixed at 5 mm above the center of slot # 1 is ON.

When SW1 is ON and as shown in Figure 3.13, the reflection coefficient curve will be below –10 dB at frequencies; 2.924, 3.35 and 3.983 GHz instead of 2.906, 3.284

and 3.923 GHz respectively when SW1 is OFF. The radiation patterns of each frequency are shown in Figure 3.14.

At frequency 4.61 GHz, the reflection coefficient is about –8.5 dB, which is some times considered as a resonance frequency for practical applications.

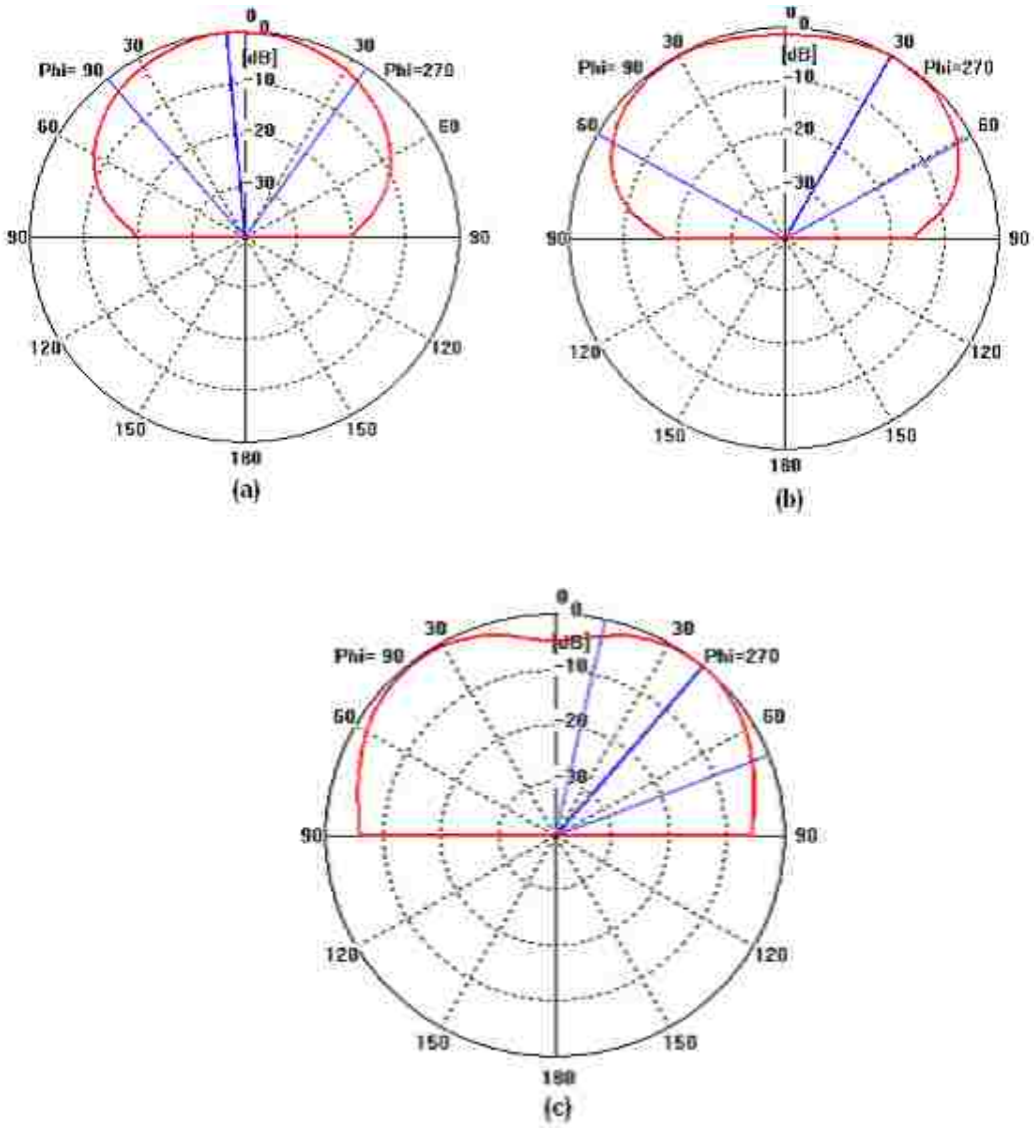

Figure 3.14: Simulated radiation patterns for a triple-band MSA when SW1 that fixed at 5 mm above the center of slot # 1 at the frequencies: (a) 2.924, (b) 3.35 and (c) 3.983 GHz.

Now by changing the position of SW1 below the center of slot # 1 with distances shown in Figure 3.15, we will give different reflection coefficient curves as follows;

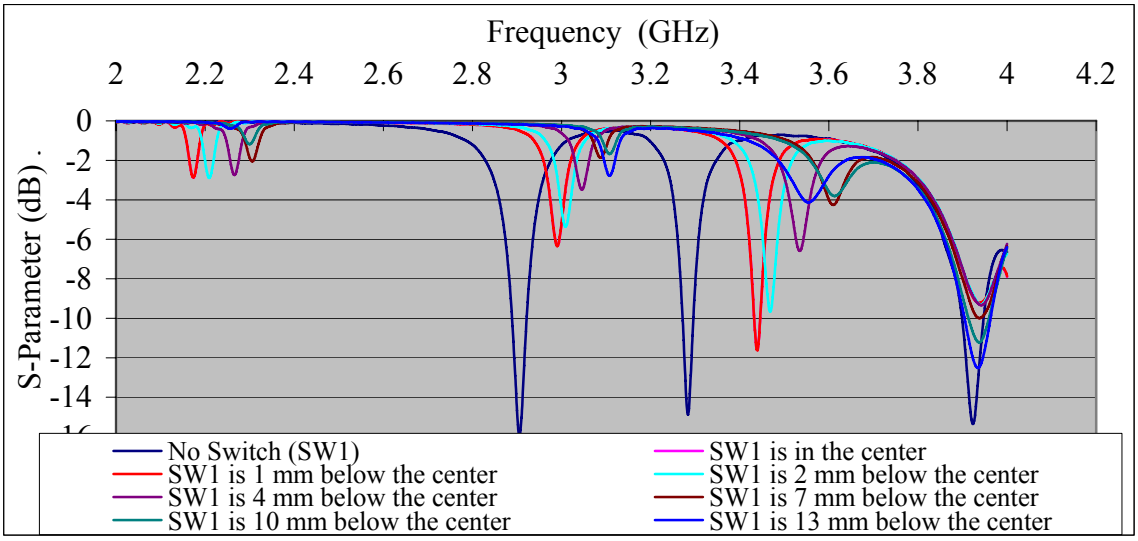

Figure 3.15: Simulated reflection coefficient curves for different positions of SW1 below the center of slot # 1.

By comparing Figure 3.15 with Figure 3.11, we see clearly that by fixing SW1 below the center of the slot, the number of resonance frequencies become lower, so the optimum case is to fix SW1 at 5 mm distance above the center of slot # 1.

The same thing is implemented to slot # 2 to determine the position of switch # 2 (SW2). Because slot # 2 is relatively long, the steps between the positions are made 4 mm to find the best place to fix SW2. By doing that and beginning from the lower edge of slot # 2 we get the results shown in Figures 3.16 and 3.17.

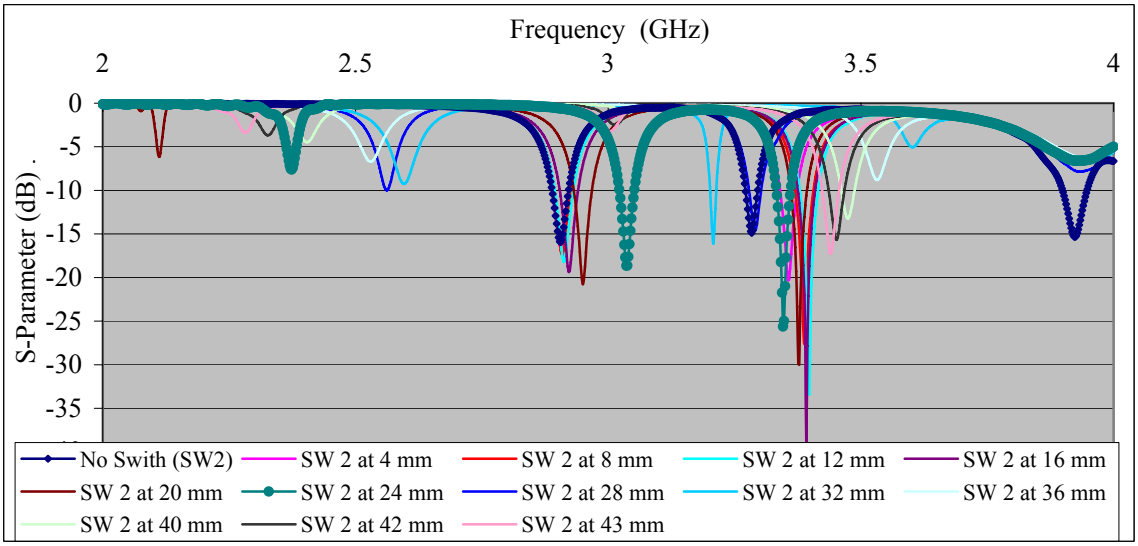

Figure 3.16: Simulated reflection coefficient curves for different positions of SW2 above the lower edge of slot # 2.

For more detailed information, Figure 3.15 is redrawn with lower frequency range as shown in Figure 3.16.

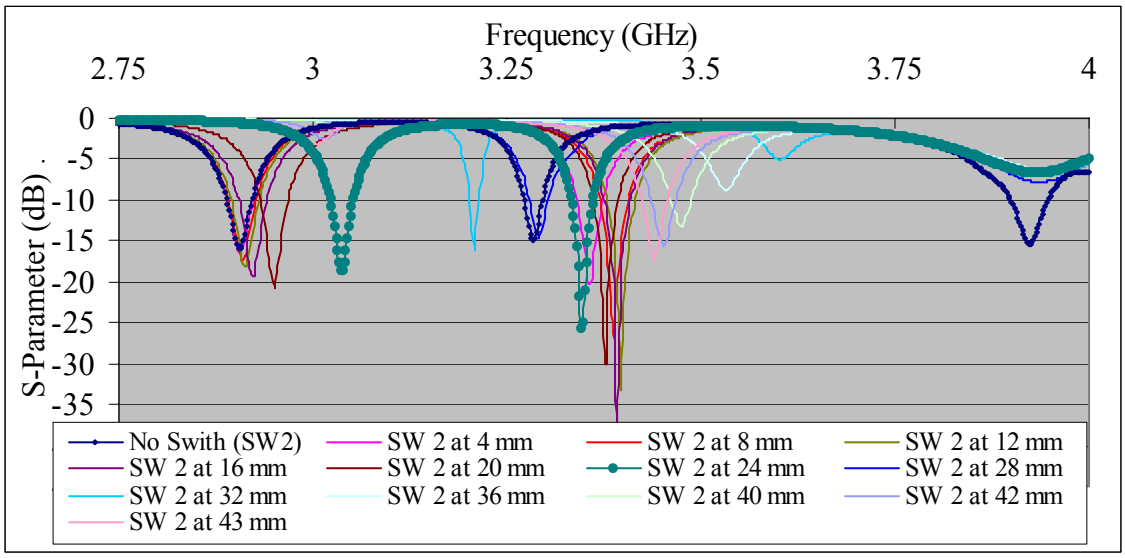

Figure 3.17: Simulated reflection coefficient curves for different positions of SW2 above the lower edge of slot # 2.

From Figures 3.16 and 3.17, the best position to fix SW2 is around 24 mm above the lower edge of slot # 2. To be more precise in determining the accurate position of SW2 that gives the best frequency diversity, we make a test for the distances 20 mm to 28 mm above the lower edge of slot # 2 by 1 mm steps. The result is shown in Figures 3.18 and 3.19.

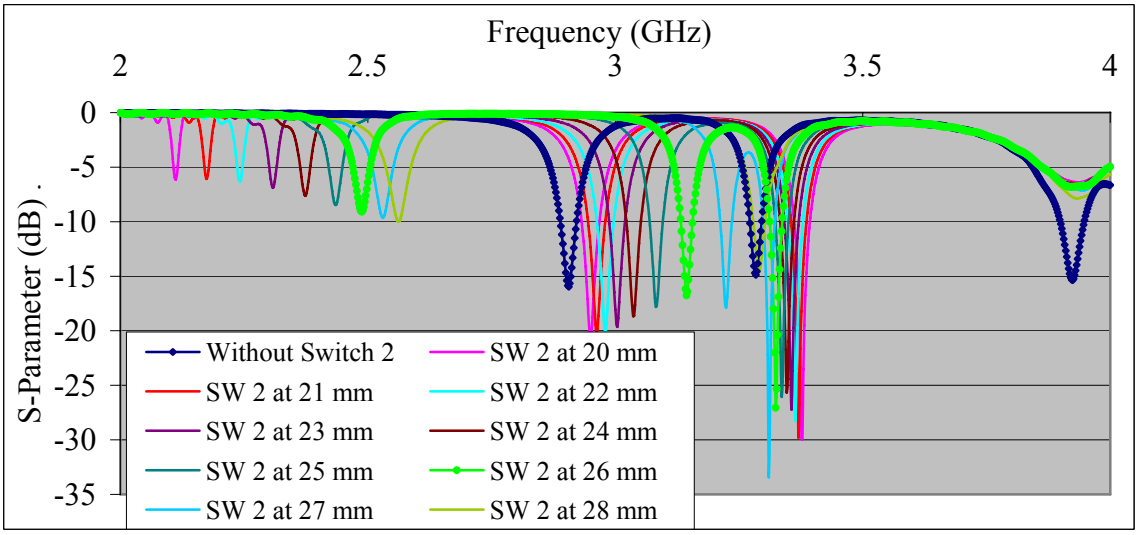

Figure 3.18: Simulated reflection coefficient curves for different positions of SW2 above the lower edge of slot # 2.

For more detailed information, Figure 3.18 is redrawn with a lower frequency range as shown in Figure 3.19.

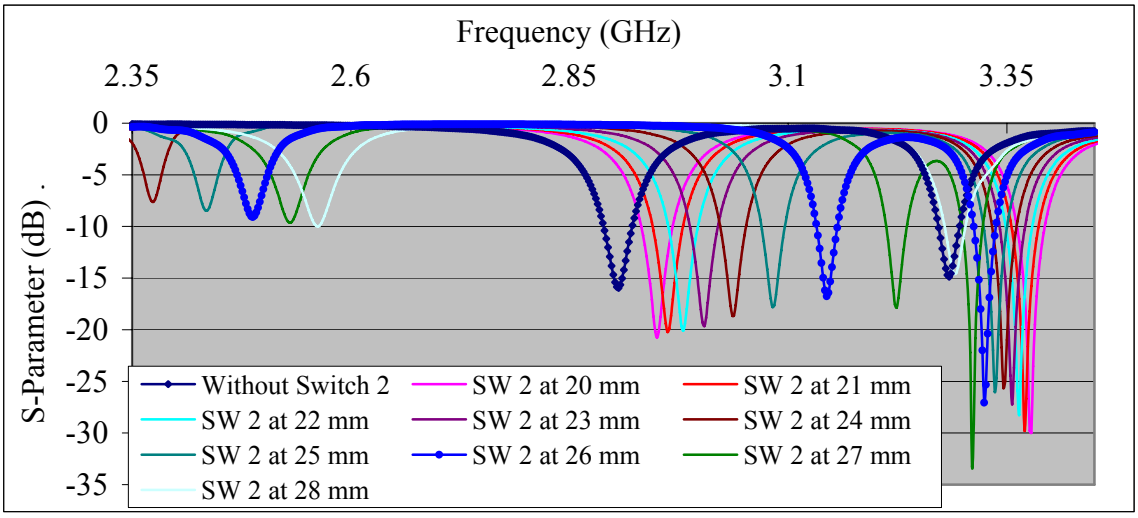

Figure 3.19: Simulated reflection coefficient curves for different positions of SW2 above the lower edge of slot # 2.

From Figures 3.18 and 3.19, the best position for SW2 that gives the best diversity is when it is 26 mm distanced from the lower edge of slot # 2 as shown in Figure 3.20.

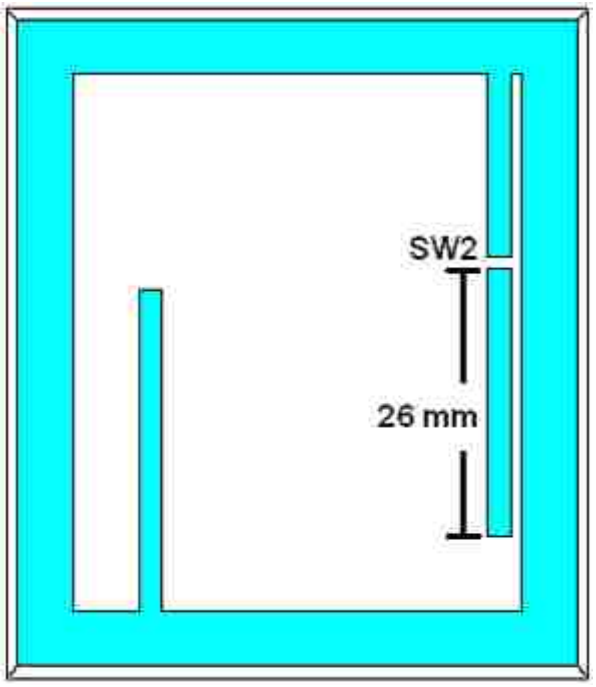

Figure 3.20: Simulated position of SW2 that gives a triple-band MSA.

When SW2 is ON, the reflection coefficient curve is almost below –10 dB when the resonance frequencies are 2.492, 3.146 and 3.326 GHz instead of 2.906, 3.284 and 3.922 GHz respectively when SW2 is OFF as shown in Figure 3.20.

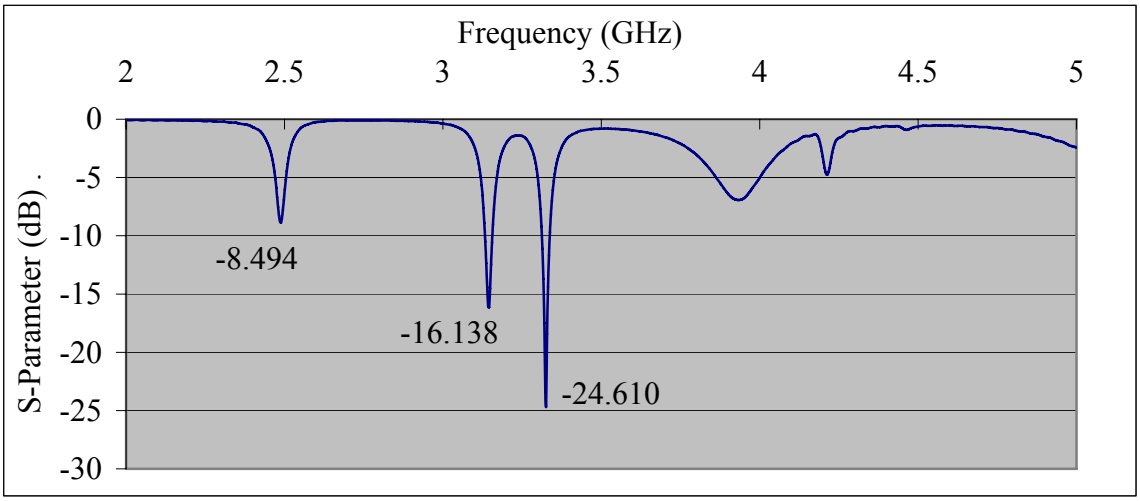

Figure 3.21: Simulated reflection coefficient curve when SW2 that fixed at 26 mm above the lower edge of slot # 2 is ON.

The radiation patterns at the three resonant frequencies when SW2 is ON are shown in Figure 3.22.

The final optimum positions of SW1 and SW2 that gives a triple-band reconfigurable MSA is shown in Figure 3.23.

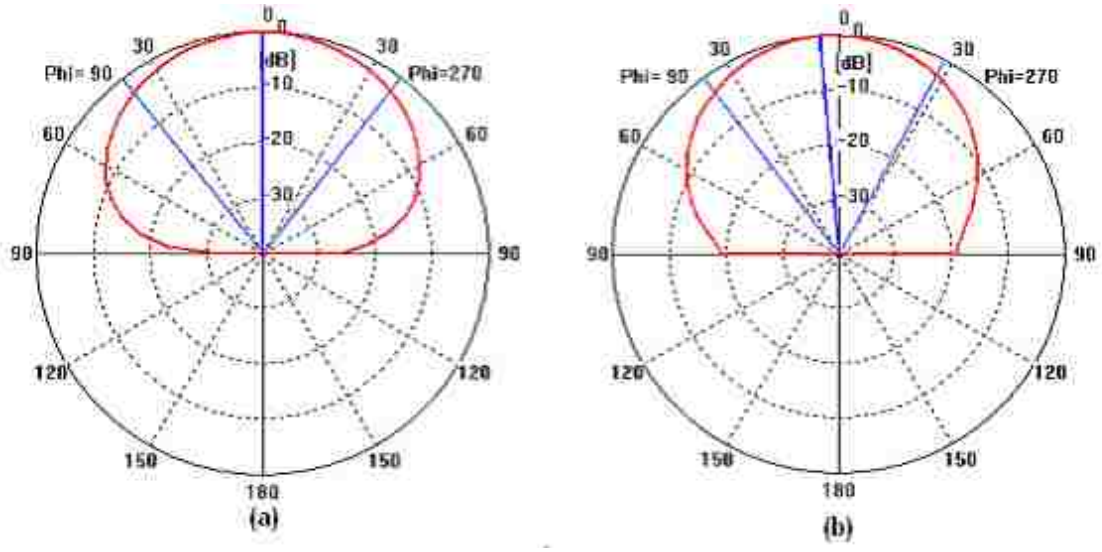

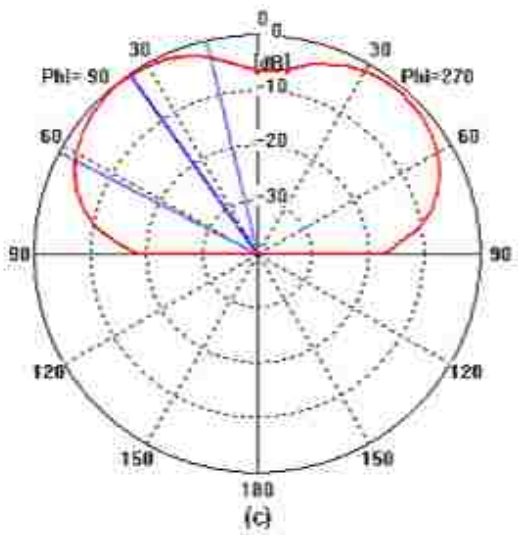

Figure 3.22: Simulated radiation patterns when SW2 is fixed at 26 mm above the lower edge of slot # 2 is ON at the frequencies: (a) 2.492, (b) 3.146 and (c) 3.326 GHz.

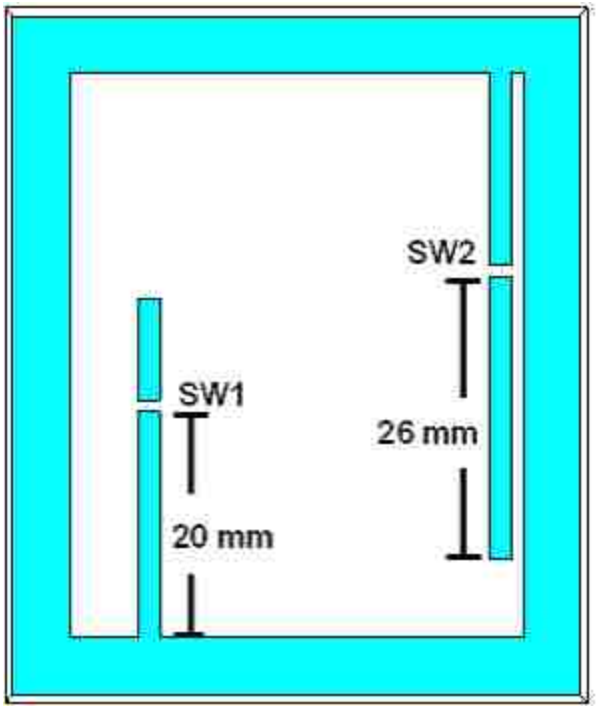

Figure 3.23: Simulated positions of SW1 and SW2 for multi-band MSA.

By switching ON both of SW1 and SW2, the reflection coefficient curve will be below –10 dB when the resonance frequencies are; 2.528, 3.152, 3.392 and 4.616 GHz. This is shown in Figure 3.24. Figure 3.25 shows the radiation patterns for these operating frequencies.

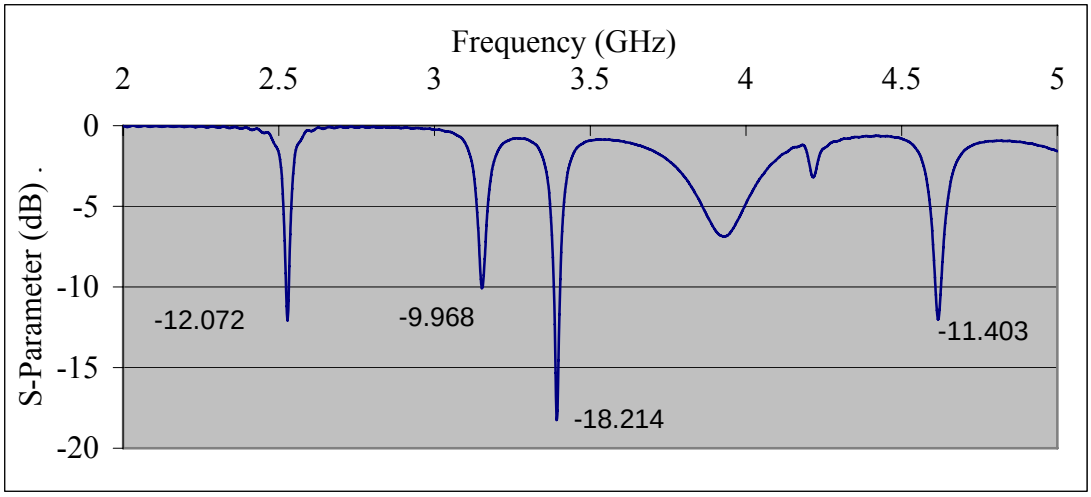

Figure 3.24: Simulated reflection coefficient curve for a multi-band MSA when SW1 and SW2 are ON.

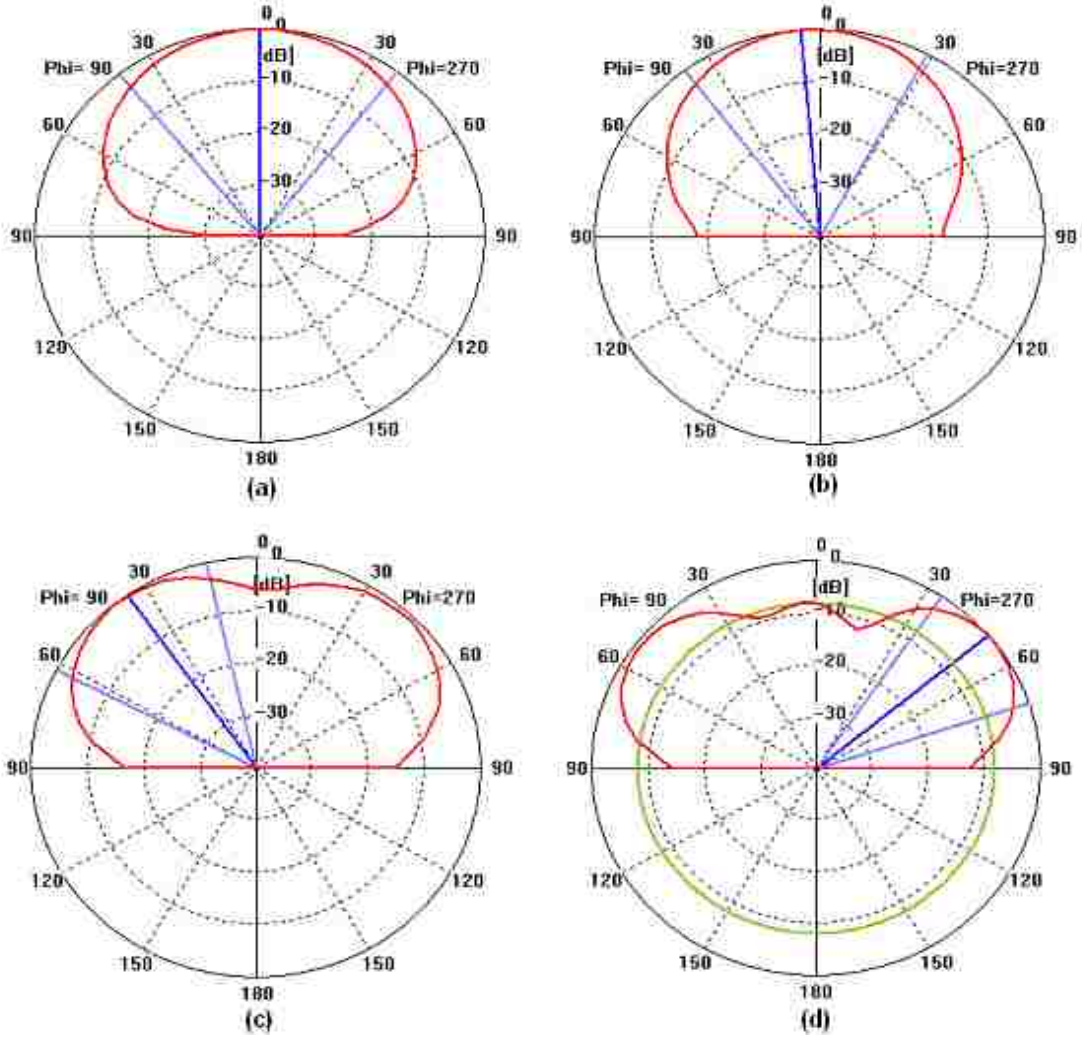

Figure 3.25: Simulated radiation patterns for multi-band MSA when SW1 and SW2 are ON at the frequencies: (a) 2.528, (b) 3.152, (c) 3.392, and (d) 4.616 GHz.

Figure 3.26 shows the reflection coefficient curves for different statuses of SW1 and SW2, these curves shows the resonance frequencies for each case.

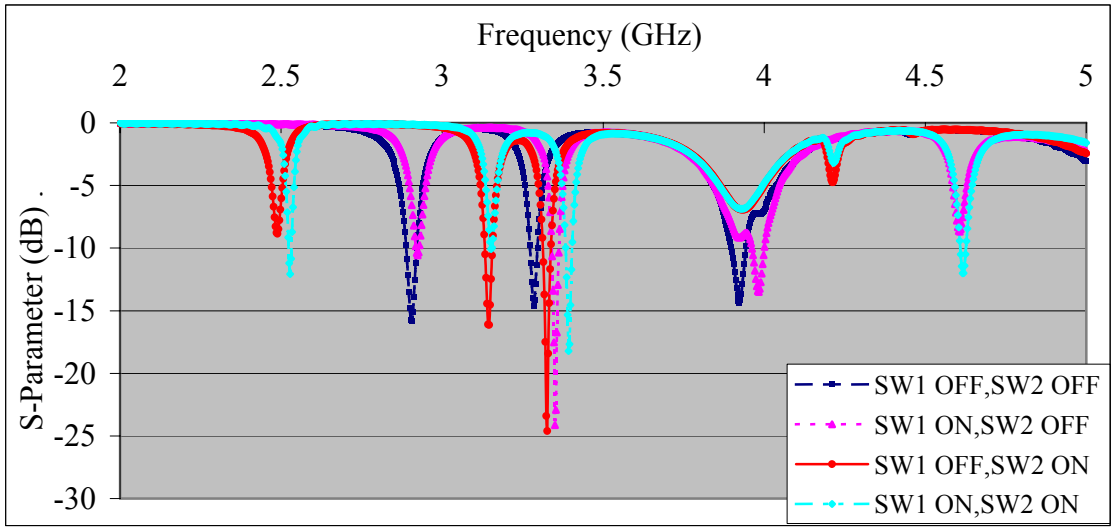

Figure 3.26: Simulated frequency diversity for a multi-band MSA for different statuses of SW1 and SW2.

3.4 Configuration of Stacked MSAs

In this section the concept of stacked MSAs are examined. The antenna shown in Figure 3.4, where both SW1 and SW2 are OFF, is covered with top layer of a substrate that has a certain dielectric constant and a certain thickness (height). The dimensions (length and width) of the top layer are 50×60 mm and a piece of metal (top patch) with $\varepsilon_r = 2.2$ and a thickness of 0.07 mm is fixed above the top layer. The initial dimensions of the top patch are 40×50 mm, and these dimensions are changed later on to get better results. In this approach, there are no direct connections between the bottom patch and the top one.

The height of the substrate in the top layer and its dielectric constant will be chosen in such a way that gives the best performance. Many experiments have been simulated for different layers of different heights and different dielectric constants as will be shown in this section.

Before adding the top layer, the reflection coefficient curve of the bottom MSA is shown in Figure 3.27.

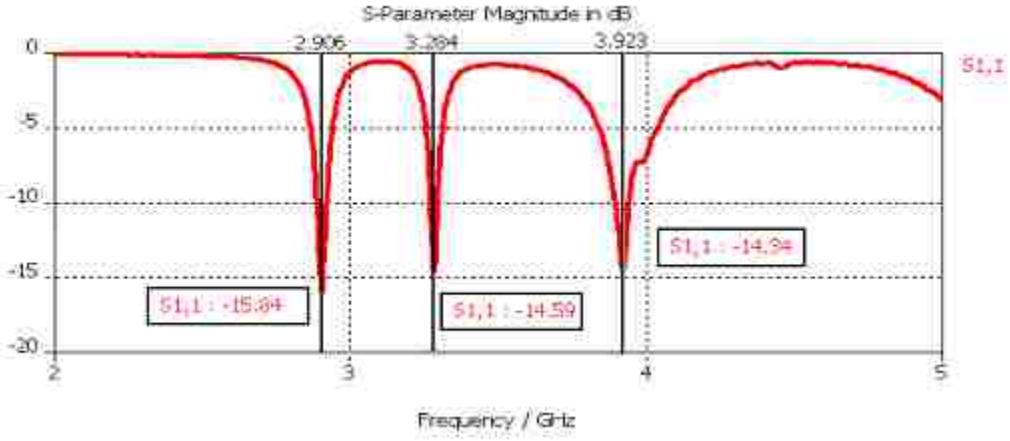

Figure 3.27: Simulated reflection coefficient curve of bottom MSA when SW1 and SW2 are OFF.

The stacked MSA is designed by adding a layer of air with ε_r = 1 and 1mm thickness. By keeping the top patch with dimensions of 40×50 mm and thickness of 0.07 mm as shown in Figure 3.28, we get the reflection coefficient curve shown in Figure 3.29.

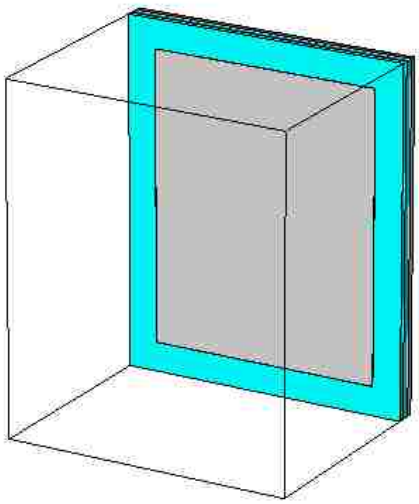

Figure 3.28: Stacked MSA with top substrate of 1 mm height and top patch dimensions of 40×50 mm.

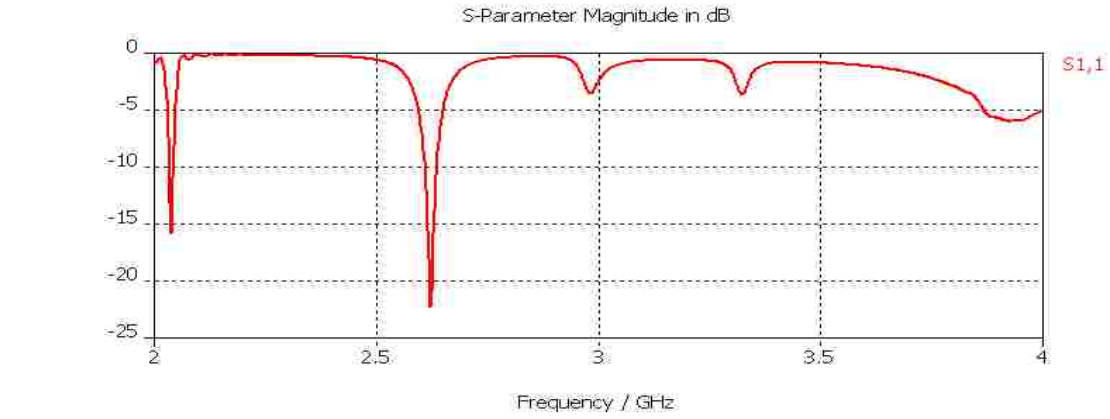

Figure 3.29: Simulated reflection coefficient curve of stacked MSA with top layer of ε_r =1 and 1 mm thickness.

By changing the dielectric constant of the top substrata, and fixing its thickness at 1 mm, we get reflection coefficient curves for materials of ε_r between (1-1.6), (1.7-2.4) and (2.5-4) as shown in Figures (3.30, 3.31 and 3.32) respectively. Detailed reflection coefficient curves for each ε_r are shown in appendix B at the end of this thesis.

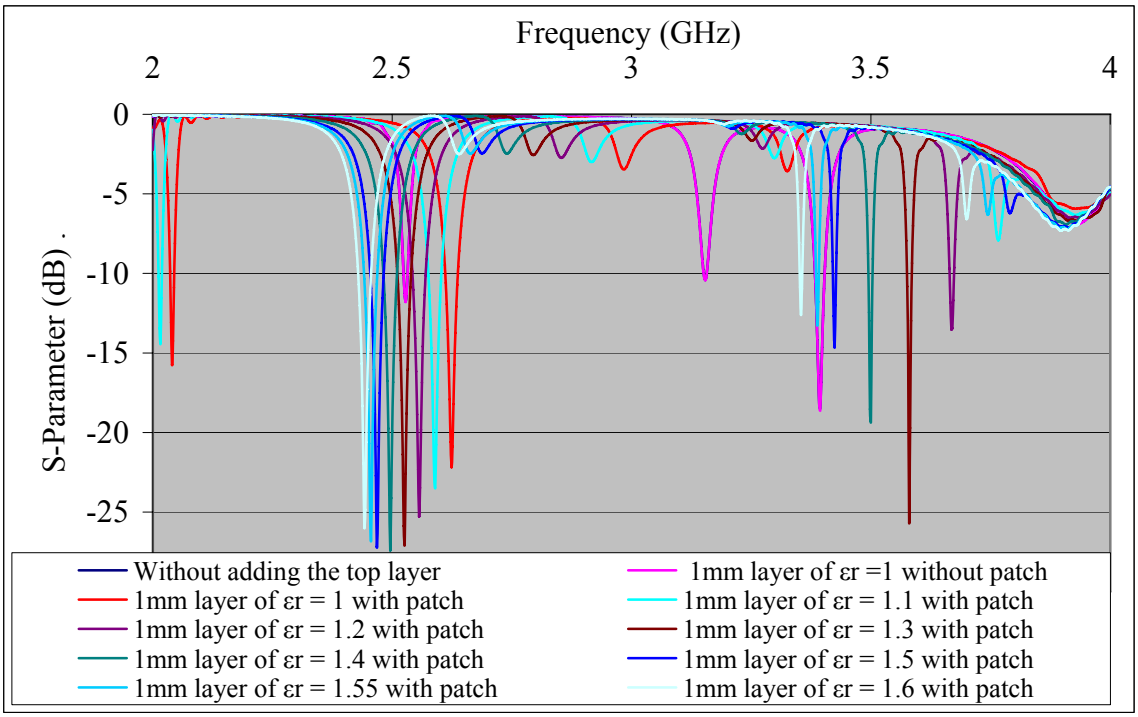

Figure 3.30: Simulated reflection coefficient curves of stacked MSAs with I mm top layer of ε_r between (1-1.6) and 1 mm thickness.

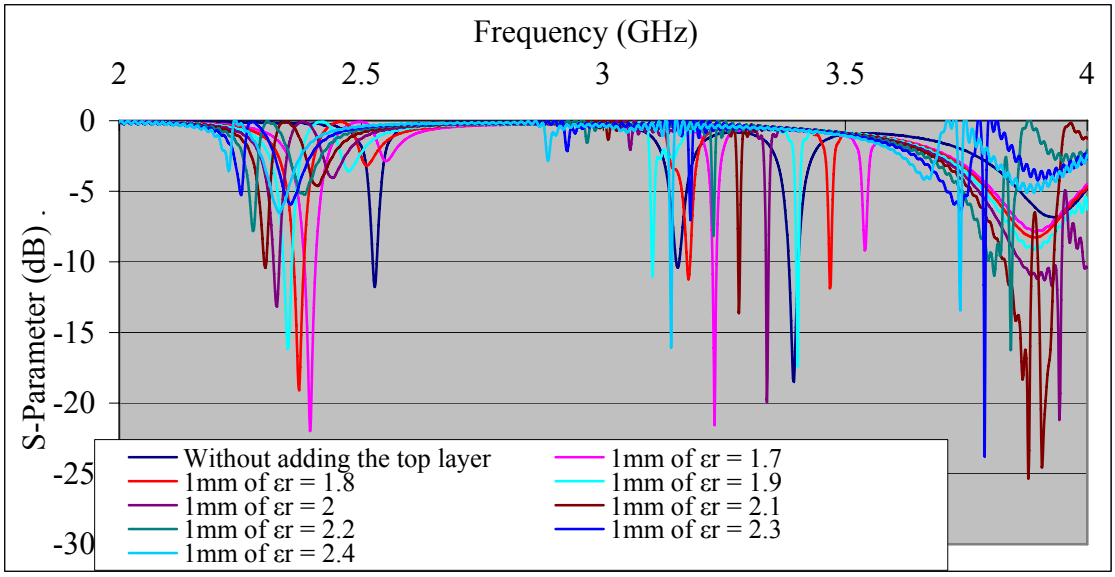

Figure 3.31: Simulated reflection coefficient curves of stacked MSAs with top layers of ε_r between (1.7-2.4) and 1 mm thickness.

Figure 3.30 shows that only two resonance frequencies are achieved. However, Figure 3.31 shows the best results that are achieved when the ε_r is between 1.9 and 2.2, where four resonance frequencies are achieved when $\varepsilon_r = 1.9$.

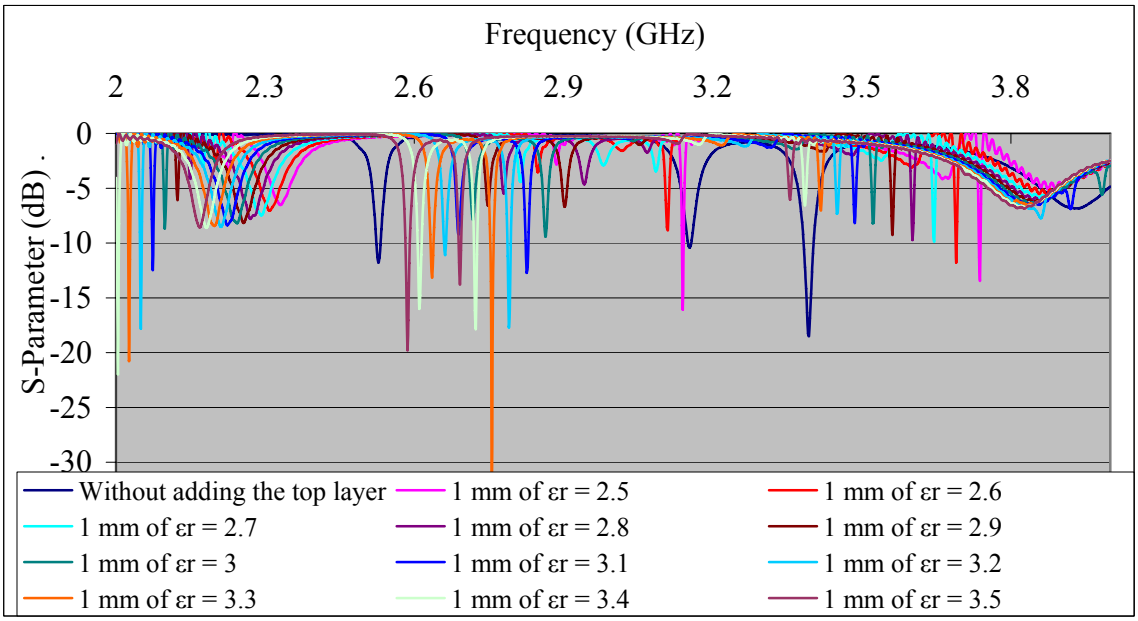

Figure 3.32: Simulated reflection coefficient curves of stacked MSAs with top layers of ε_r between (2.5-3.5) and 1 mm thickness.

From Figure 3.31, the best results are achieved when ε_r is between 3.2 and 3.4, where we get four resonance frequencies when $\varepsilon_r = 3.3$

To improve the bandwidth and efficiency and to increase the number of resonance frequencies of the staked MSA, the thickness of the top substrate has to be increased, also the dimensions of the top patch suppose to be increased to get better results. By changing the thickness of the top substrate to 1.588 mm instead of 1 mm (for practical purposes) and the dimensions of top patch to be 45×55 mm with keeping its thickness equals 0.07 mm as shown in Figure 3.32, better performance is achieved.

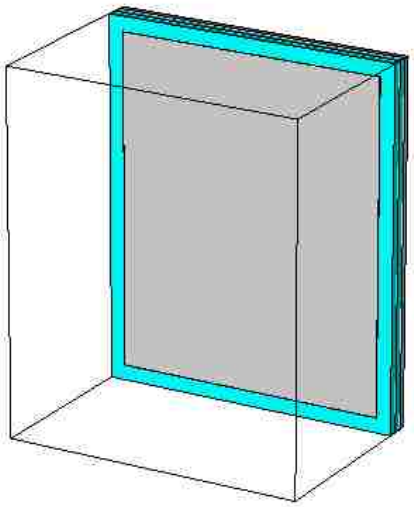

Figure 3.33: Stacked MSA with top substrate of 1.588 mm thickness and top patch dimensions of 40×50 mm.

Many experiments are simulated for different ε_r from 1 to 2 to get a stacked MSA with optimum performance. The best results are achieved when the ε_r is between 1.4 and 1.7. The detailed reflection coefficient curves are shown in Appendices C and D.

Figures 3.34, 3.35 and 3.36 show the reflection coefficient curves when dielectric constants equal 1.43, 1.44 and 1.45 respectively.

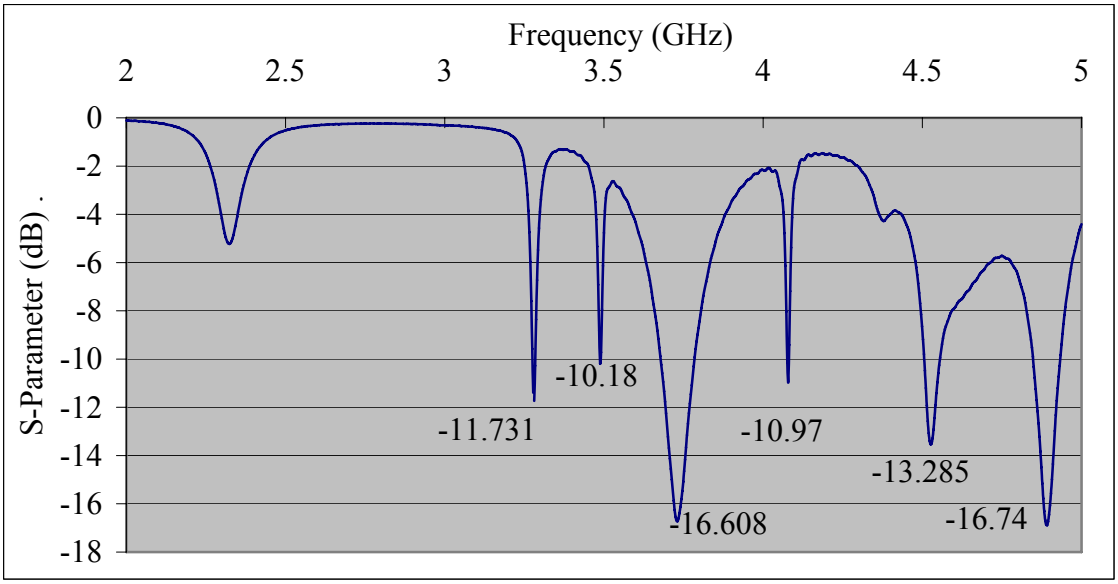

Figure 3.34: Simulated reflection coefficient curve of stacked MSA with 1.588 mm top layer of ε_r = 1.43.

- When ε_r = 1.43, antenna will resonate at the following frequencies; 3.281, 3.488, 3.737, 4.079,4.532 and 4.895 GHz.

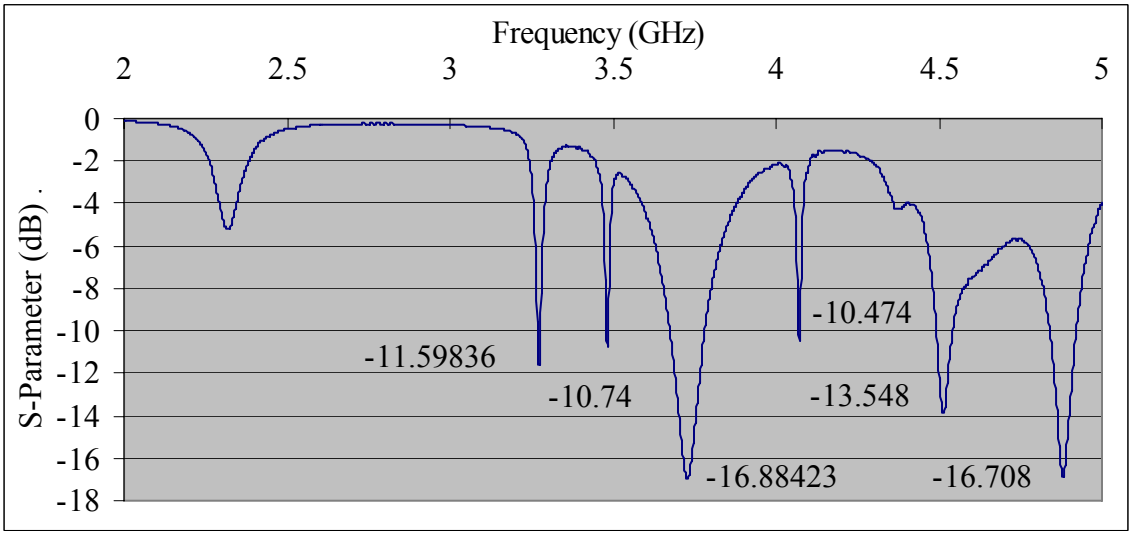

Figure 3.35: Simulated reflection coefficient curve of stacked MSA with 1.588 mm top layer of ε_r = 1.44.

- When ε_r =1.44, antenna will resonate at the following frequencies; 3.275, 3.482, 3.734, 4.073,4.52 and 4.886 GHz.

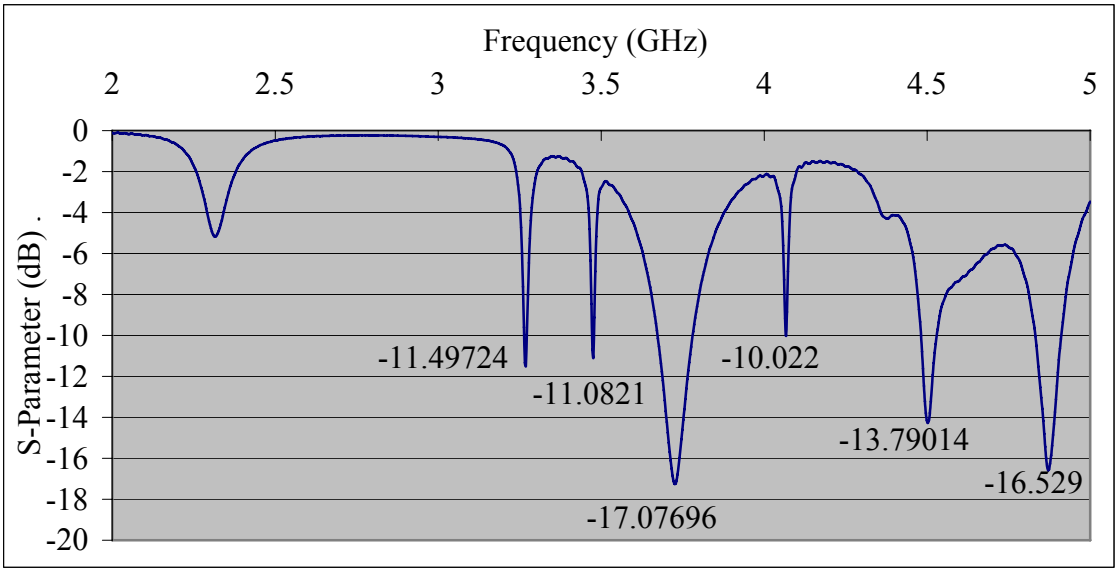

Figure 3.36: Simulated reflection coefficient curve of stacked MSA with 1.588 mm top layer of ε_r = 1.45.

- When ε_r = 1.45, antenna will resonate at the following frequencies; 3.269, 3.476, 3.731, 4.065,4.508 and 4.874 GHz.

The best reflection coefficient curve is achieved when the ε_r = 1.44 as shown in Figure 3.35. The simulated radiation patterns for these resonance frequencies achieved are shown in Figure 3.37.

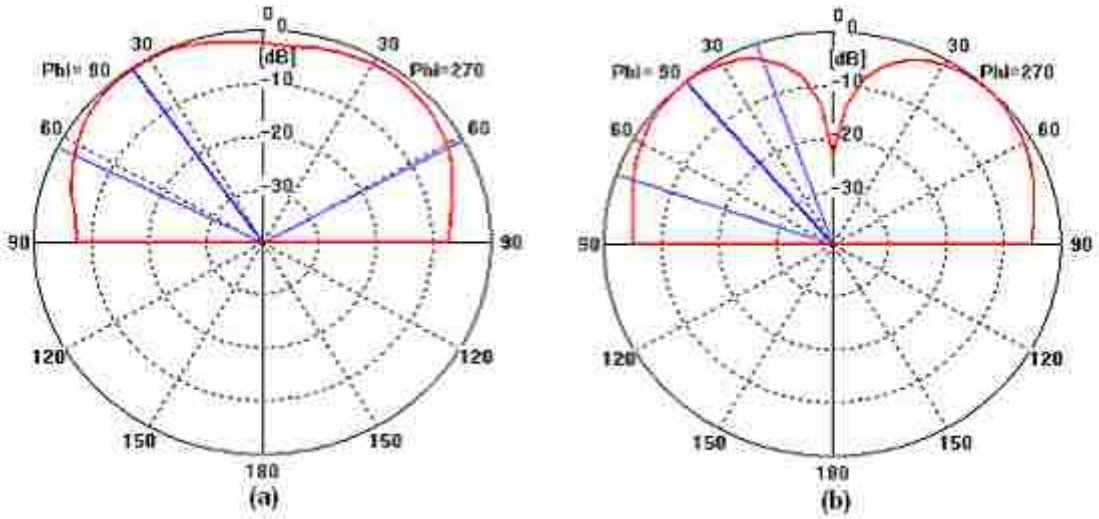

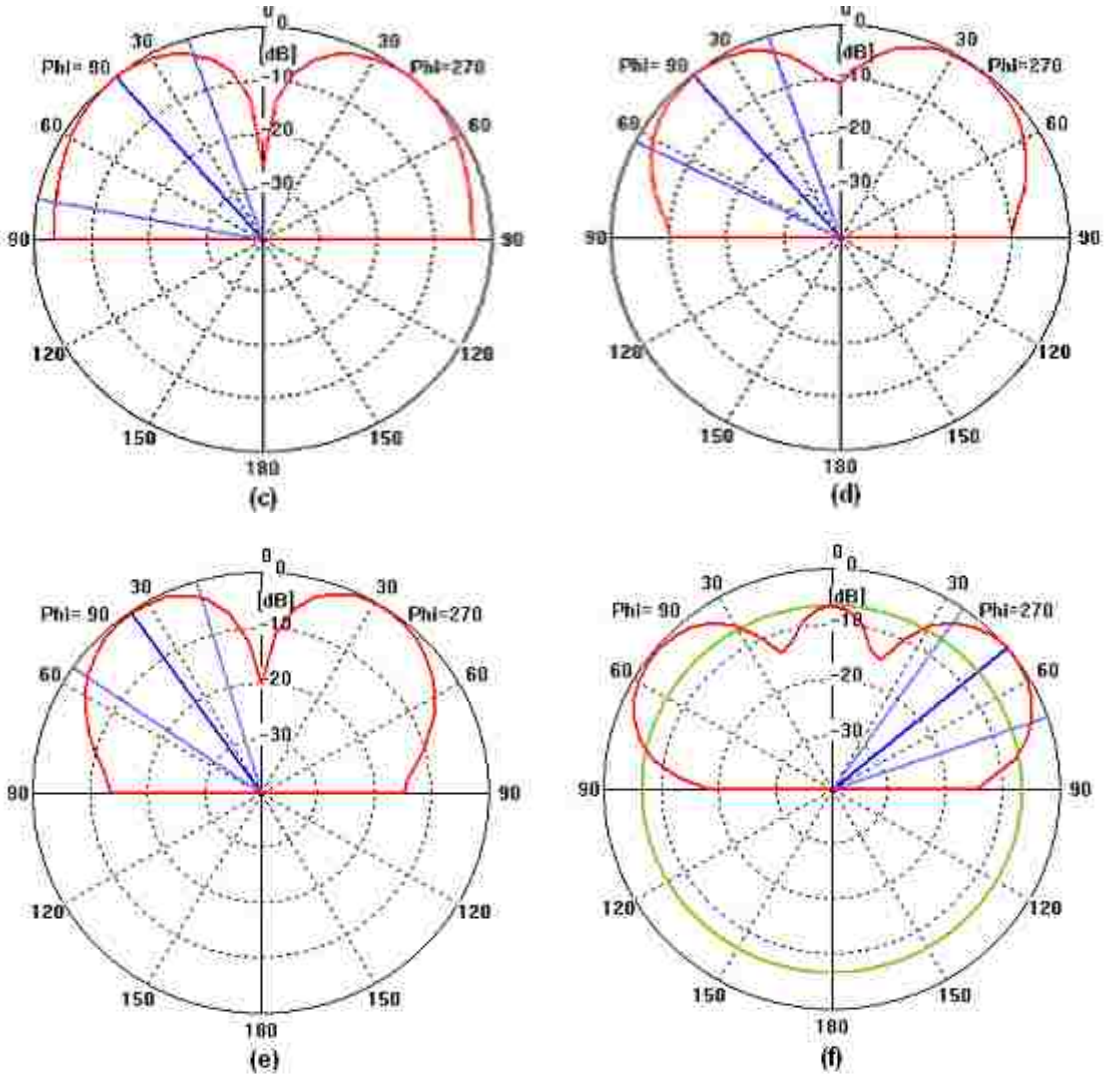

Figure 3.37: Simulated radiation patterns of stacked MSA with top layer of ε_r = 1.44 at the frequencies: (a) 3.275, (b) 3.482, (c) 3.734, (d) 4.073, (e) 4.52 and (f) 4.886 GHz.

Distort in the radiation pattern of the antenna in the main beam direction occurs due to the radiated surface wave results in increase the side-lobe and back-lobe levels. This surface wave radiation can be minimized by adding metallic strips (called parasitic strips) parallel to the radiating edges of the patch. However the size of parasitic strips is too large for a normal patch antenna.

A comparison between a conventional MSA and a stacked MSA with adding top layer of ε_r = 1.44 for different statuses of SW1 and SW2 are shown in Figures 3.38 and 3.39.

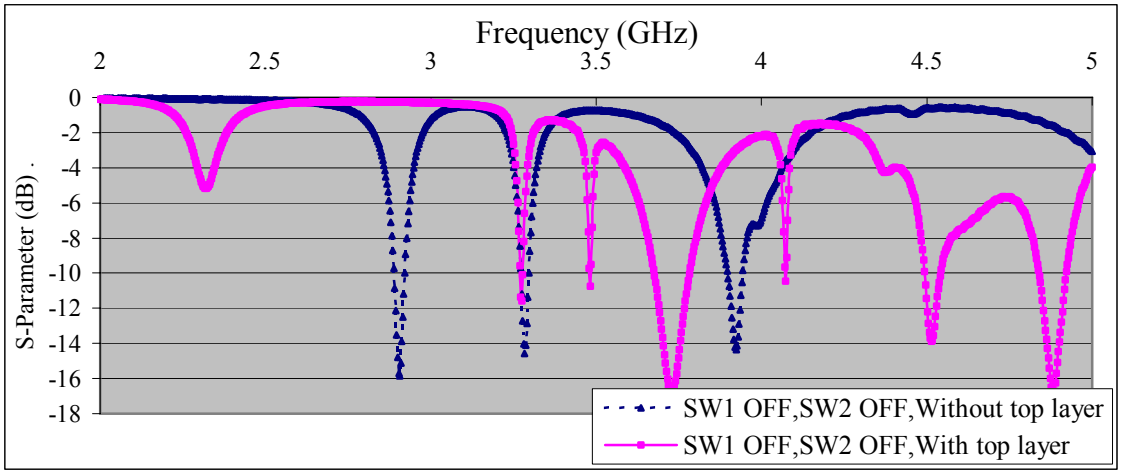
Frequency (GHz)
2
2.5
3
3.5
4
4.5
5
0
-2
-4
-6
-8
-10
-12
-14
-16
-18
S-Parameter (dB) .
SW1 OFF,SW2 OFF,Without top layer
SW1 OFF,SW2 OFF,With top layer

(a)

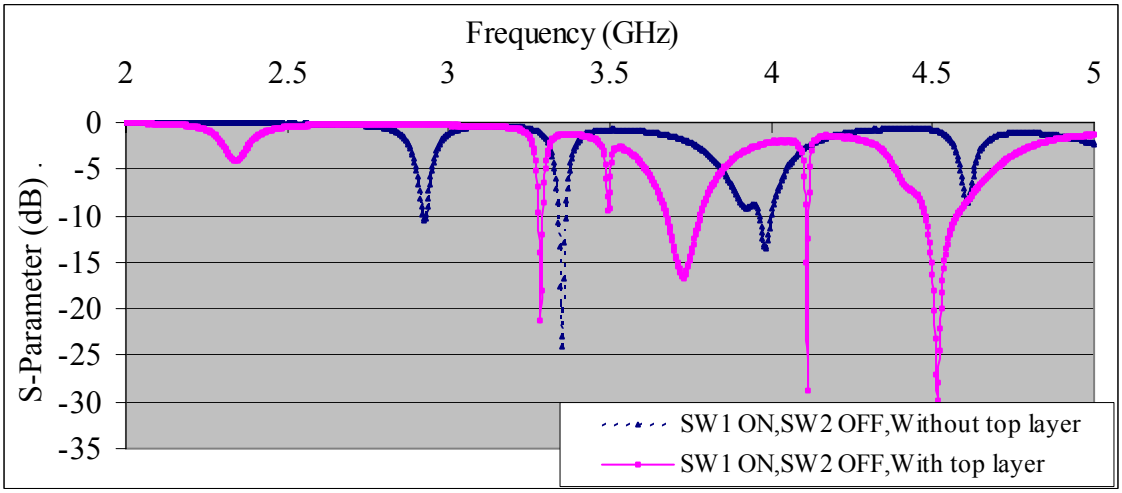
Frequency (GHz)
2
2.5
3
3.5
4
4.5
5
0
-5
-10
-15
-20
-25
-30
-35
S-Parameter (dB) .
SW1 ON,SW2 OFF,Without top layer
SW1 ON,SW2 OFF,With top layer

(b)

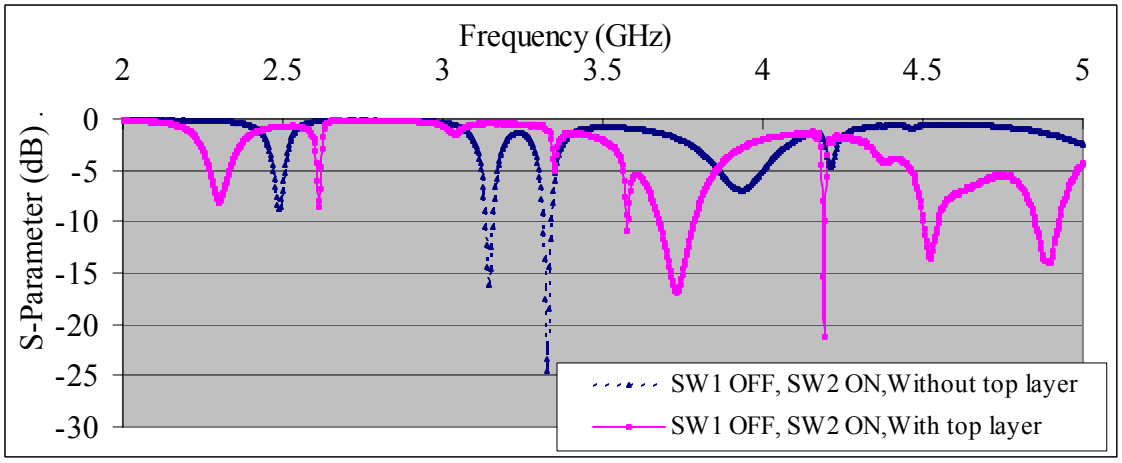
Frequency (GHz)
2
2.5
3
3.5
4
4.5
5
0
-5
-10
-15
-20
-25
-30
S-Parameter (dB) .
SW1 OFF, SW2 ON,Without top layer
SW1 OFF, SW2 ON,With top layer

(c)

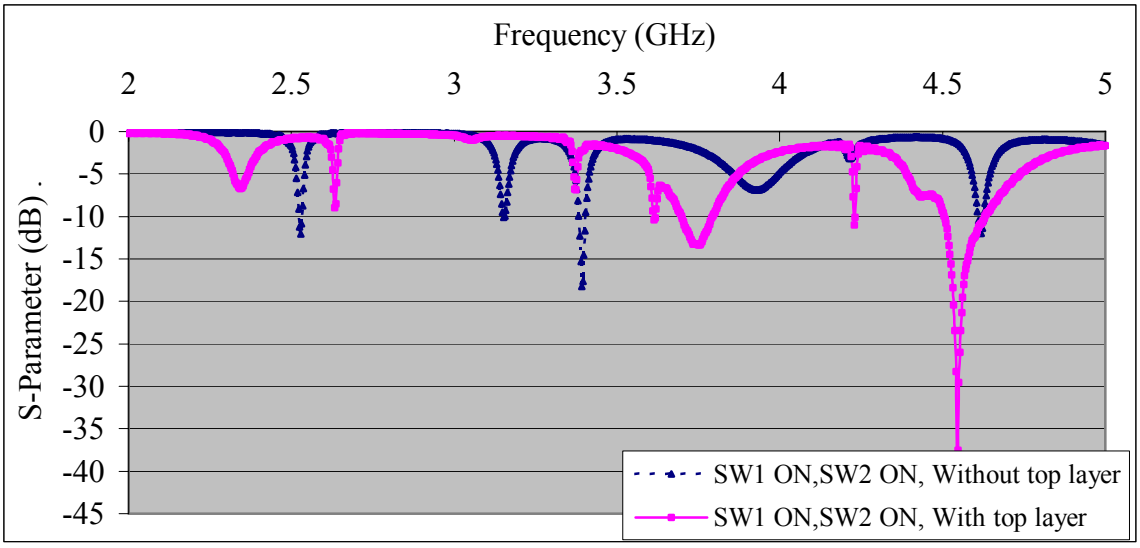

(d)

Figure 3.38: Simulated reflection coefficient curves of stacked MSA with / without adding the top layer of ε_r =1.44 when (a) SW1and SW2 are OFF, (b) SW1 ON, SW2 OFF, (c) SW1 OFF, SW2 ON, (d) SW1and SW2 are ON.

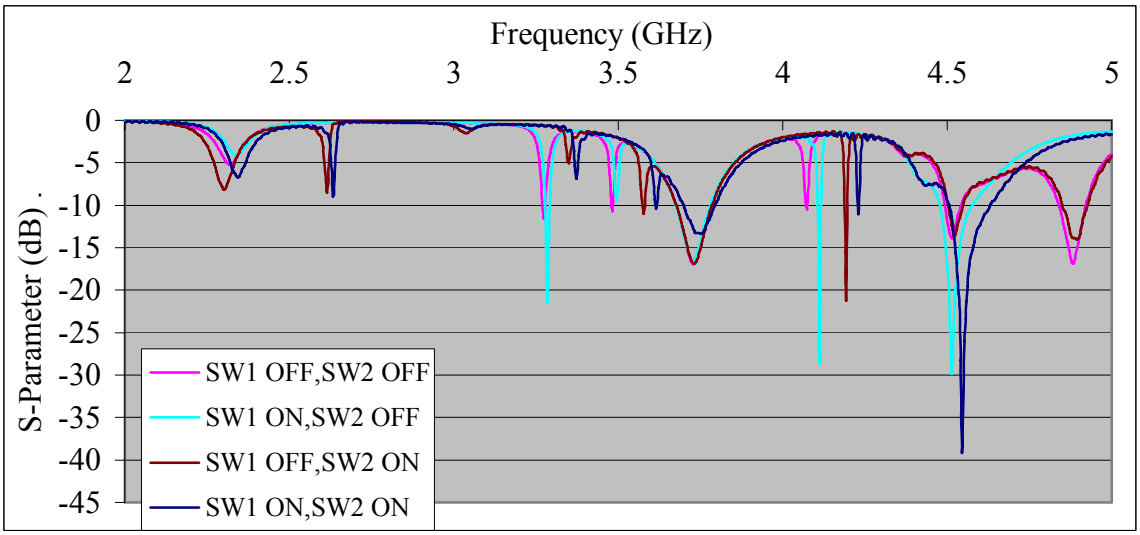

Figure 3.39: Simulated reflection coefficient curves of stacked MSA with/ without adding the top layer of ε_r = 1.44 for different statuses of SW1 and SW2.

We try now to increase the ε_r to 4.4. Simulations that have been done so far will repeated again with ε_r of the top layer equals 4.4 instead of 1.44. Also the dimensions of top patch will remains 45×55 mm and its thickness is 0.07. Again the bottom MSA will

control the reconfigurability by changing the statuses of the switches as shown in Figure 3.23.

- When SW1 and SW2 are OFF, the reflection coefficient curve is shown in Figure 3.40.

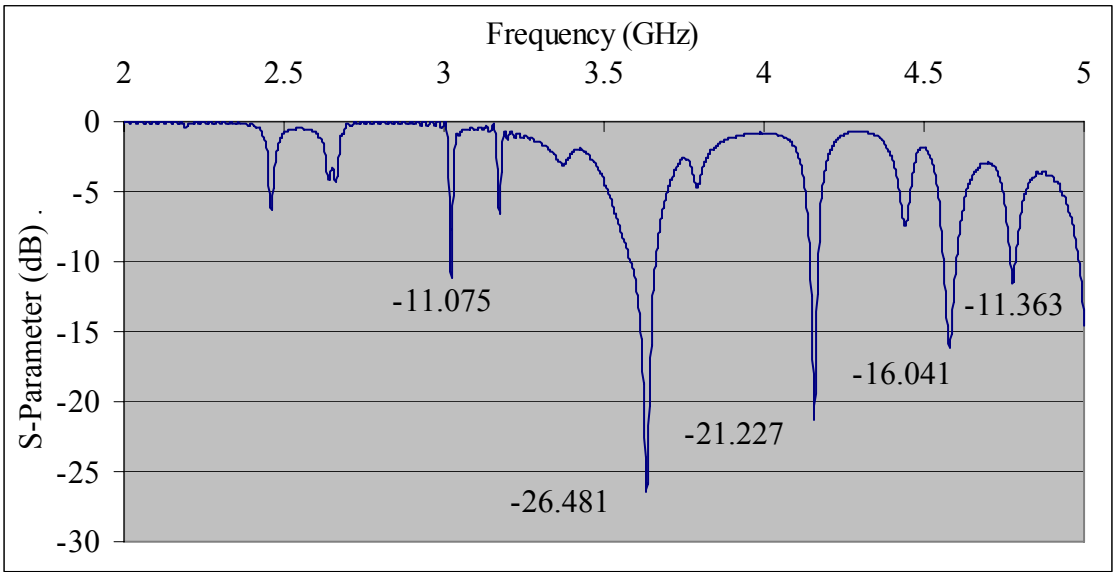

Figure 3. 40: Simulated reflection coefficient curve of stacked MSA with top layer of ε_r = 4.4 when SW1 and SW2 are OFF.

The resonance frequencies of this antenna are 3.023, 3.632, 4.157, 4.583 and 4.781 GHz, and the simulated radiation patterns for these frequencies are shown in Figure 3.41.

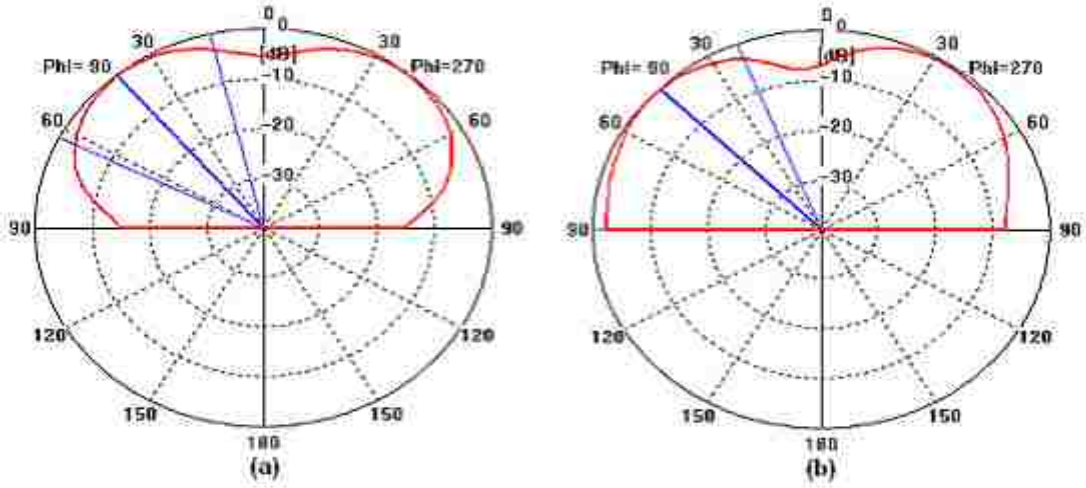

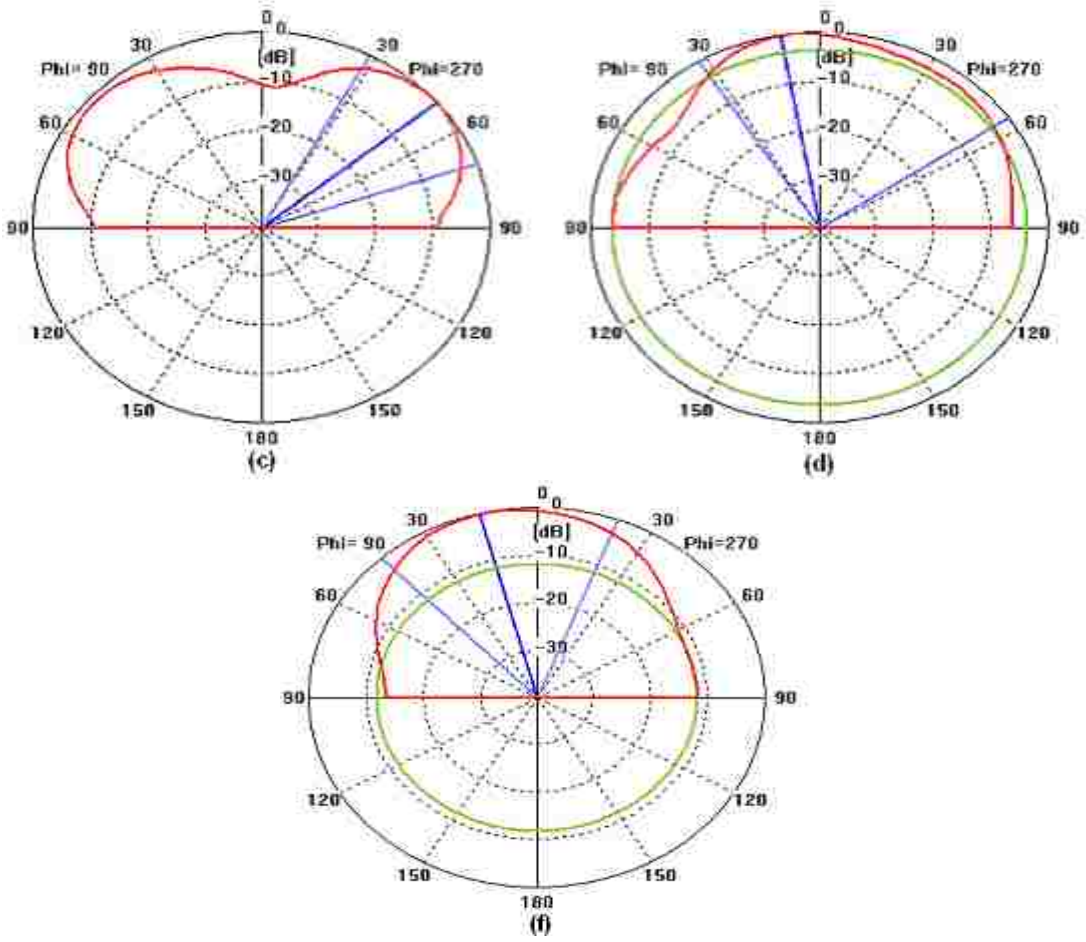

Figure 3.41: Simulated radiation patterns of stacked MSA with top layer of $\varepsilon_r = 4.4$ when SW1 and SW2 are OFF at the frequencies: (a) 3.023, (b) 3.632, (c) 4.157, (d) 4.583 and (f) 4.781 GHz.

- When SW1 is ON and SW2 is OFF, the reflection coefficient curve is shown in Figure 3.42.

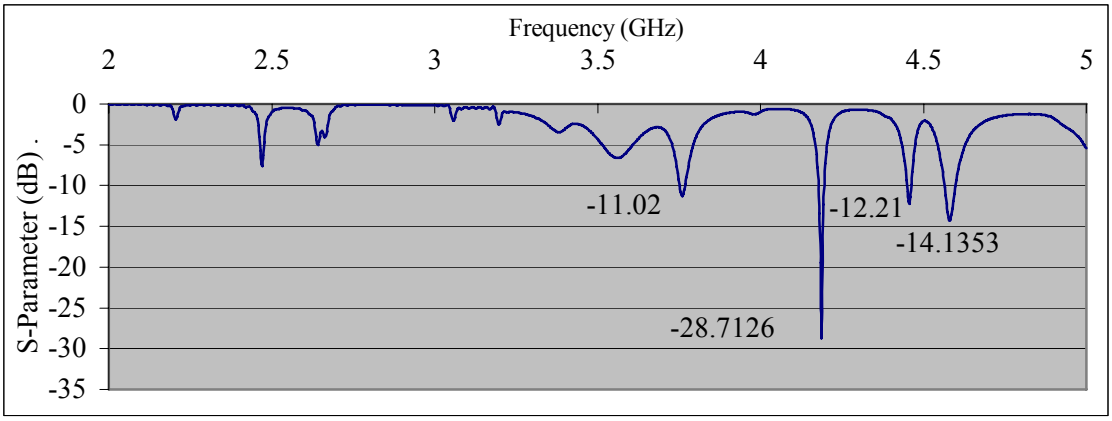

Figure 3.42: Simulated reflection coefficient curve of stacked MSA with top layer of $\varepsilon_r = 4.4$ when SW1 is ON and SW2 is OFF.

The resonant frequencies of this antenna are 3.764, 4.187, 4.457 and 4.586 GHz, and the simulated radiation patterns for these frequencies are shown in Figure 3.43.

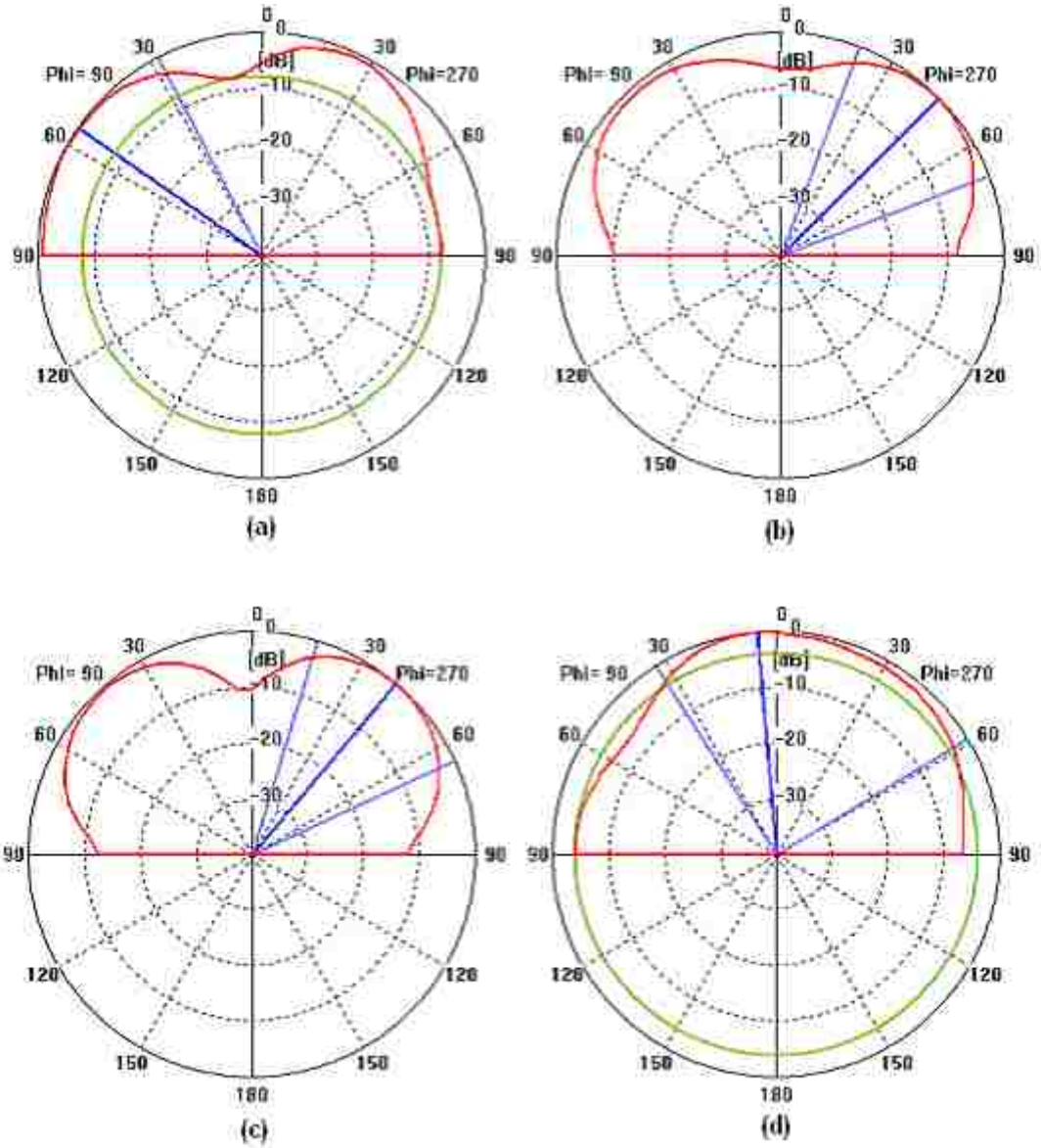

Figure 3.43: Simulated radiation pattern of stacked MSA with top layer of $\varepsilon_r = 4.4$ at the frequencies: (a) 3.764, (b) 4.187, (c) 4.457 and (d) 4.586 GHz.

- When SW1 is OFF and SW2 is ON, the reflection coefficient curve is shown in Figure 3.44.

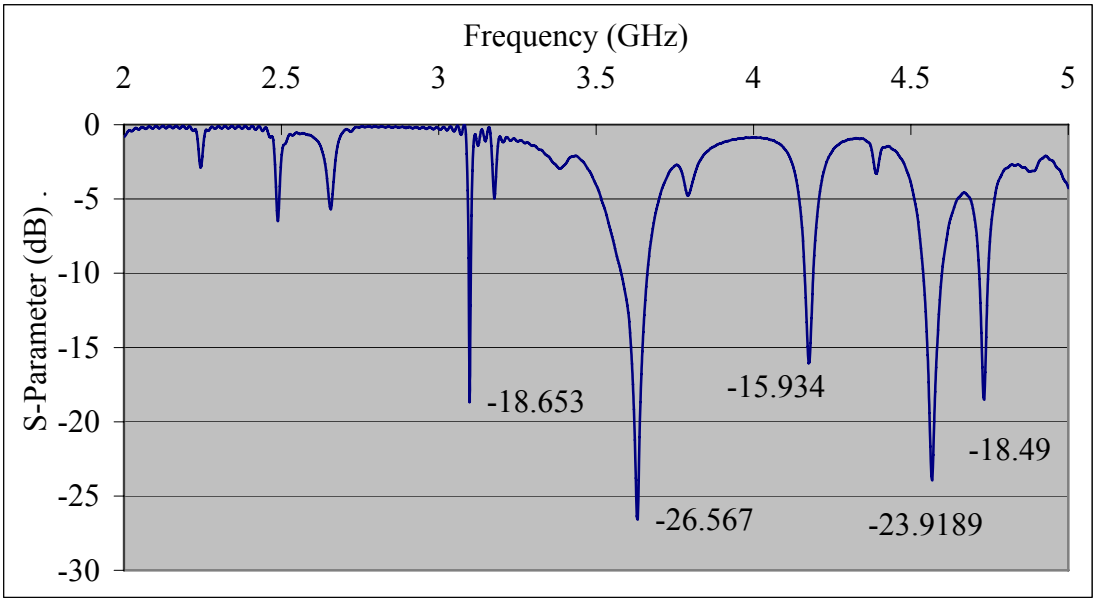

Figure 3.44: Simulated reflection coefficient curve stacked MSA with top layer of $\varepsilon_r = 4.4$ when SW1 is OFF and SW2 is ON.

The resonance frequencies of this antenna are 3.098, 3.632, 4.178, 4.568 and 4.733GHz, and the simulated radiation patterns for these frequencies are shown in Figure 3.45.

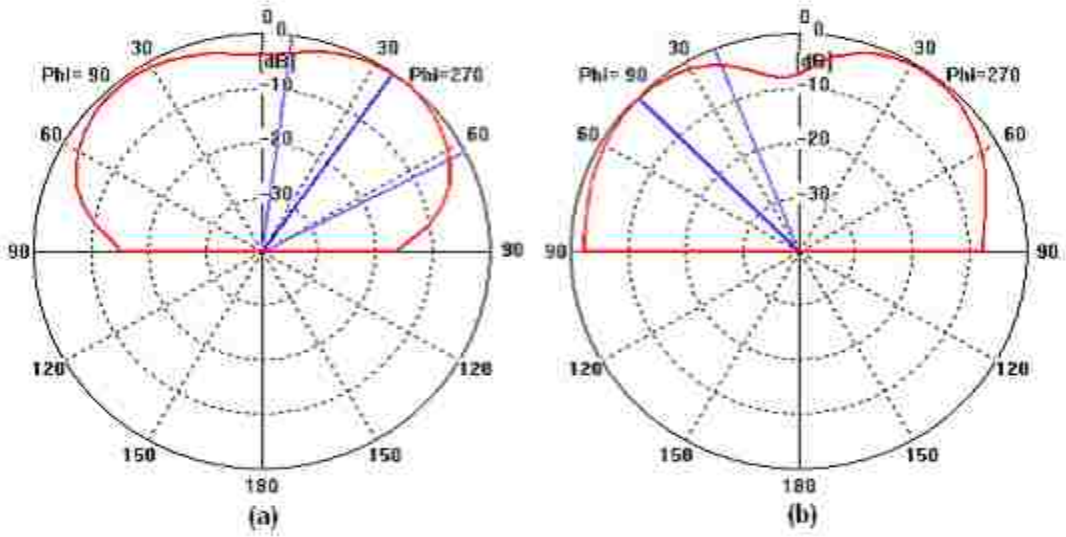

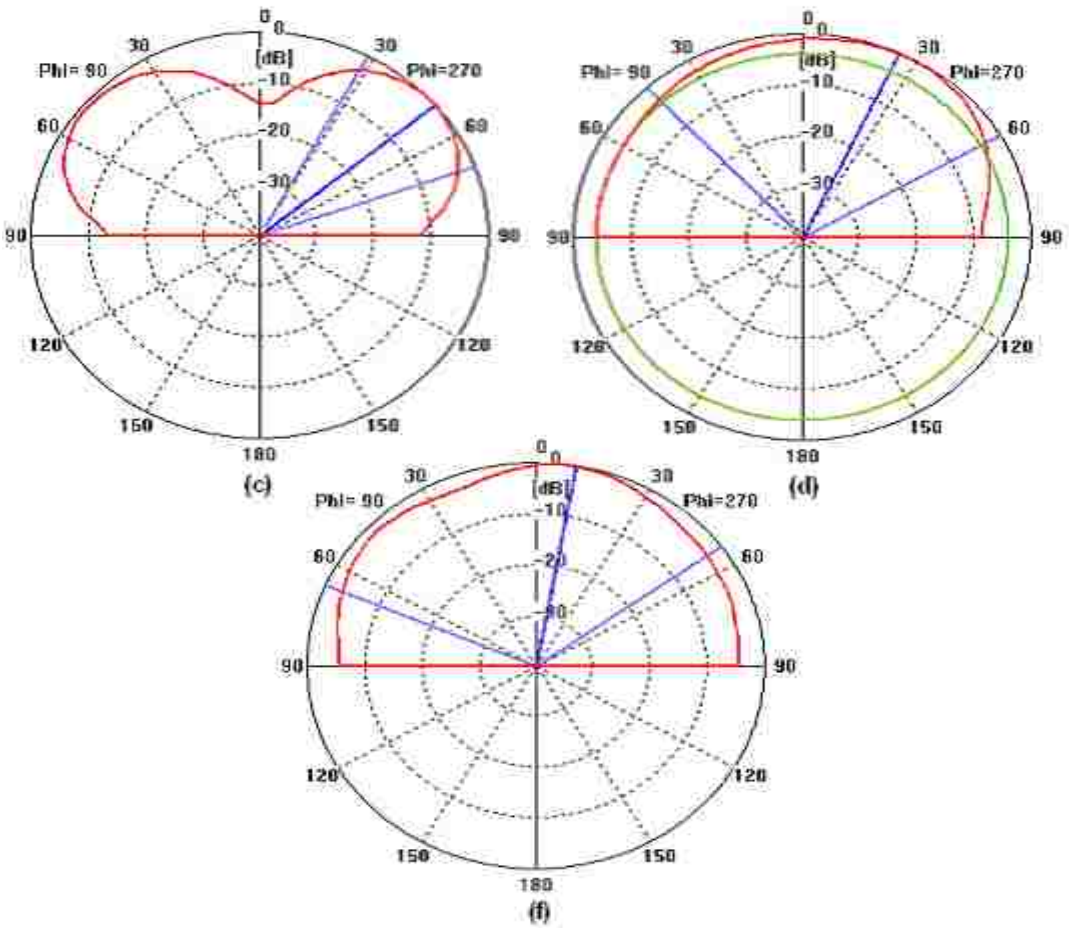

Figure 3.45: Simulated radiation patterns of stacked MSA with top layer of $\varepsilon_r = 4.4$ at the frequencies: (a) 3.098, (b) 3.632, (c) 4.178, (d) 4.568 and (f) 4.733GHz.

- When SW1 and SW2 are ON, the reflection coefficient curve is shown in Figure 3.46.

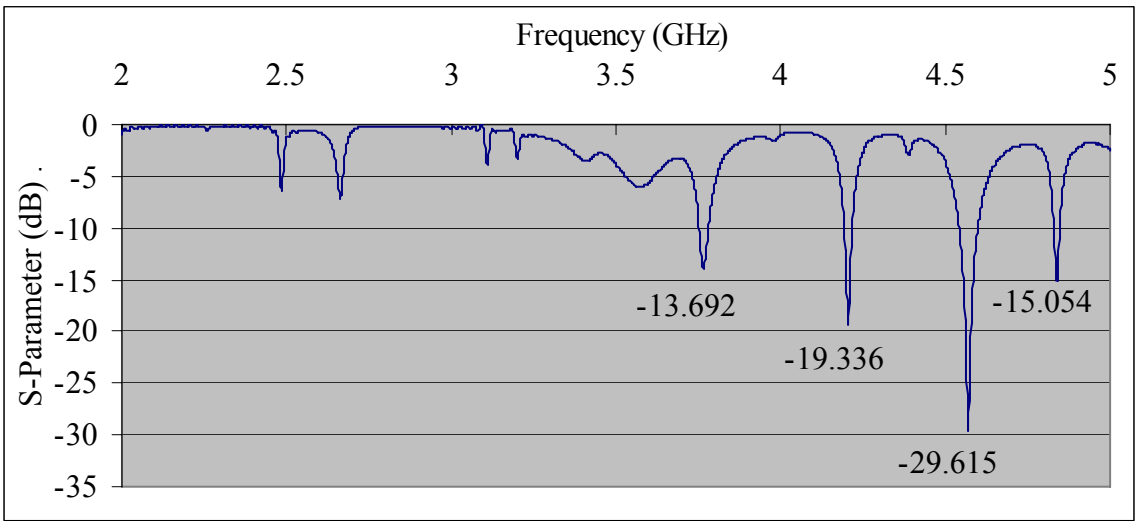

Figure 3.46: Simulated reflection coefficient curve of stacked MSA with top layer of $\varepsilon_r = 4.4$ when SW1 and SW2 are ON.

The resonance frequencies of this antenna are 3.77, 4.205, 4.571 and 4.841 GHz, and the simulated radiation patterns for these frequencies are shown in Figure 3.47.

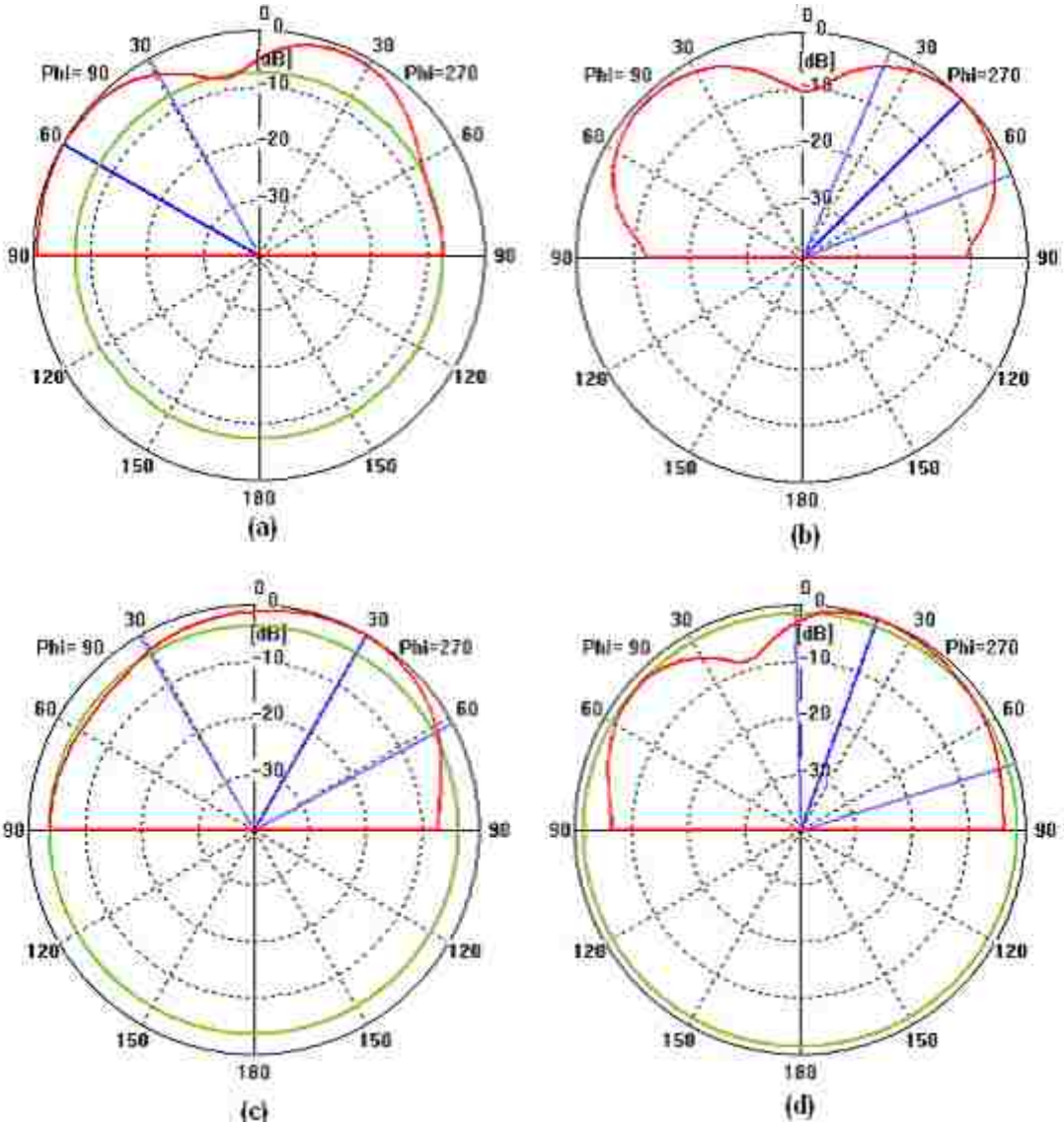

Figure 3.47: Simulated radiation patterns of stacked MSA with top layer of $\varepsilon_r = 4.4$ at the frequencies: (a) 3.77, (b) 4.205, (c) 4.571 and (d) 4.841 GHz.

A comparison between a triple-band MSA and a stacked MSA with adding top layer of ε_r equals 4.44 for different statuses of SW1 and SW2 are shown in Figures 3.48.

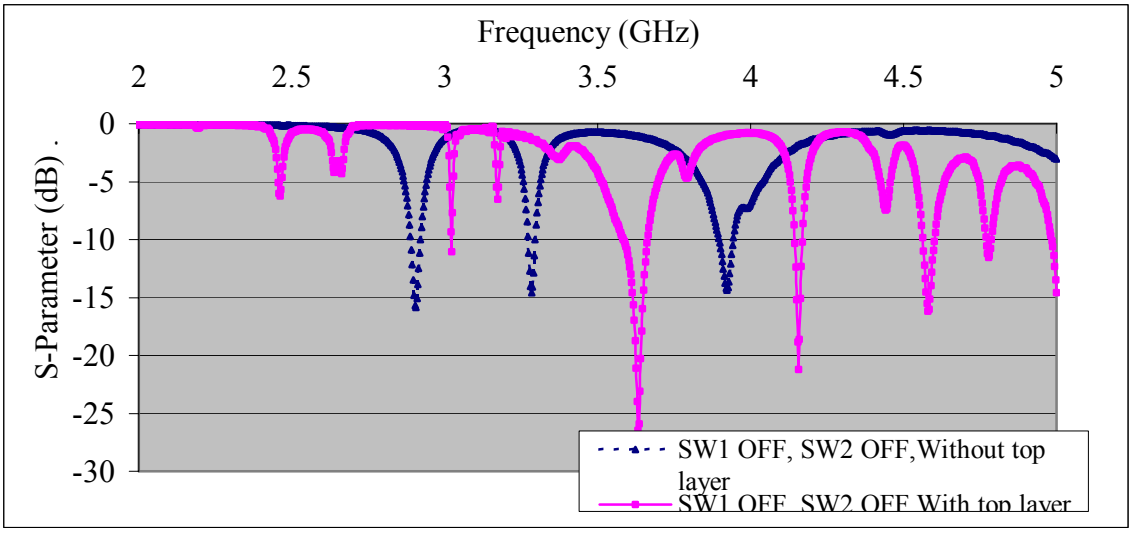
Frequency (GHz)
2
2.5
3
3.5
4
4.5
5
S-Parameter (dB) .
0
-5
-10
-15
-20
-25
-30
SW1 OFF, SW2 OFF,Without top layer
SW1 OFF, SW2 OFF With top layer

(a)

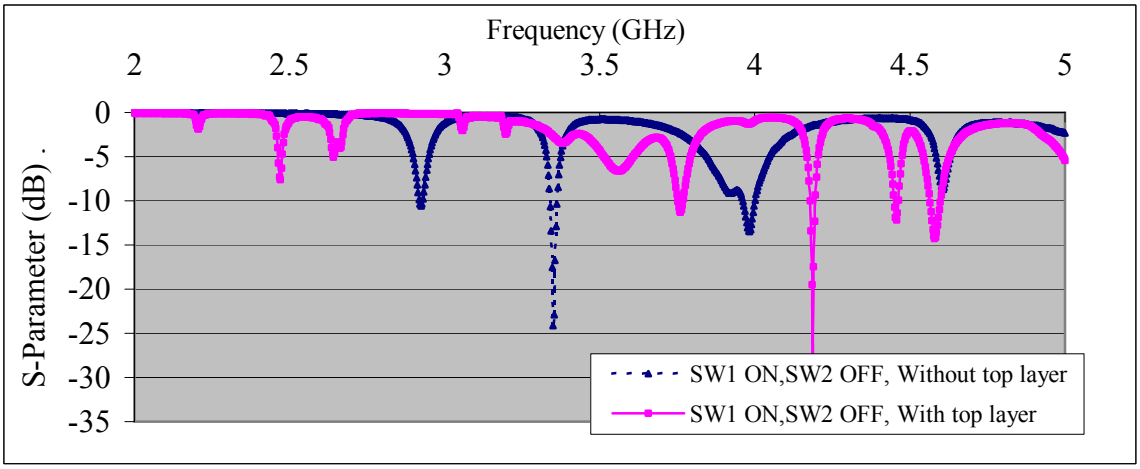
Frequency (GHz)
2
2.5
3
3.5
4
4.5
5
S-Parameter (dB) .
0
-5
-10
-15
-20
-25
-30
-35
SW1 ON,SW2 OFF, Without top layer
SW1 ON,SW2 OFF, With top layer

(b)

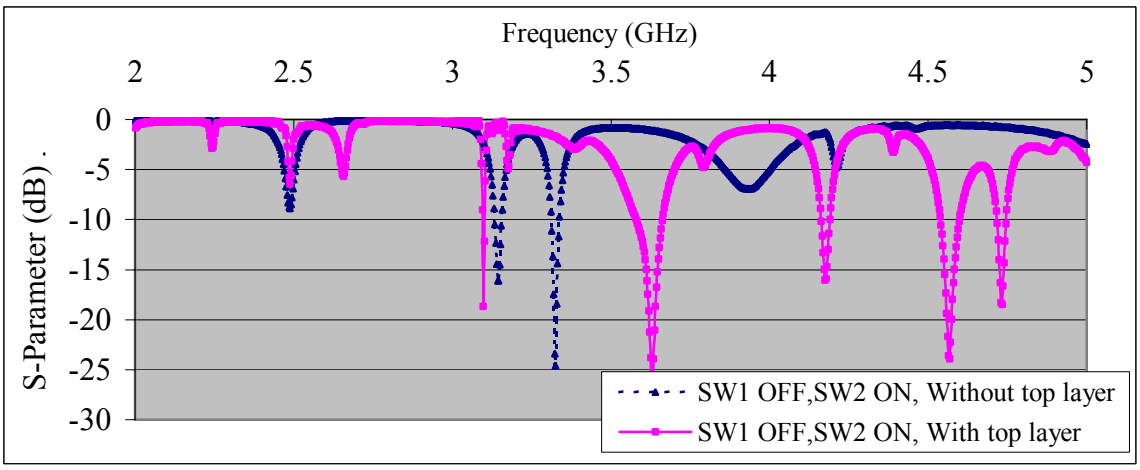
Frequency (GHz)
2
2.5
3
3.5
4
4.5
5
S-Parameter (dB) .
0
-5
-10
-15
-20
-25
-30
SW1 OFF,SW2 ON, Without top layer
SW1 OFF,SW2 ON, With top layer

(c)

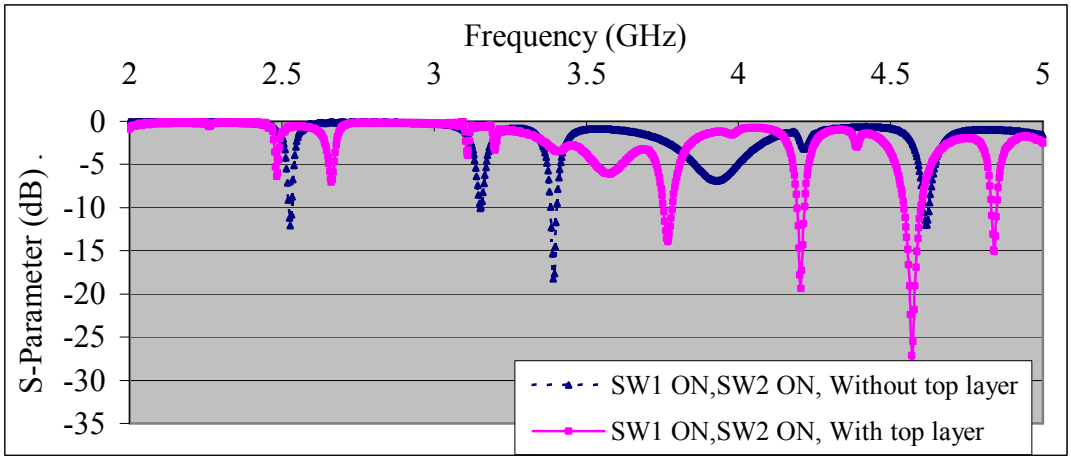

(d)

Figure 3.48: Simulated reflection coefficient curve of stacked MSA with / without adding top layer of ε_r = 4.4 when (a) SW1 and SW2 are OFF, (b) SW1 ON, SW2 OFF, (c) SW1 OFF, SW2 ON, (d) SW1 and SW2 are ON.

A comparison between different reflection coefficient curves for different situations of SW1 and SW2 are shown in Figure 3.49.

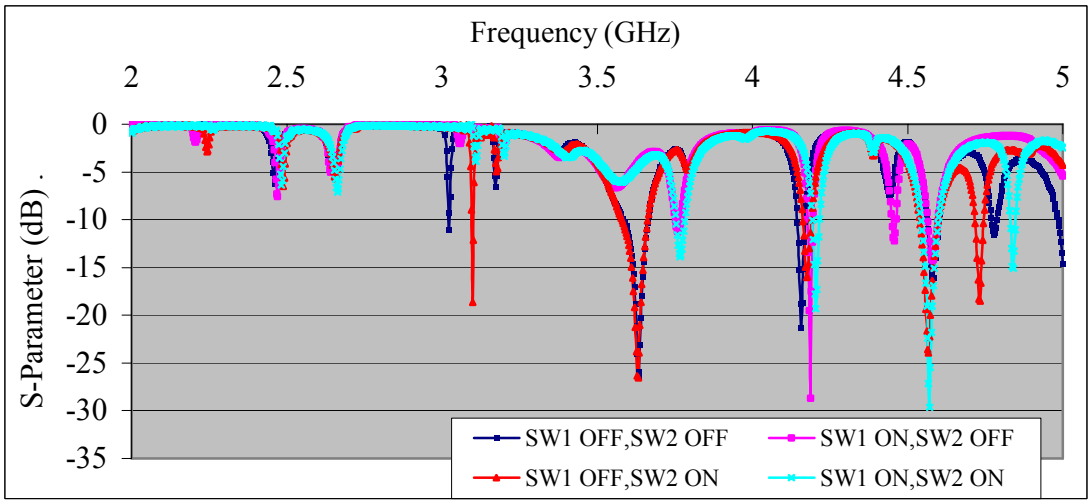

Figure 3.49: Simulated reflection coefficient curves of stacked MSA with top layer of ε_r = 4.4 for different statuses of SW1 and SW2.

3.5 Configuration of Stacked MSAs with Inverted Patches

When the top and bottom patches of Figure 3.27 are switched, where the bottom patch with its slots becomes the top patch and the top patch becomes the bottom one of the new antenna as shown in Figure 3.50. ε_r is 2.2 for the bottom layer and 1.44 for the top layer.

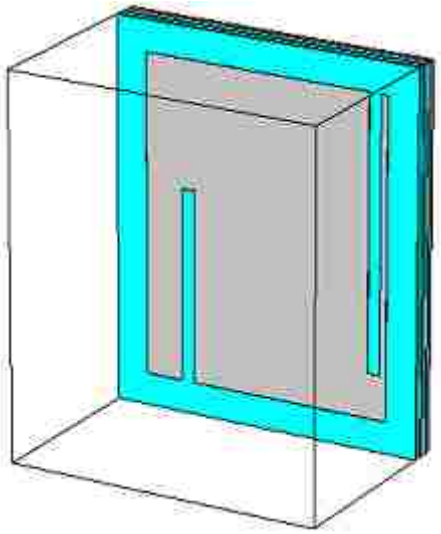

Figure 3.50: Simulated stacked MSA with top layer of ε_r = 1.44.

To obtain reconfigurability in stacked MSA with inverted patches, switches are added to the slots in the same places as shown before in the last section, where SW1 is added to slot # 1 and SW2 is added to slot # 2. The results of all statuses of the switches are as follows;

- When SW1 and SW2 are OFF, the reflection coefficient curve is shown in Figure 3.51.

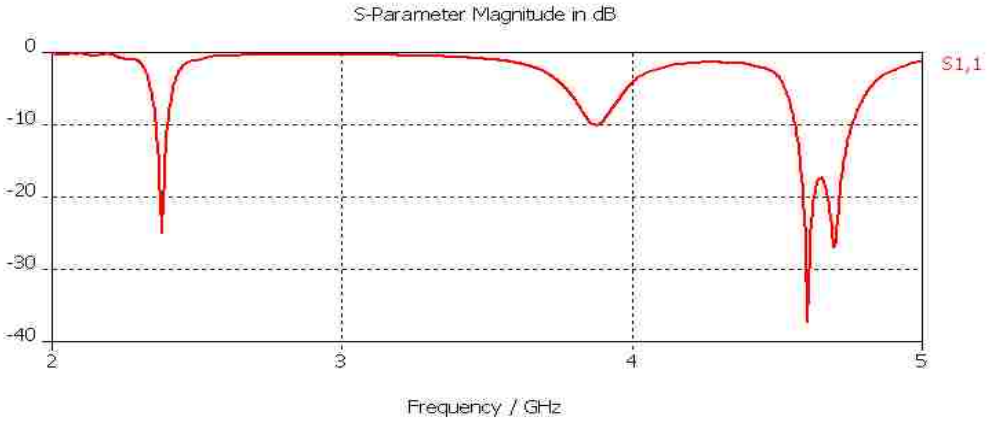

Figure 3.51: Simulated reflection coefficient curve of stacked MSA with top layer of ε_r = 1.44 when SW1 and SW2 are OFF.

- When SW1 is ON and SW2 is OFF, the reflection coefficient curve is shown in Figure 3.52

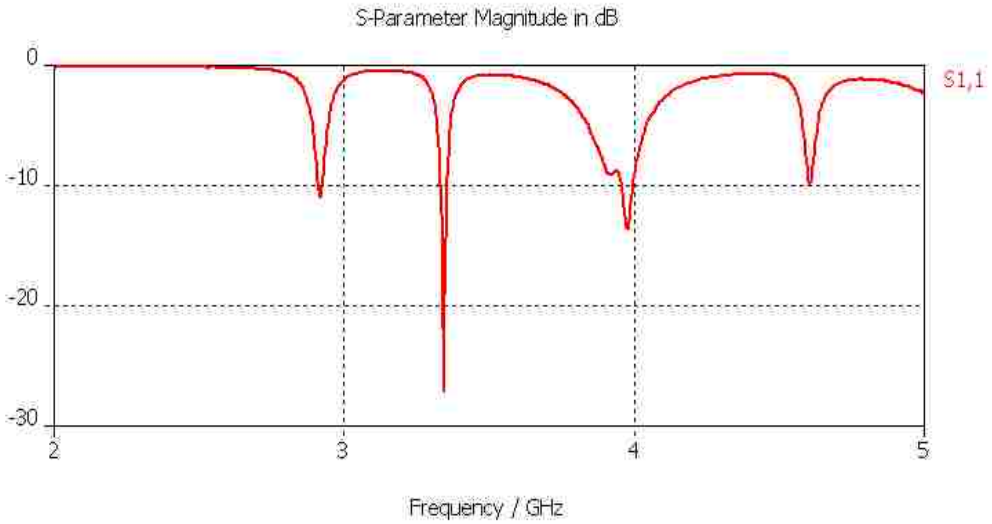

Figure 3.52: Simulated reflection coefficient curve of stacked MSA with top layer of ε_r = 1.44 when SW1 is ON and SW2 is OFF.

- When SW1 is OFF and SW2 is ON, the reflection coefficient curve is shown in Figure 3.53

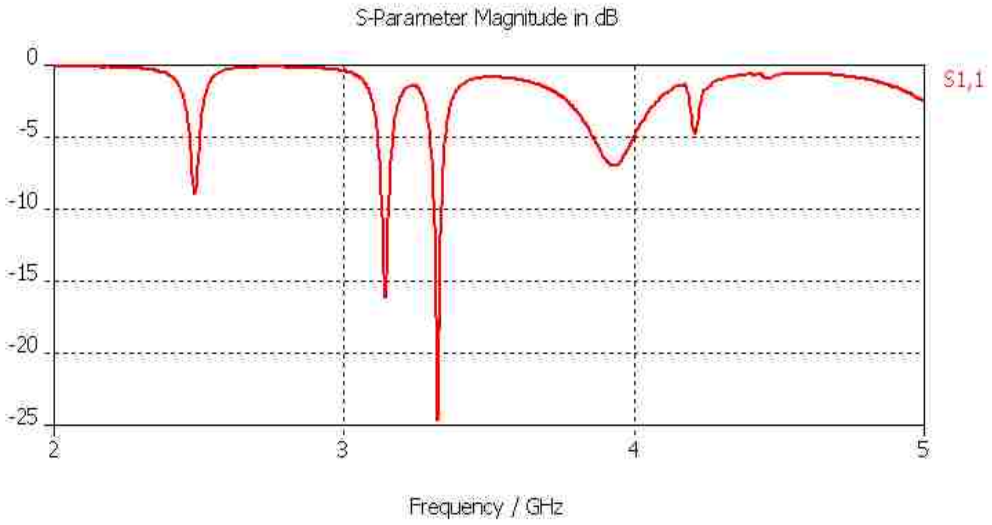

Figure 3.53: Simulated reflection coefficient curve of stacked MSA with top layer of ε_r = 1.44 when SW1 is OFF and SW2 is ON.

- When SW1 and SW2 are ON we get the reflection coefficient curve shown in Figure 3.54

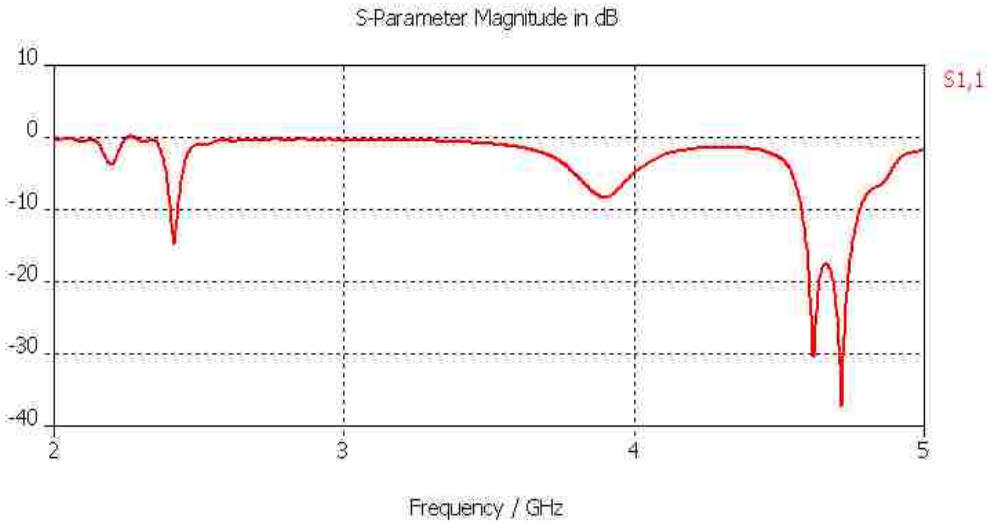

Figure 3.54: Simulated reflection coefficient curve of stacked MSA with top layer of ε_r = 1.44 when SW1 and SW2 are ON.

To increase the number of resonance frequencies we should reduce the dimensions of the bottom patch by scaling it with a certain value. By trying many values, the best results are achieved when 0.7 scales the bottom patch. The new dimensions of the bottom patch are as follows;

W=35 mm, *L*= 28 mm, and the coordinate of the feeding point is (7.75, 17.5) mm, where the origin of this coordinate is the lower left corner of the bottom patch as shown in Figure 3.55.

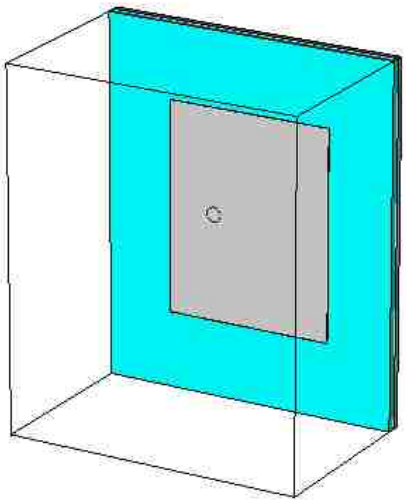

Figure 3.55: Conventional bottom MSA with patch scaled by 0.7.

- When SW1 and SW2 are OFF we get the reflection coefficient curve shown in Figure 3.56.

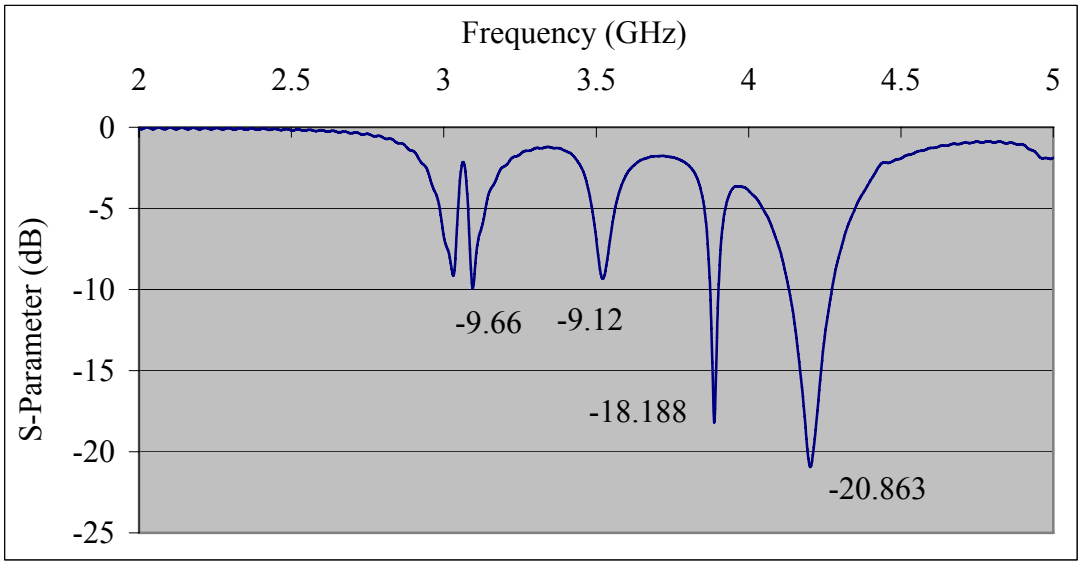

Figure 3.56: Simulated reflection coefficient curve of stacked MSA with top layer of ε_r = 1.44 and with bottom patch scaled by 0.7 when SW1 and SW2 are OFF.

The resonance frequencies of the antenna are 3.098, 3.527, 3.887 and 4.205 GHz, and the simulated radiation patterns for these frequencies are shown in Figure 3.57.

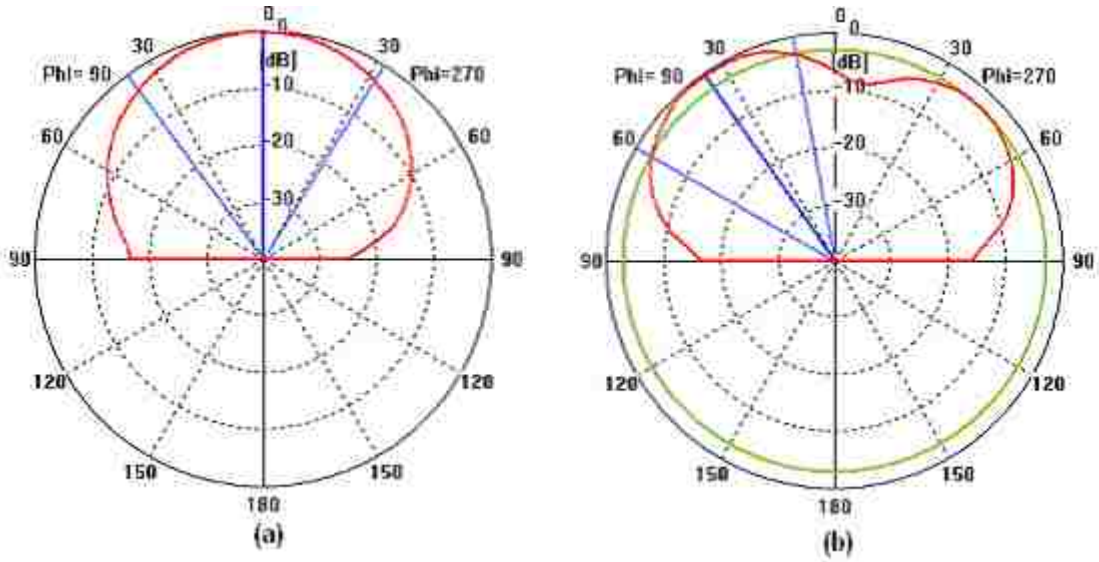

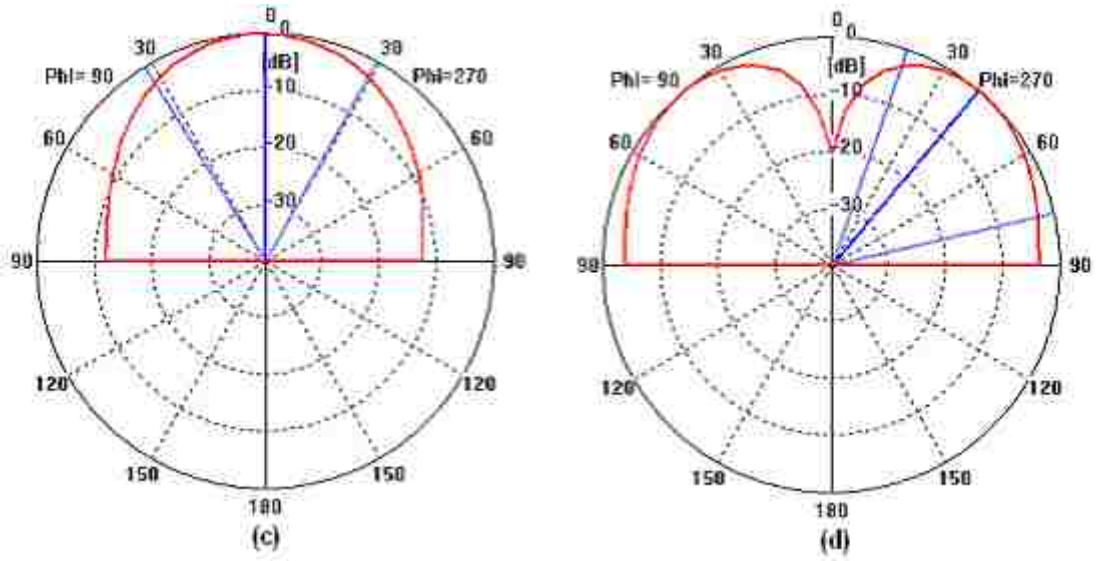

Figure 3.57: Simulated radiation patterns of stacked MSA with top layer of ε_r = 1.44 and with bottom patch scaled by 0.7 when SW1 is OFF and SW2 is OFF at the frequencies: (a) 3.098, (b) 3.527, (c) 3.887 and (d) 4.205 GHz.

- When SW1 is ON and SW2 is OFF we get the reflection coefficient curve shown in Figure 3.58.

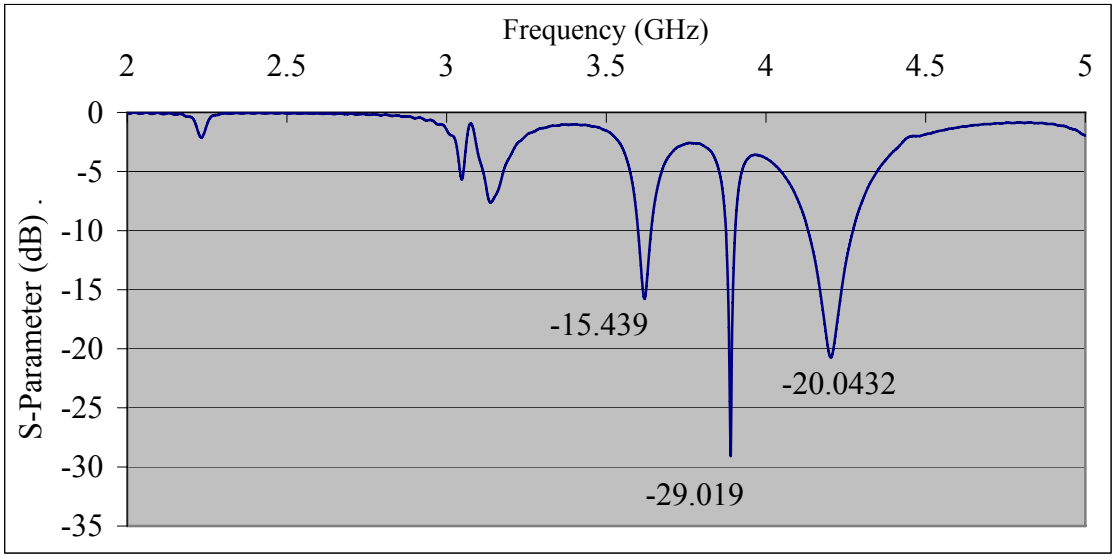

Figure 3.58: Simulated reflection coefficient curve of stacked MSA with top layer of ε_r = 1.44 and with bottom patch scaled by 0.7 when SW1 is ON and SW2 is OFF.

The resonance frequencies of the antenna are 3.623, 3.89 and 4.211 GHz, and the simulated radiation patterns for these frequencies are shown in Figure 3.59.

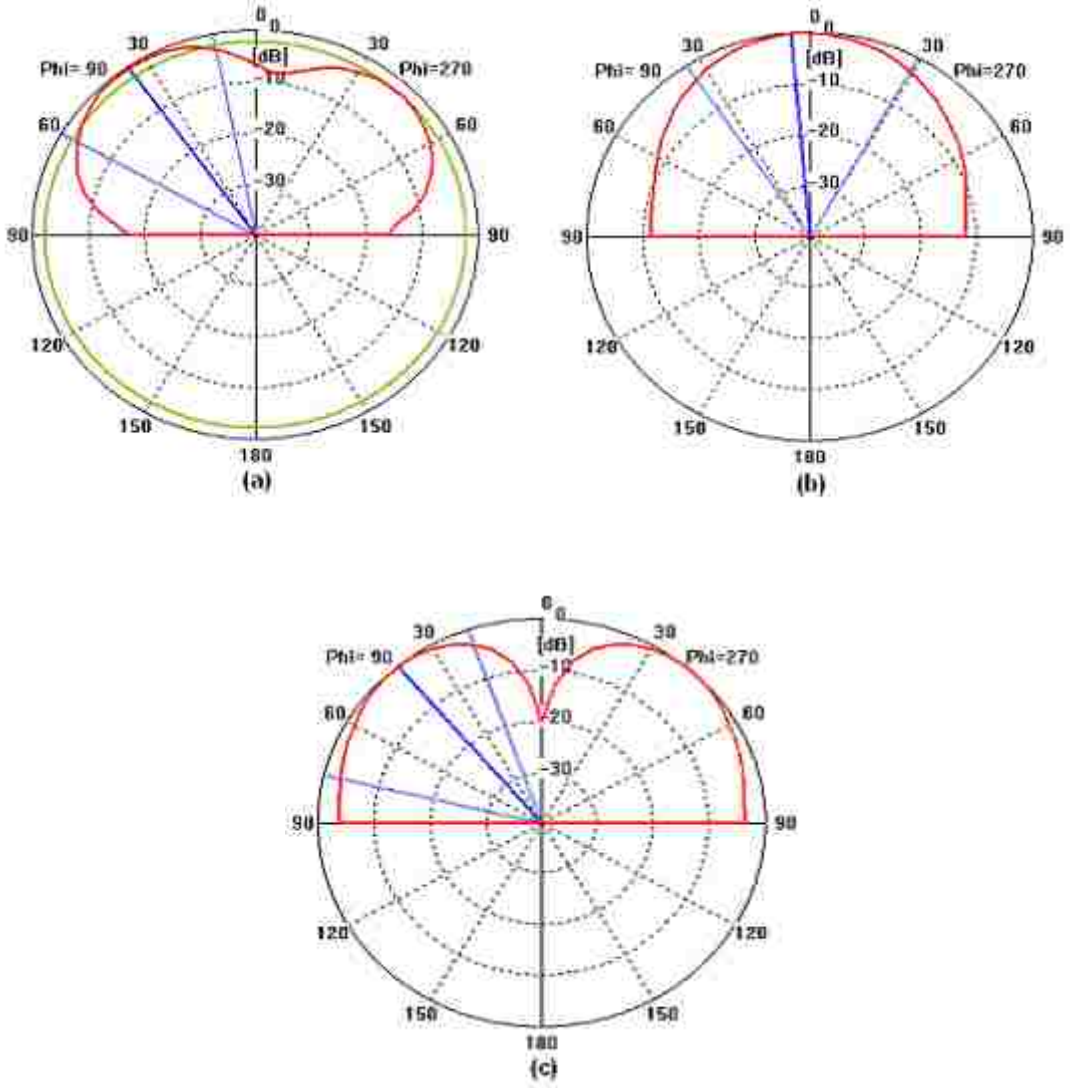

Figure 3.59: Simulated radiation patterns of stacked MSA with top layer of $\varepsilon_r = 1.44$ and with bottom patch scaled by 0.7 when SW1 is ON and SW2 is OFF at the frequencies: (a) 3.623, (b) 3.89 and (c) 4.211 GHz.

- When SW1 is OFF and SW2 is ON we get the reflection coefficient curve shown in Figure 3.60.

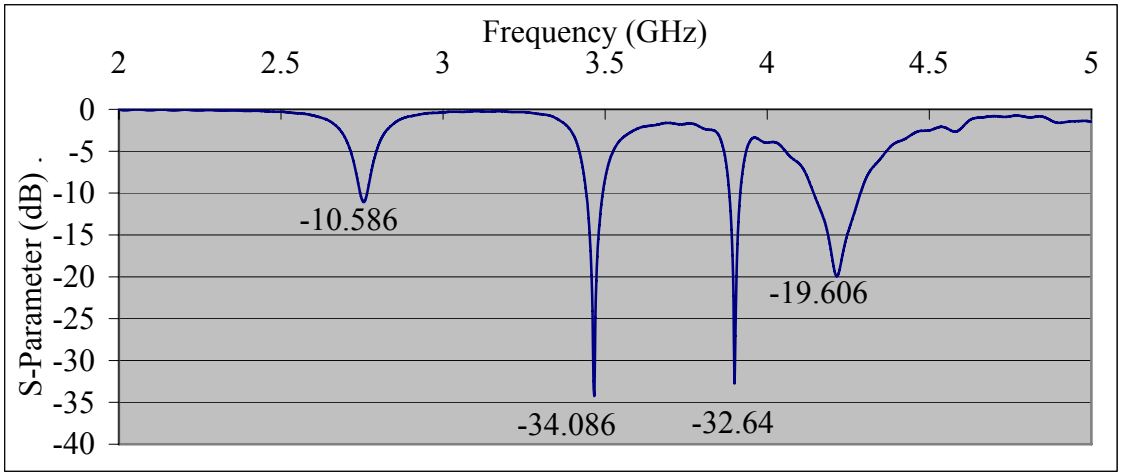

Figure 3.60: Simulated reflection coefficient curve of stacked MSA with top layer of ε_r = 1.44 and with bottom patch scaled by 0.7 when SW1 is OFF and SW2 is ON.

The resonance frequencies of the antenna are 2.762, 3.467, 3.899 and 4.22 GHz, and the simulated radiation patterns for these frequencies are shown in Figure 3.61.

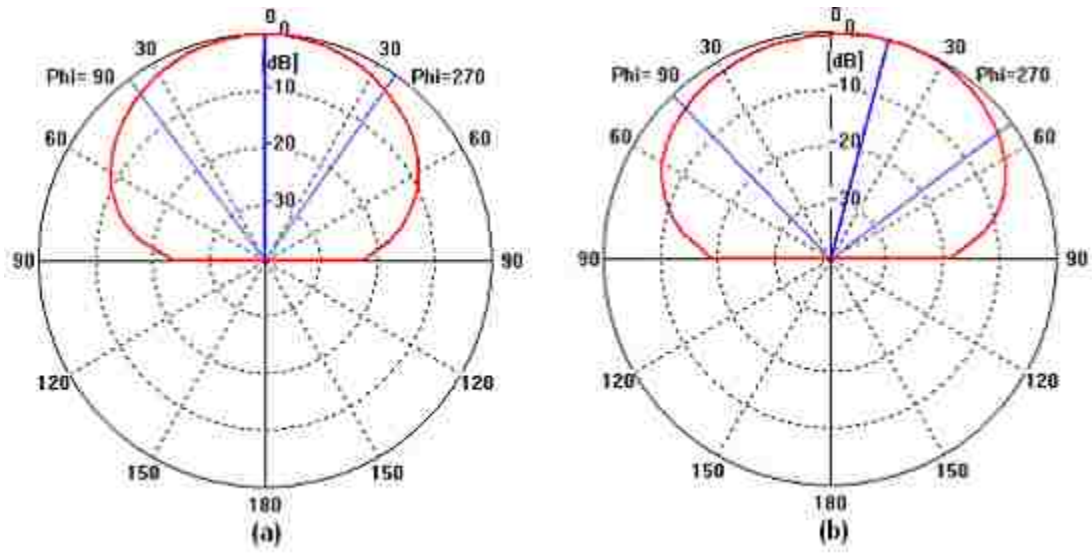

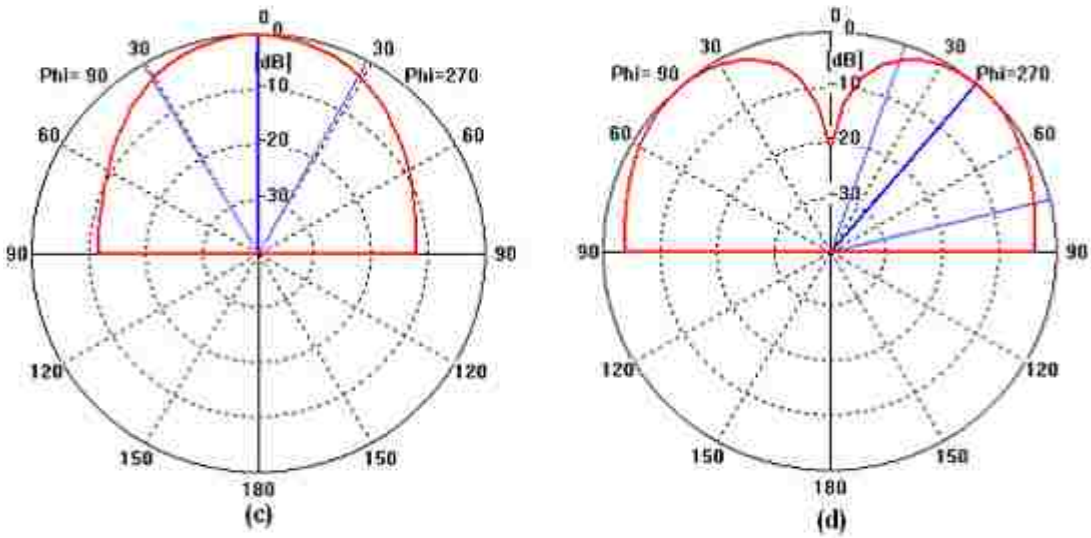

Figure 3.61: Simulated radiation patterns of stacked MSA with top layer of ε_r = 1.44 and with bottom patch scaled by 0.7 when SW1 is OFF and SW2 is ON at the frequencies: (a) 2.762, (b) 3.467, (c) 3.899 and (d) 4.22 GHz.

- When SW1 and SW2 are ON we get the reflection coefficient curve shown in Figure 3.62.

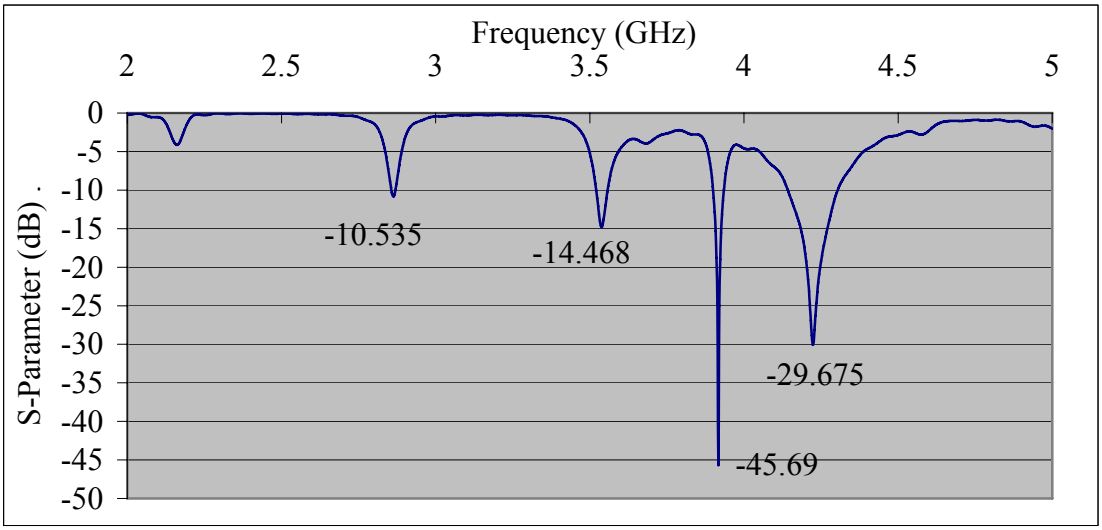

Figure 3.62: Simulated reflection coefficient curve of stacked MSA with top layer of ε_r = 1.44 and with bottom patch scaled by 0.7 when SW1 and SW2 are ON.

The resonance frequencies of the antenna are 2.867, 3.542, 3.917 and 4.226 GHz, and the simulated radiation patterns for these frequencies are shown in Figure 3.63.

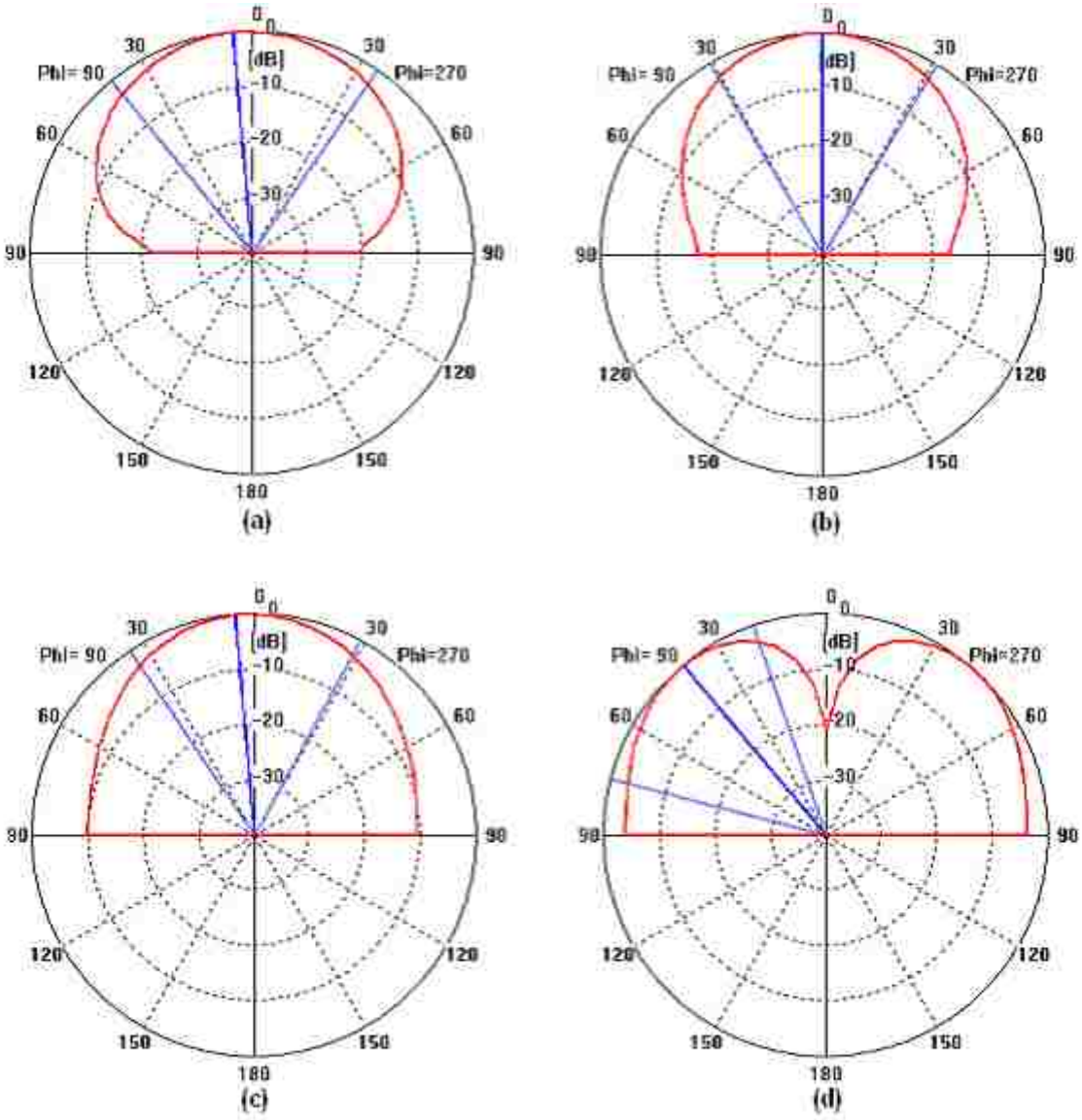

Figure 3.63: Simulated radiation patterns of stacked MSA with top layer of $\varepsilon_r = 1.44$ and with bottom patch scaled by 0.7 when SW1 and SW2 are ON at the frequencies: (a) 2.867, (b) 3.542, (c) 3.917 and (d) 4.226 GHz.

The reflection coefficient curves for different statuses of SW1 and SW2 of the stacked MSA are shown in Figure 3.64.

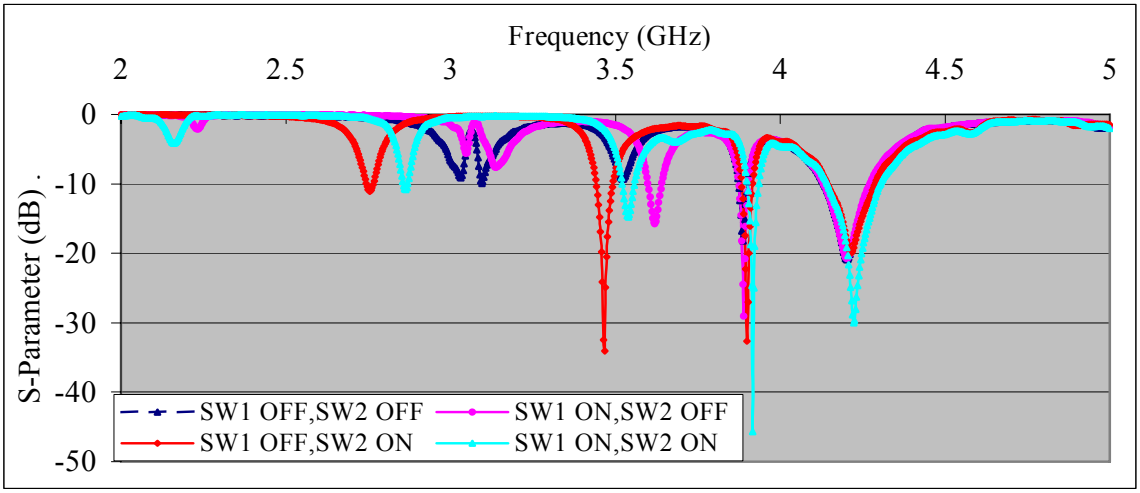

Figure 3.64: Simulated reflection coefficient curves of stacked MSA with top layer of $\varepsilon_r = 1.44$ and with bottom patch scaled by 0.7 for different statuses of SW1 and SW2.

Now ε_r will be changed to 4.4 instead of 1.44 where the dimensions of top patch will remains 40×50 mm and its thickness is 0.07 mm, and the bottom patch is still scaled by the factor 0.7.

Figure 3.65 shows a comparison between the reflection coefficient curves for original MSA, original MSA scaled by factor of 0.7 and original MSA with adding only a top layer of 1.588 mm thickness and $\varepsilon_r = 4.4$ above the scaled bottom patch, where this will move resonance frequencies from the original place.

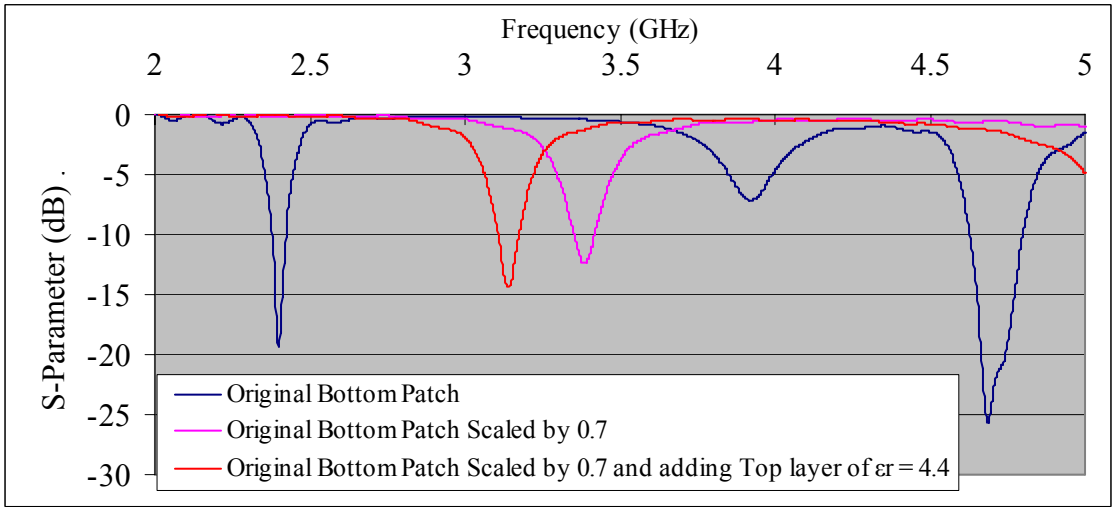

Figure 3.65: Simulated reflection coefficient curves for original MSA, original MSA scaled by factor of 0.7 and original MSA with adding a top layer of $\varepsilon_r = 4.4$.

After adding the top patch, which contains two slots as shown in Figure 3.64, and after adding the switches (SW1 and SW2), different reflection coefficient curves are achieved for different statuses of the switches as follows;

- When SW1 and SW2 are OFF, the reflection coefficient curve is shown in Figure 3.66.

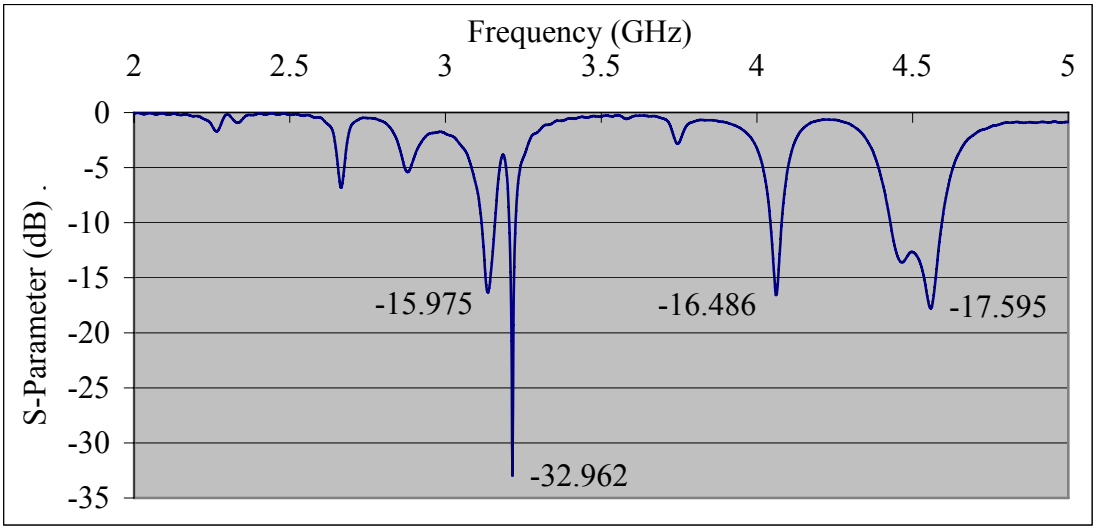

Figure 3. 66: Simulated reflection coefficient curve of stacked MSA with top layer of ε_r = 4.4 and with bottom patch scaled by 0.7 when SW1 and SW2 are OFF.

The resonance frequencies of this antenna are 3.14, 3.215, 4.064 and 4.565 GHz, and the simulated radiation patterns for these frequencies are shown in Figure 3.67.

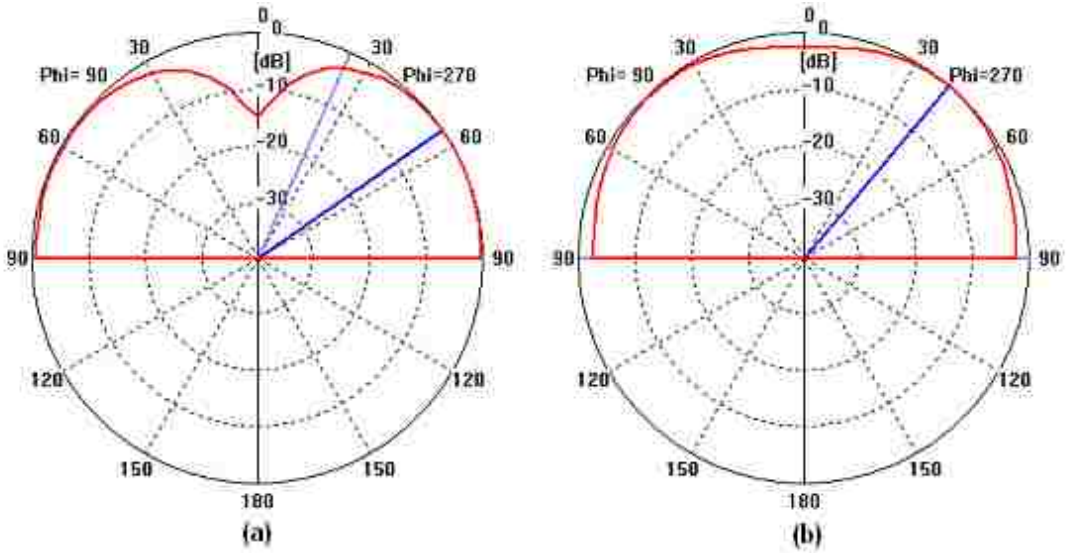

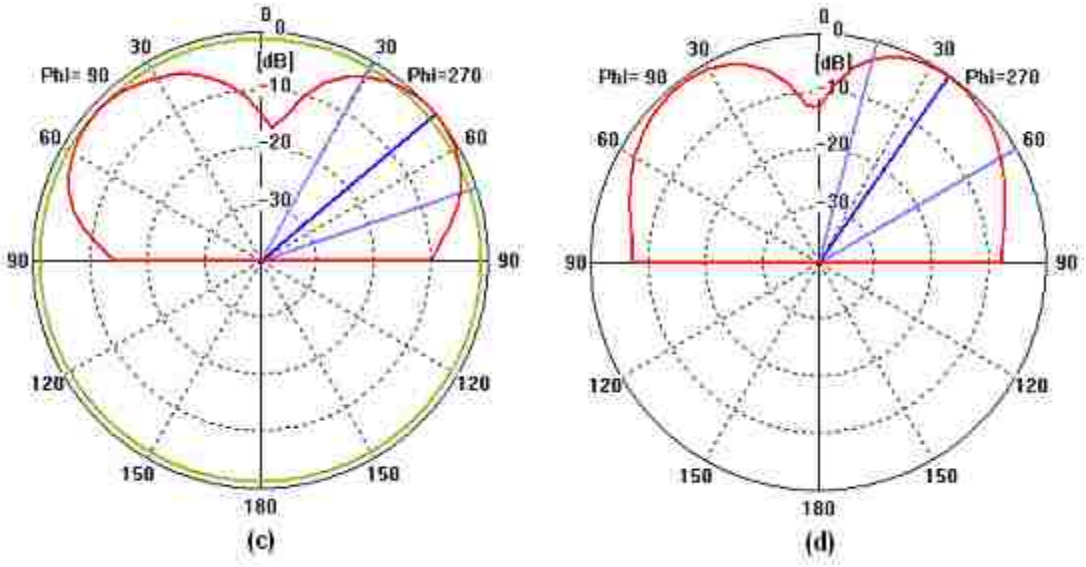

Figure 3.67: Simulated radiation patterns of stacked MSA with top layer of ε_r = 4.4 and with bottom patch scaled by 0.7 when SW1 is OFF and SW2 is OFF at the frequencies: (a) 3.14, (b) 3.215, (c) 4.064 and (d) 4.565 GHz.

- When SW1 is ON and SW2 is OFF, the reflection coefficient curve is shown in Figure 3.68.

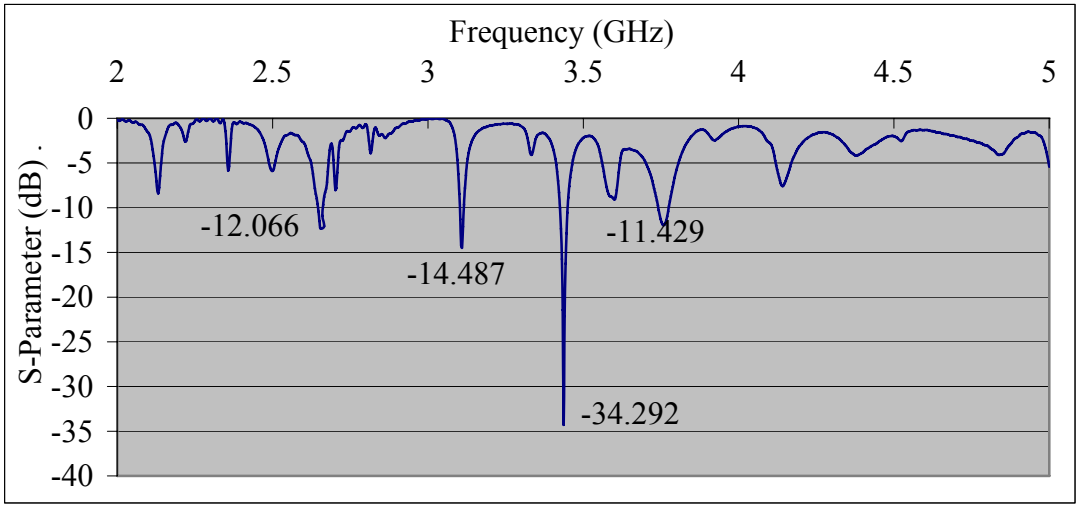

Figure 3.68: Simulated reflection coefficient curve of stacked MSA with top layer of ε_r = 4.4 and with bottom patch scaled by 0.7 when SW1 is ON and SW2 is OFF.

The resonance frequencies of this antenna are 2.657, 3.11, 3.437 and 3.767 GHz and the simulated radiation patterns for these frequencies are shown in Figure 3.69.

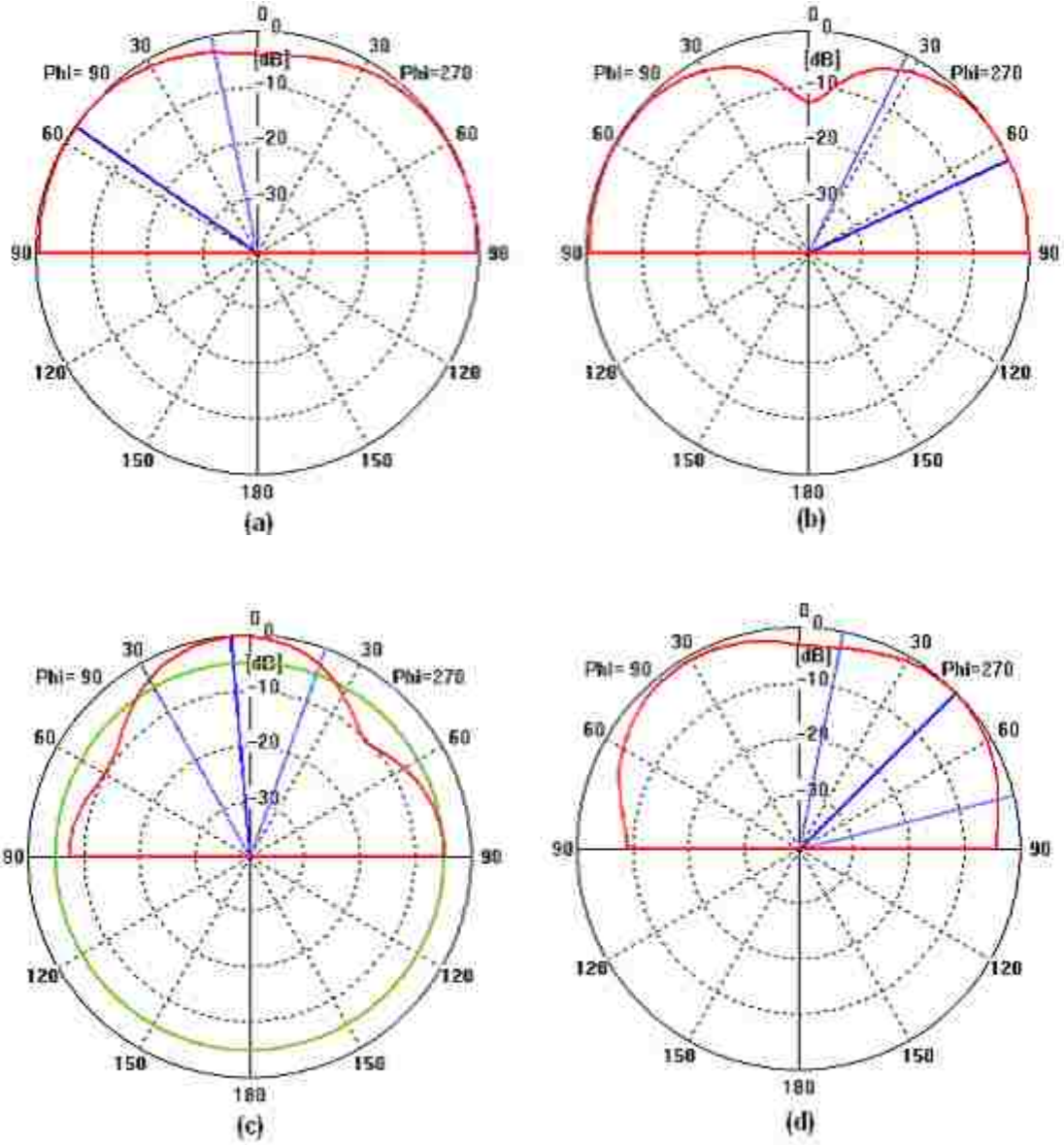

Figure 3.69: Simulated radiation patterns of stacked MSA with top layer of $\varepsilon_r = 4.4$ and with bottom patch scaled by 0.7 when SW1 is ON and SW2 is OFF at the frequencies: (a) 2.657, (b) 3.11, (c) 3.437 and (d) 3.767 GHz.

- When SW1 is OFF and SW2 is ON, the reflection coefficient curve is shown in Figure 3.70.

The resonance frequencies of this antenna are 2.057, 2.679, 3.149, 4.079 and 4.49 GHz and the simulated radiation patterns for these frequencies are shown in Figure 3.71.

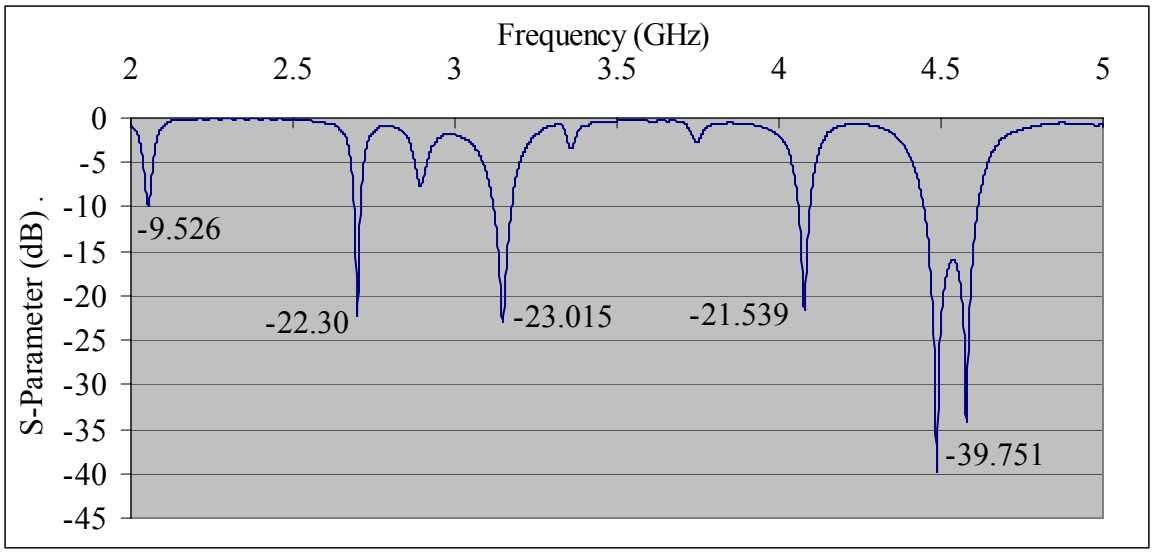

Figure 3.70: Simulated reflection coefficient curve of stacked MSA with top layer of $\varepsilon_r = 4.4$ and with bottom patch scaled by 0.7 when SW1 is OFF and SW2 is ON.

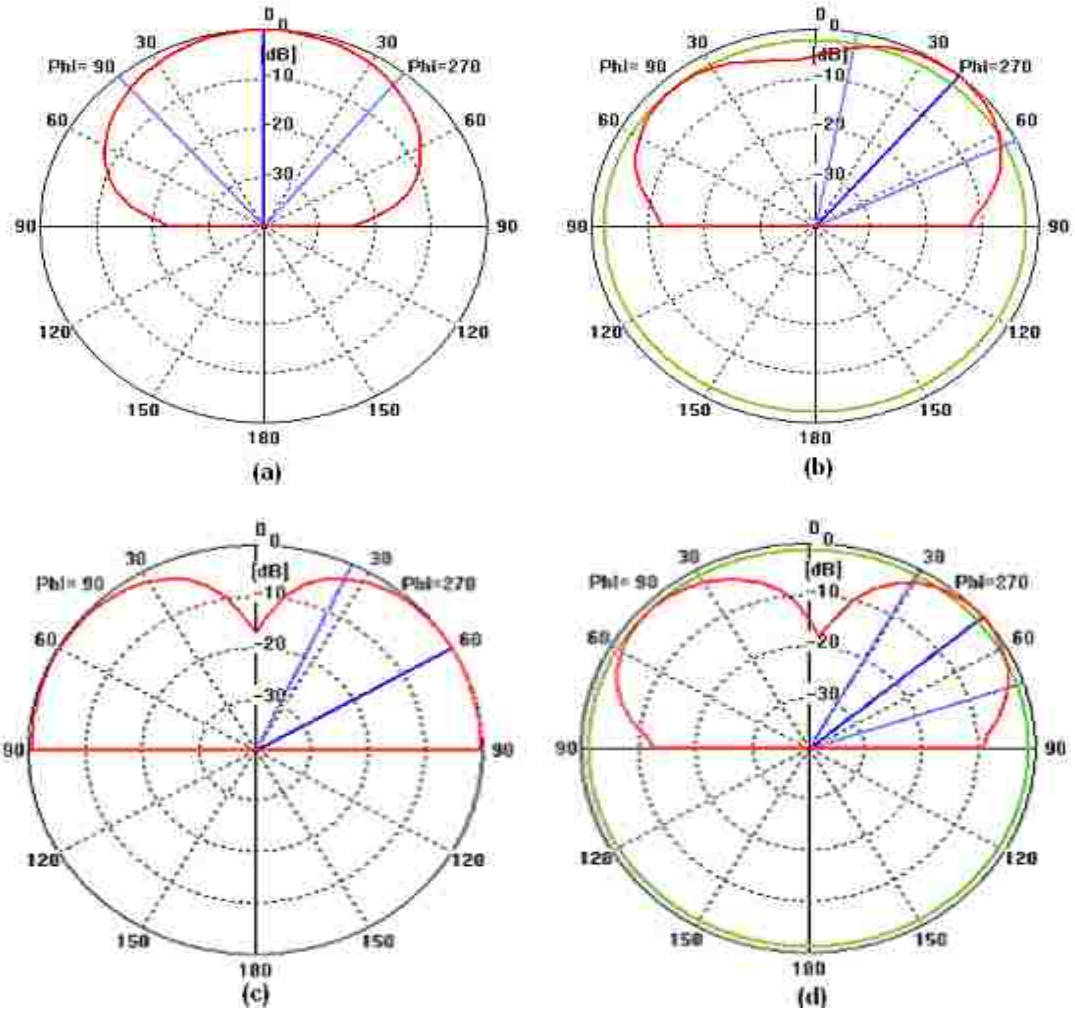

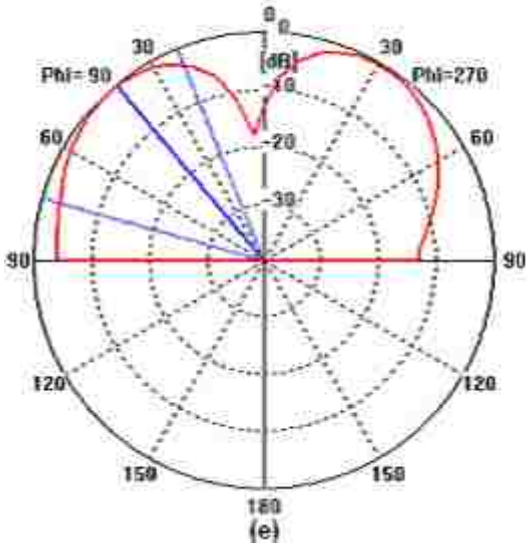

Figure 3.71: Simulated radiation patterns of stacked MSA with top layer of ε_r = 4.4 and with bottom patch scaled by 0.7 when SW1 is OFF and SW2 is ON at the frequencies: (a) 2.057, (b) 2.679, (c) 3.149, (d) 4.079 and (e) 4.49 GHz.

- When SW1 and SW2 are ON, the reflection coefficient curve is shown in Figure 3.72.

The resonance frequencies of this antenna are 2.12, 2.768 and 3.164 GHz and the simulated radiation patterns for these frequencies are shown in Figure 3.73.

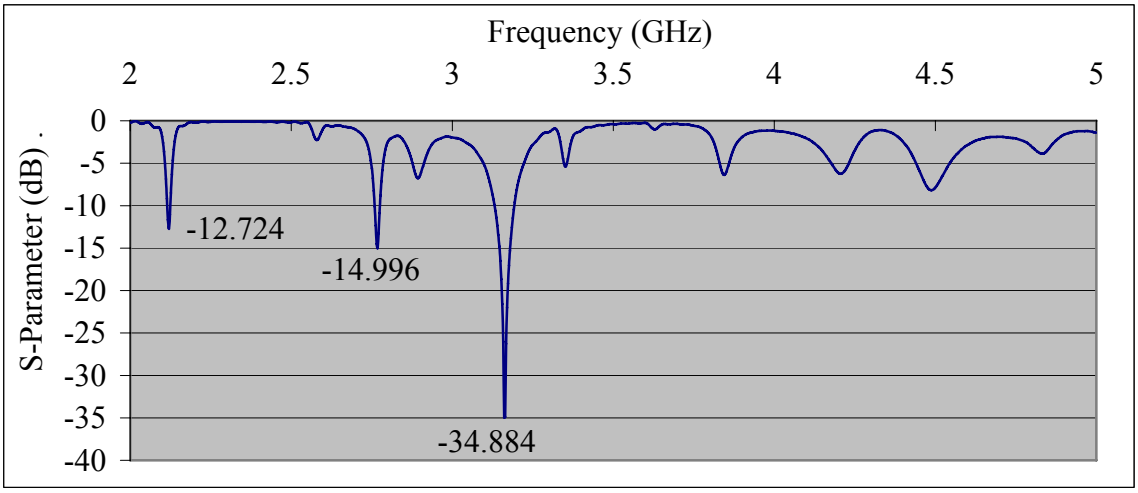

Figure 3.72: Simulated reflection coefficient curve of stacked MSA with top layer of ε_r = 1.44 and with bottom patch scaled by 0.7 when SW1 and SW2 are ON.

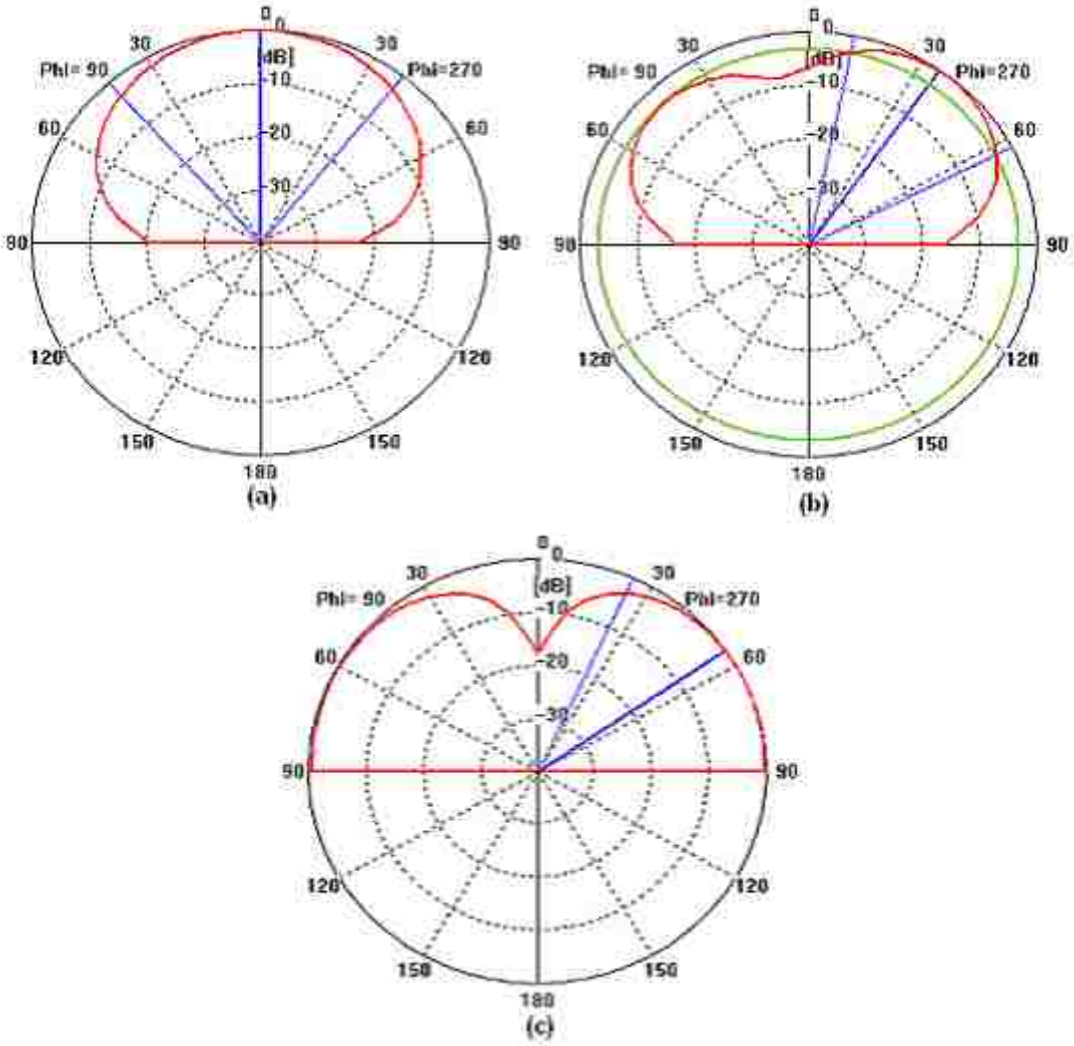

Figure 3.73: Simulated radiation patterns of stacked MSA with top layer of $\varepsilon_r = 4.4$ and with bottom patch scaled by 0.7 when SW1 and SW2 are ON at the frequencies: (a) 212, (b) 2.768, and (c) 3.164 GHz.

A comparison between different reflection coefficient curves for different statuses of SW1 and SW2 are shown in Figure 3.74.

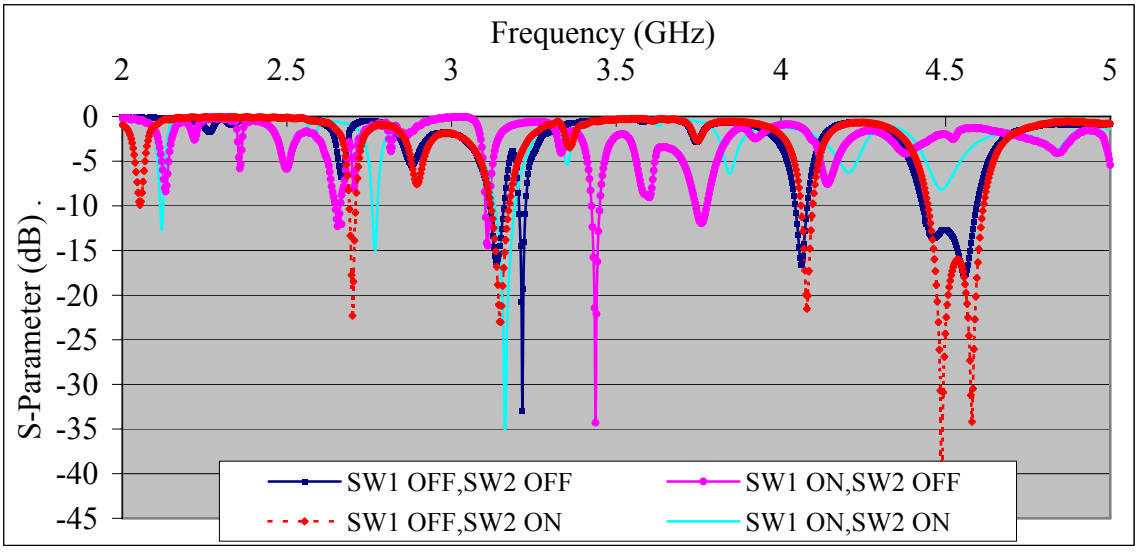

Figure 3.74: Simulated reflection coefficient curves of stacked MSA with top layer of $\varepsilon_r = 4.4$ and with bottom patch scaled by 0.7 for different statuses of SW1 and SW2.

3.6 Summary

In this chapter the calculations needed to find the dimensions of the conventional MSA using transmission line model is presented. After that stacked MSAs are simulated using CST MWS for different dielectric constants and different dielectric layers thicknesses. Results are shown and comparison between reflection coefficients curves before and after adding the top layer of the stacked MSA is presented. As a general care, the number of resonance frequencies when the top layer is of dielectric constant $\varepsilon_r = 4.4$ is lower than it for dielectric constant $\varepsilon_r = 1.44$.

Chapter 4

Experimental Results and Conclusion

4.1 Introduction

The designed antennas simulated in the last chapter are fabricated and tested. The fabricated antennas are built using Rogers 5880 of ε_r = 2.2 and thickness 1.588 mm as well as Rogers 5880 of ε_r = 2.2. The antennas are fabricated by using a new model of the LPKF laser and electronic company called ProtoMat S62 shown in Figure 4.1.

Figure 4.1: ProtoMat S62 machine.

ProtoMat S62 is a compact high-speed plotter used for complex PCB's, single-sided, double-sided and multilayer mixed-signal boards, RF and microwave boards.

ProtoMat S62 provides unequaled precision and performance for quickly and easily milling and drilling circuit board prototypes.

LPKF Circuit Cam software is installed with the plotter to import data from any package (as CST MWS in our case). Board Master software is also installed to control the operation of the plotter. For more details see [43] and [44].

Agilent 8720D network analyzer is used to measure the magnitude of the reflection coefficient (S_{11}) of the fabricated antennas that agrees well the simulated results shown in chapter three of this thesis.

4.2 Fabrication Processes

To fabricate a certain patch antenna that simulated using CST MWS, we follow the following procedure;

- Fix the simulated microstrip antenna in CST MWS main window.
- Press File icon then Export then DXF then Enter to get a DXF file that is exported to fit LPKF Circuit Cam software as shown in Figure 4.2.

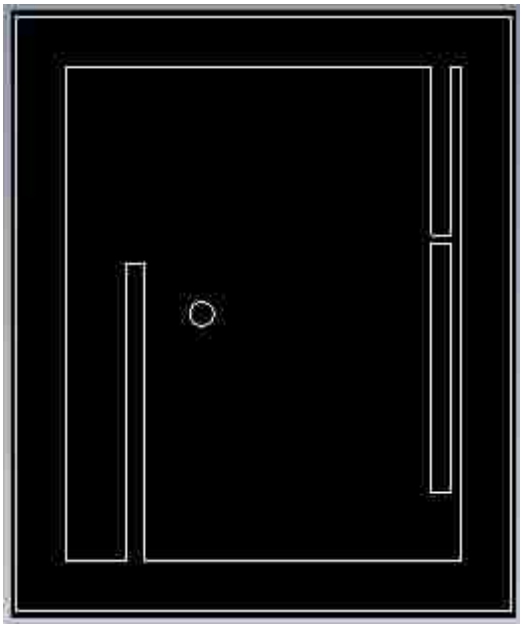

Figure 4.2: Simulated MSA saved as DXF file.

- Using LPKF Circuit Cam software, Import DXF file to LPKF Circuit Cam by pressing File then Import DXF file then a window will open asking about file type which is DXF

in our case, the layer which is top, and list of apertures which is DXF mm unit, and then press Import.

- After getting the imported DXF file press Insert then Rubout Area and choose the unneeded layer to be rubbed out which is either top or bottom layer according to the application.
- Use the tools shown in the left column to rub out unneeded metal.
- Press Edit then Insulate to choose some specified tools which is suitable to the design needed then press Run.
- Press File then export then LPKF then LKPF circuit board plotter and save the file that fits Board Master software.
- Using Board Master software, press File then Import then LMD/ LPR then import the needed file saved in the last step.
- Switch ProtoMat S62 ON, then fix the dielectric board and locate the working area using Board Master software.
- From Board Master software choose milling top/ bottom from the bar located on the top lift corner then press All+ icon then press Start to begin fabricating MSA.
- After ProtoMat S62 finishing its duty the dielectric board is cut to fit the specified dimensions and a coaxial connecter is fixed to feed the fabricated MSA.
- Agilent 8720D network analyzer is used to measure the magnitude of the reflection coefficient (S_{11}).

4.3 Experimental Results

After finishing the fabrication of the antennas that was simulated so far, we end up with the experimental results that agree well the results obtained from simulation part.

4.3.1 Configuration of Fabricated Stacked MSA

The bottom patches of the antennas simulated in section 3.2.1 of the last chapter are fabricated where the measured results are as follows;

- When SW1 and SW2 are OFF, the fabricated bottom antenna is shown in Figure 4.3 and the reflection coefficient curve is shown in Figure 4.4.

Figure 4.3: Fabricated bottom MSA with two slots when SW1 and SW2 are OFF.

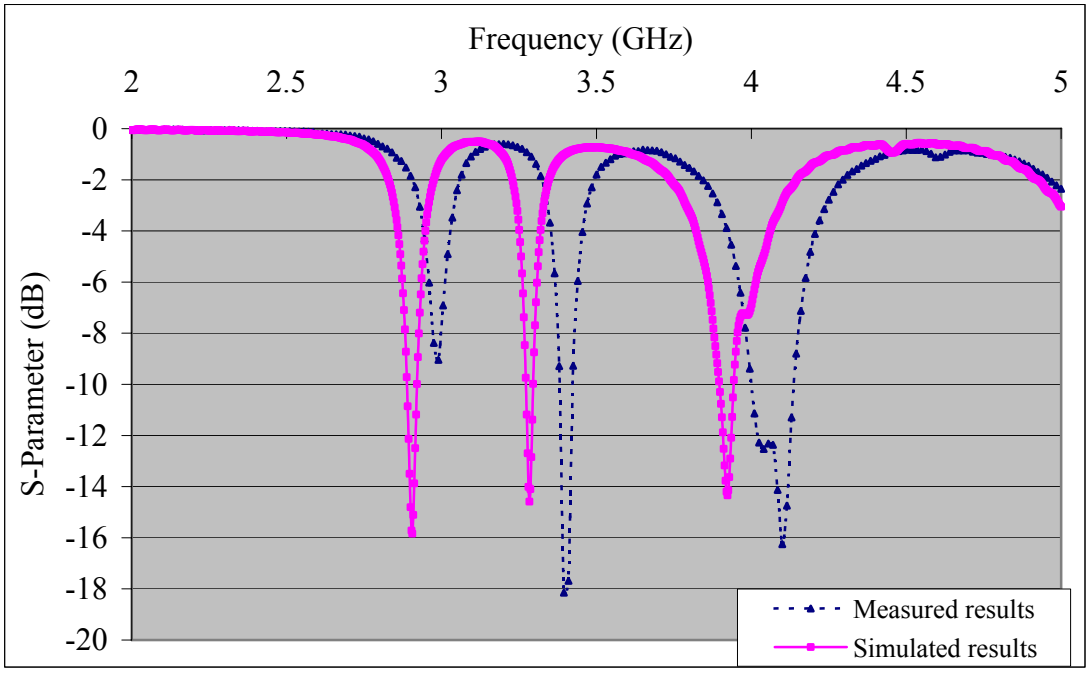

Figure 4.4: Measured reflection coefficient curve of fabricated bottom MSA with two slots when SW1 and SW2 are OFF.

- When SW1 is ON and SW2 is OFF, the fabricated bottom antenna is shown in Figure 4.5 and the reflection coefficient curve is shown in Figure 4.6.

Figure 4.5: Fabricated bottom MSA with two slots when SW1 is ON and SW2 is OFF.

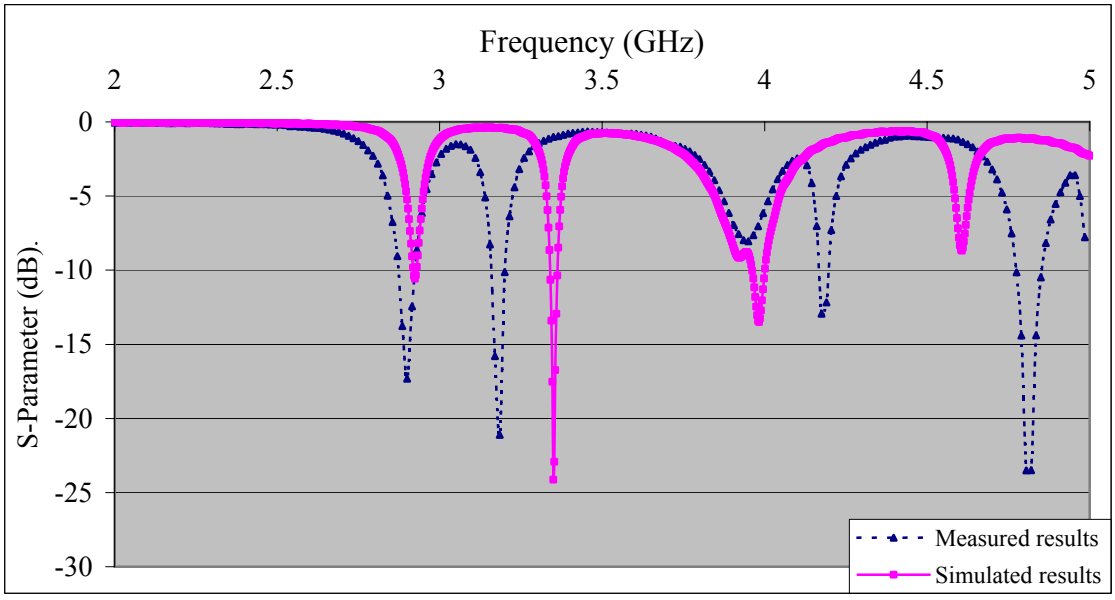

Figure 4.6: Measured reflection coefficient curve of fabricated bottom MSA with two slots when SW1 is ON and SW2 is OFF.

- When SW1 is OFF and SW2 is ON, the fabricated bottom antenna is shown in Figure 4.7 and the reflection coefficient curve is shown in Figure 4.8.

Figure 4.7: Fabricated bottom MSA with two slots when SW1is OFF and SW2 is ON.

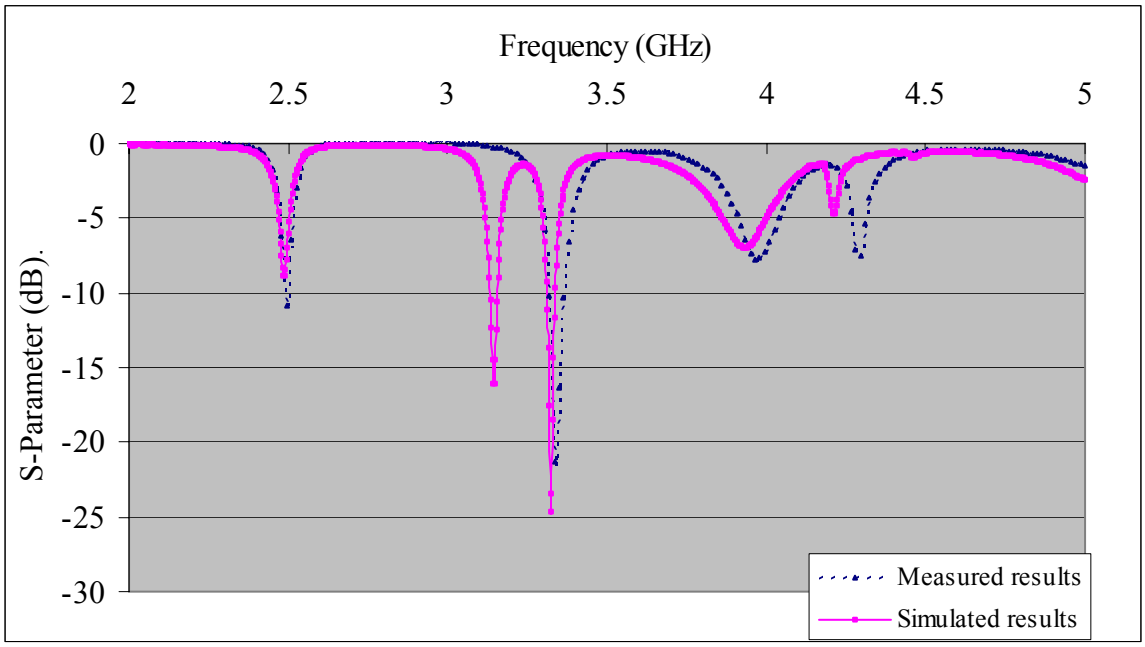

Figure 4.8: Measured reflection coefficient curve of fabricated bottom MSA with two slots when SW1 is OFF and SW2 is ON.

- When SW1 and SW2 are ON, the fabricated bottom antenna is shown in Figure 4.9 and the reflection coefficient curve is shown in Figure 4.10.

Figure 4.9: Fabricated bottom MSA with two slots when SW1 and SW2 are ON.

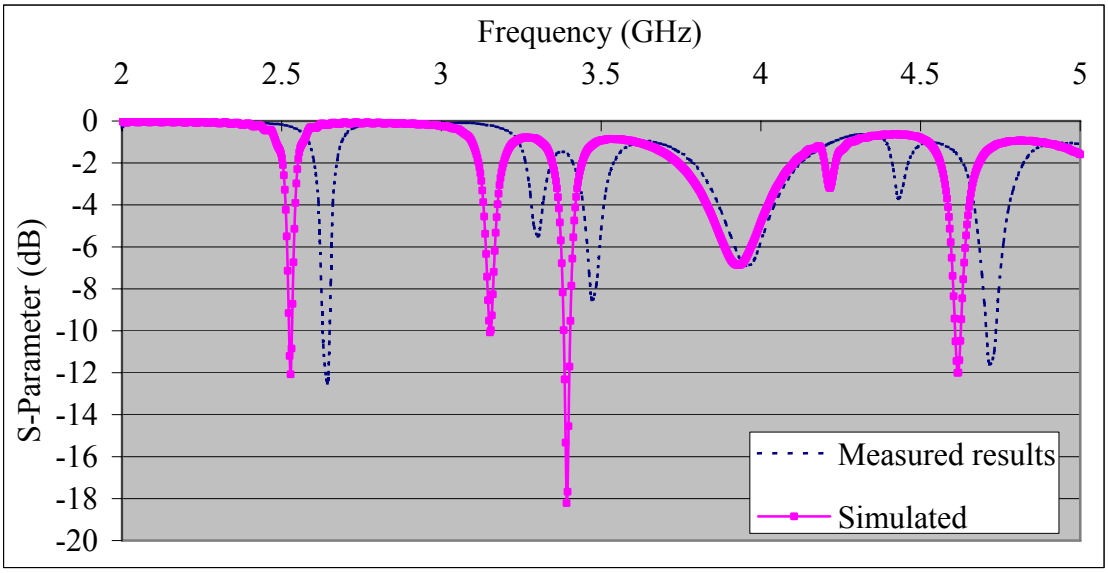

Figure 4.10: Measured reflection coefficient curve of fabricated bottom MSA with two slots when SW1 and SW2 are ON.

A comparison between different reflection coefficients for different statuses of SW1 and SW2 are shown in Figure 3.71.

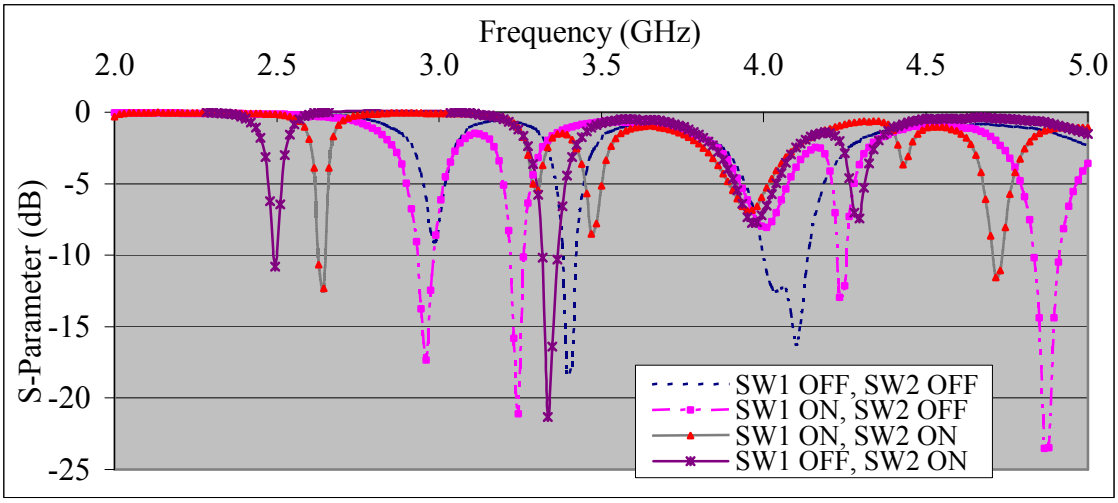

Figure 4.9: Measured reflection coefficient curves of MSA with two slots for different statuses of SW1 and SW2.

After adding the top layer of $\varepsilon_r = 4.4$ that has a patch of size 45×55 to fabricate the stacked MSA, we get the reflection coefficient curves for different statuses of SW1 and SW2 of the fabricated bottom antenna as follows;

- When SW1 and SW2 are OFF the reflection coefficient curve is shown in Figure 4.10.

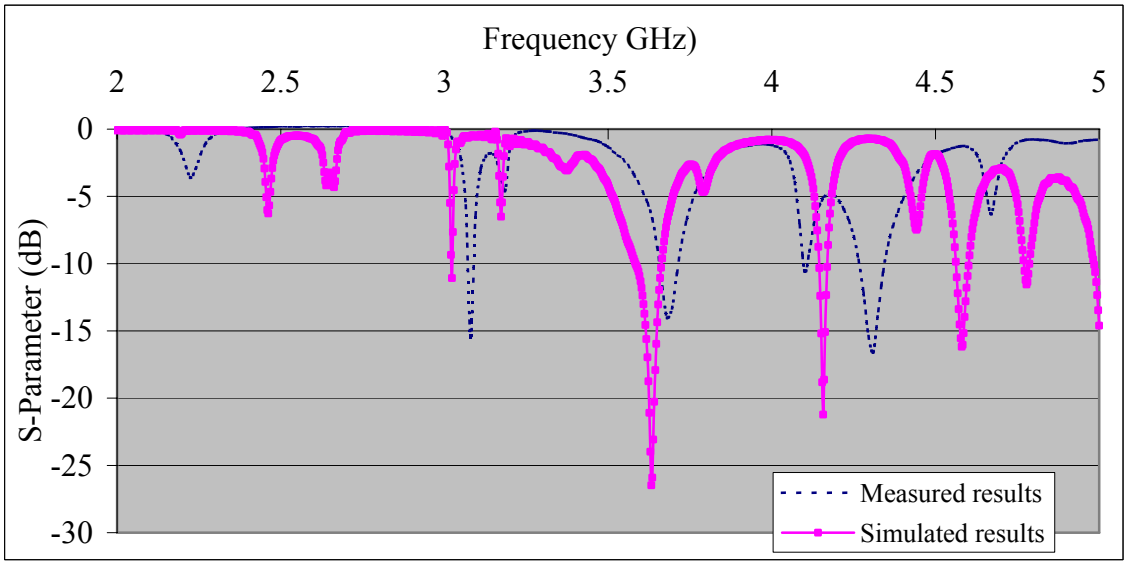

Figure 4.10: Measured and simulated reflection coefficient curves of stacked-MSA with two slots when SW1 and SW2 are OFF.

- When SW1 is ON and SW2 is OFF the reflection coefficient curve is shown in Figure 4.11.

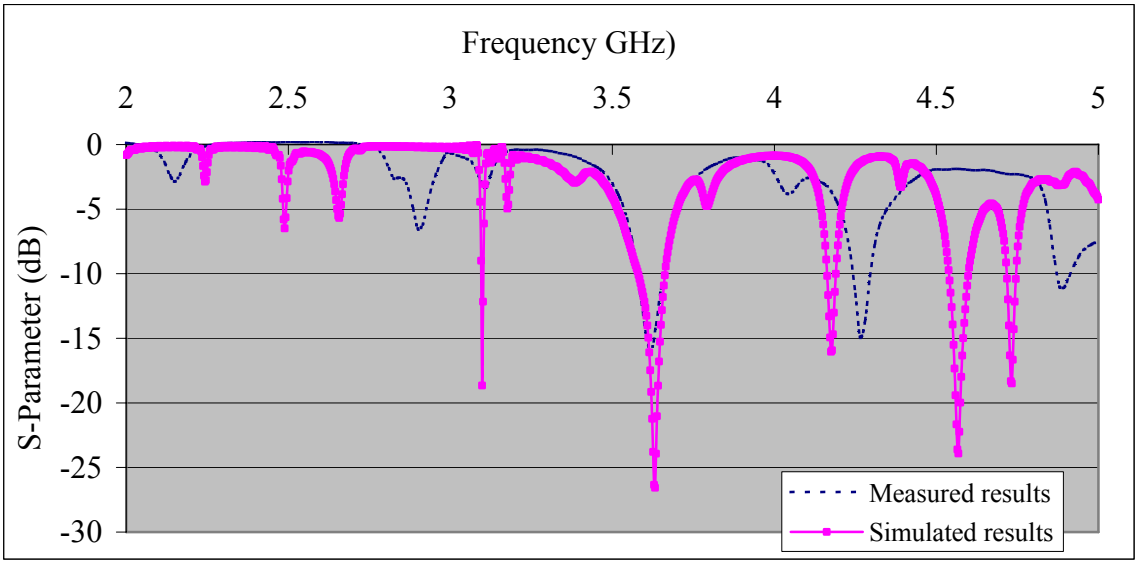

Figure 4.11: Measured and simulated reflection coefficient curves of stacked-MSA with two slots when SW1 is ON and SW2 is OFF.

- When SW1 is OFF and SW2 is ON the reflection coefficient curve is shown in Figure 4.12.

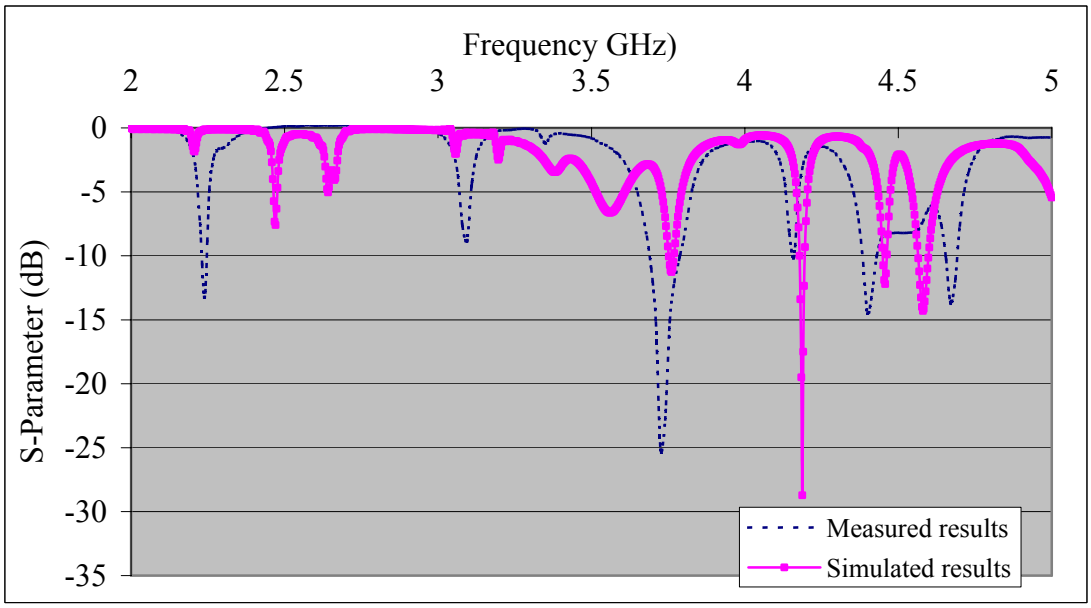

Figure 4.12: Measured and simulated reflection coefficient curves of stacked-MSA with two slots when SW1 is OFF and SW2 is ON.

- When SW1 and SW2 are ON the reflection coefficient curves is shown in Figure 4.13.

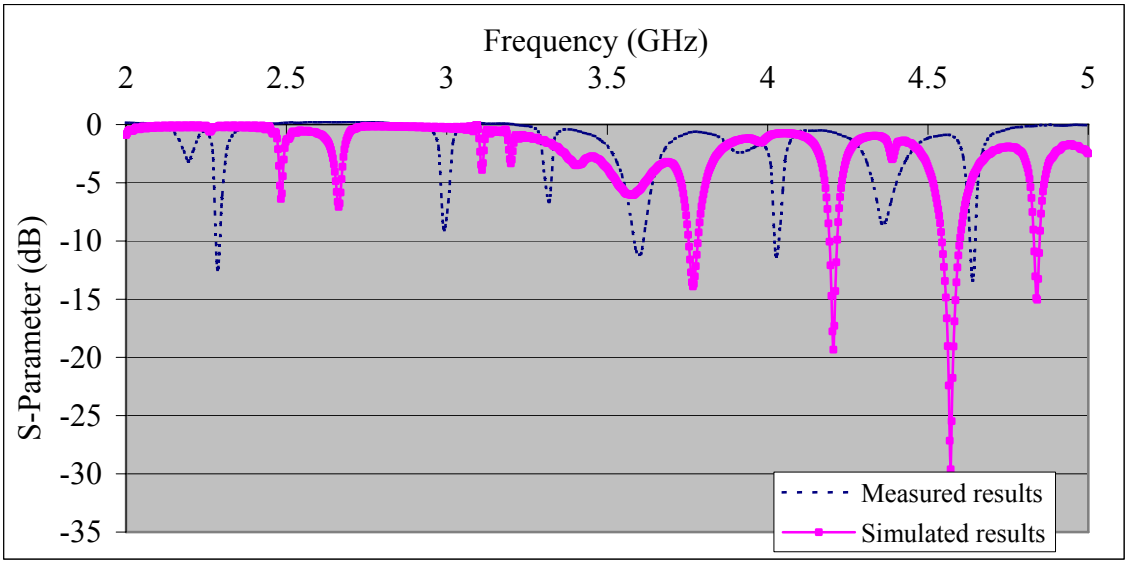

Figure 4.13: Measured and simulated reflection coefficient curves of stacked-MSA with two slots when SW1 and SW2 are ON.

A comparison between different reflection coefficients for different statuses of SW1 and SW2 are shown in Figure 4.14.

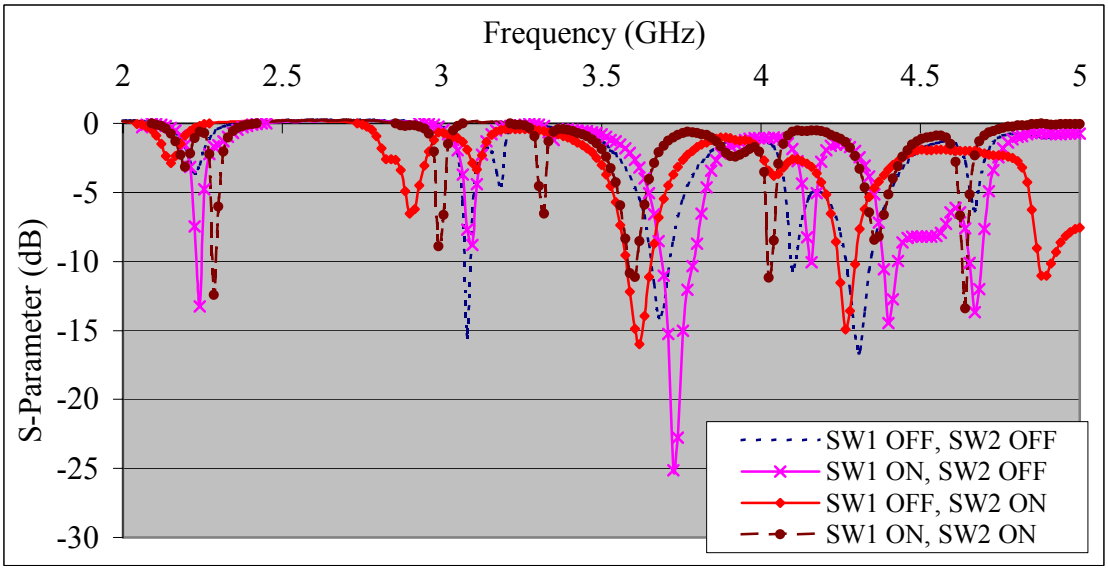

Figure 4.14: Measured reflection coefficient curves of stacked-MSA with two slots with different statuses of SW1 and SW2.

4.3.2 Configuration of Fabricated Stacked MSA with Inverted Patches

The bottom patch of the antenna simulated in section 3.2.2 of the last chapter is fabricated as shown in Figure 4.10 and its reflection coefficient curve is shown in Figure 4.11.

Figure 4.16: Fabricated conventional MSA with patch scaled by 0.7.

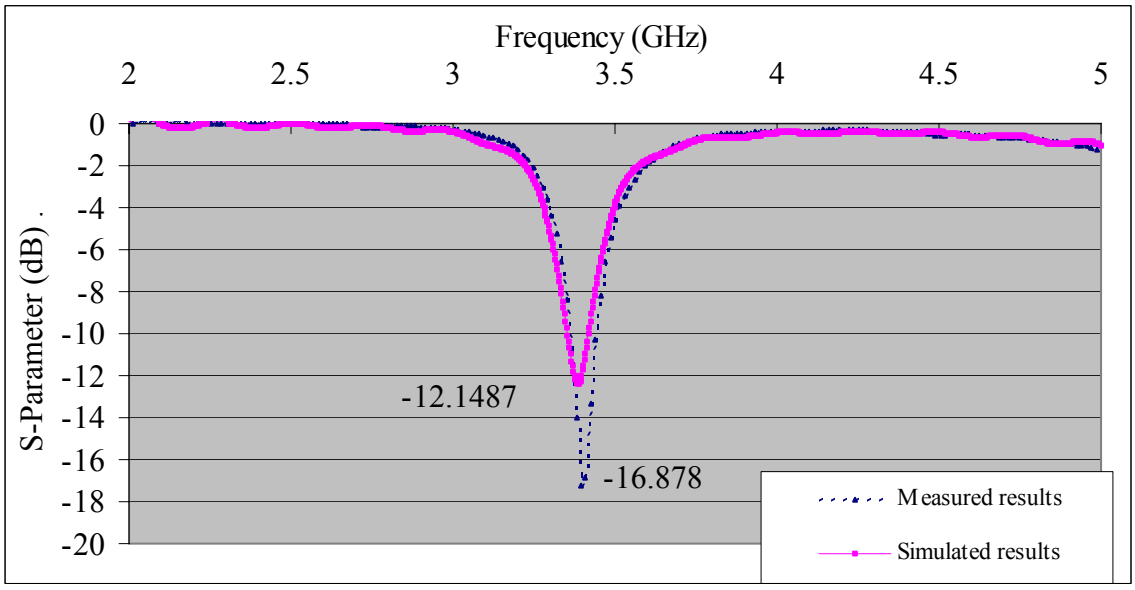

Figure 4.17: Measured and simulated reflection coefficient curve of fabricated conventional MSA with patch scaled by 0.7.

After adding the top layer of $\varepsilon_r = 4.4$ which has two slots and two switches. Figure 4.18 shows the top layer when SW1 and SW2 are both ON. A reconfigurable reflection coefficient curves for different statuses of SW1 and SW2 of stacked MSA with top layer of $\varepsilon_r = 4.4$ is shown In Figure 4.19.

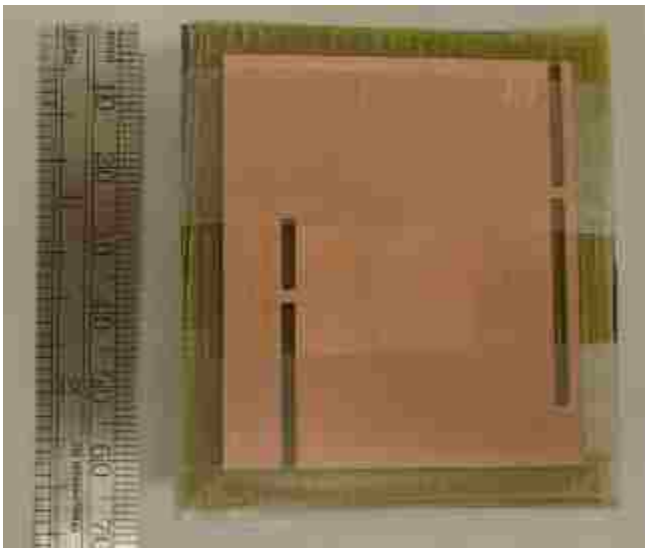

Figure 4.18: Fabricated stacked-MSA with top layer of $\varepsilon_r = 4.4$ when SW1 and SW2 are ON.

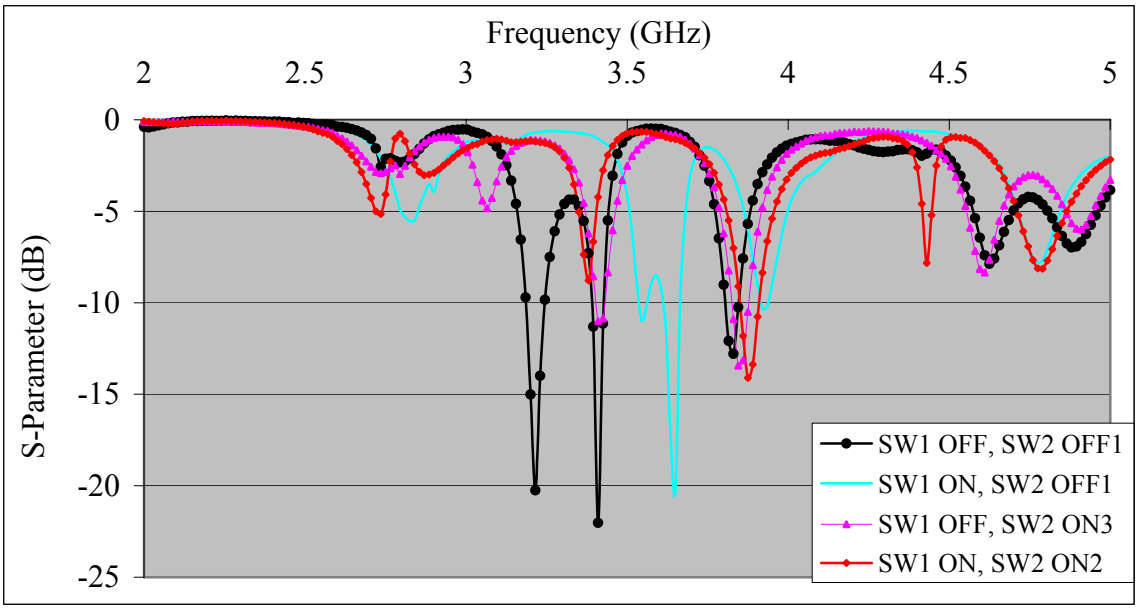

Figure 4.19: Measured reflection coefficient curves of fabricated stacked-MSA of top layer with two slots with different statuses of SW1 and SW2.

Figures 4.14 and 4.19 show practical reconfigurability of two different stacked MSAs that enables us to accommodate more than one service using the same antenna and can be easily integrated with packaging structures. By changing the statuses of the switches, the operating frequencies will be moved. Modern mobile, satellite and wireless communication systems exploit this convenient cost effective technique by designing a single antenna operates more than single resonance frequency instead of designing multiple antennas to do this task.

The resonance frequency can be adjusted by changing the shape of the radiating element such as modifying the position of the feeding point or by changing the statuses of the switches. For practical applications, PIN diodes or copper tapes are used to make switching instead of switches shown in Figures 4.5, 4.7, 4.9 and 4.18.

For some results presented so far in this chapter, there is small shift between simulated and measured reflection coefficient curves. There are many reasons standing behind that such as the difference in dielectric constant between layers used in simulations and ones used in fabricating antennas. Thus, when ε_r for layers used in fabricating antennas equals 2.23 instead of 2.2 and 4.45 instead of 4.4, a small shift in reflection coefficient curves is yielded. Also in fabrication process and while removing parts of the patches, ProtoMat S62 machine might remove a little bit more parts than required dimensions during milling process which cases small shift in resonant frequencies of the fabricated antennas. This is besides air gaps exist between the stacked layers which affect somehow the values of resonant frequencies.

The size of the feeding gap and its location influence the impedance matching, in other words they affect the resonant frequencies. In the other hand, increasing in the probe diameter cases decrease in the probe inductive, which decreases the total inductance of the antenna and as a result the resonance frequencies slightly shift upwards.

4.4 Future Work

There are many additions that are suggested for future work such as;

- Inserting PIN diodes to make switching process more convenient for practical applications.

- Shorting techniques such as shorting pins and shorting walls are highly recommended to achieve a shift in resonance frequencies and to reduce the patch size. To get maximum shifting, the shorting pins have to be placed very close to the patch edge. However, for thick layers and in order to reduce the inductive loading, the shorting pins have to be close to the feeding point.
- The resonance frequencies can be tuned by varying the length of the slots, where by increasing the path length of the surface current, the resonance frequencies are reduced. Also chopping the two diagonally opposite corners of the patch makes the resonance frequencies of the mode along this diagonal to be higher than that for a mode along the unchopped diagonal.
- Using thicker dielectric materials for the top layer that is to make the distance between the parasitic patch and the feeding patch about a half wavelength to enhance the gain of stacked MSA. On the other hand, in order to have a wider bandwidth, the distance between the parasitic patch and the feeding patch must be made very small. Thus, a compromise must be implemented to get the optimum gain and bandwidth simultaneously. Using high dielectric constant substrates and modifying the basic patch shapes, the probe inductance problem can be overcome.

4.5 Conclusion

New reconfigurable-staked MSAs of operating frequencies in the range of (2-5) GHz are designed, fabricated and tested in this thesis. The experimental results agreed well with the results obtained from simulations performed in chapter three. In the first antenna slots are added to conventional rectangular (bottom) patch to obtain triple resonance frequencies, also switches are added to slots in order to control the reconfigurability of the staked MSAs. The positions and dimensions of slots and switches are optimally chosen to give as many resonant frequencies as possible. By adjusting the statuses of the switches, which are optimally fixed along the slots, the values of resonance frequencies can be controlled, thus achieving frequency reconfigurability.

By placing another MSA on the top of the bottom antenna with slots the number of resonance frequencies are increased, which is the main contribution of this thesis, and the bandwidth and gain of the overall MSA are enhanced. A dielectric layer separates the

two antennas where the dielectric constant and the thickness of the top layer are carefully optimized to get maximum number of resonance frequencies, bandwidth and gain of the staked MSA. The second antenna is the same as the first one but with switching top and bottom patches. Several results are included to verify the validity of the newly designed antenna.

Appendices
Appendix A

MATLAB program No. 1

```
clear all; close all;
%Define Constants


c=30e9;% in cm/s.          %Free-Space Velocity of Light.
fr=2.4e9;                  %Center (Resonant) Frequency be 2.4 GHz.
h=.1588;% in cm            %The Height of the Substrate.
Lumda=c/fr;%in cm
er=2.2;                    %The Dielectric Constant.
W=sqrt(2/(er+1))*c/(2*fr) %Width of the Antenna (cm).


 %Relative Dielectric Constant.
ereff=((er+1)/2)+((er-1)/2)*(1+12*(h/W))^-.5

%Fringing Field Contribution to Antenna Length.

deltaL=.412*h*(ereff+.3)*((W/h)+.264)/((ereff-.258)*((W/h)+.8))

L=30e9/(2*fr*sqrt(ereff))-2*deltaL   %Physical Length.
Leff=L+2*deltaL                      %Effective Length.
X=2*pi/Lumda;                        %Wave Number.

% Numerical Integral to Find the Conductance of one Slot.
Y=0;
for theta=0:.001:pi;
    M=((sin(.5*X*W*cos(theta))/cos(theta))^2*(sin(theta))^3);
    Y=Y+M;
end
G1=1/(120*pi^2)*.001*Y

% Numerical Integral to Find the Mutual Conductance Between the Slot.

R=0;
for theta=0:.001:pi;

k=((sin(.5*X*W*cos(theta))/cos(theta))^2*(sin(theta))^3)*besselj(0,X*L*
sin(theta));
    R=R+k;
end
G12=1/(120*pi^2)*.001*R

Rin=1/(2*(G1+G12))      %Characteristic Impedance of Transmission Line

% The Distance Between the Radiating Edge and the Feeding Point.

solve('(cos(pi*u/L))^2-50/Rin')
```

MATLAB program No. 2

```
clear all; close all;
%Define Constants

syms x z
L=.04;          %Length of the Antenna (m).
W=.050;         %Width of the Antenna (m).
h=.001588;      %The Height of the Substrate (m).
epsr=2.2;       %The Dielectric Constant.
f=2.4*10^9;     %Center (Resonant) Frequency be 2.4 GHz.
c=3*10^8;       %Free-Space Velocity of Light.
lamda0=c/f;
k0=2*pi/lamda0;% Integral to Find the Conductance of one Slot.
Y=0;
I1=int((sin(.5*k0*W*cos(x))/cos(x))^2*(sin(x))^3,x,0,pi);
G1=I1/(120*(pi^2));
% Numerical Integral to Find the Mutual Conductance Between the Slots.
sum=0;
for y=.0001:.001:pi;
     R
=(sin(.5*k0*W*cos(y))/cos(y))^2*BESSELJ(0,k0*L*sin(y))*(sin(y))^3;
sum=sum+R;
 end
 G12=(1/(120*(pi^2)))*sum*.001;
 Rin=1/(2*(G1+G12))      %Characteristic Impedance of Transmission Line
  solve('(cos(pi*u/L))^2-50/Rin')    % The Distance Between the
Radiating Edge and the Feeding Point (m).
```

Appendix B

For stacked MSA with top substrate (layer) of 1 mm height and top patch dimensions of 40×50.

Reflection coefficient curves for stacked MSA with top layer of ε_r between (1.1- 4).

- For $\varepsilon_r = 1.1$

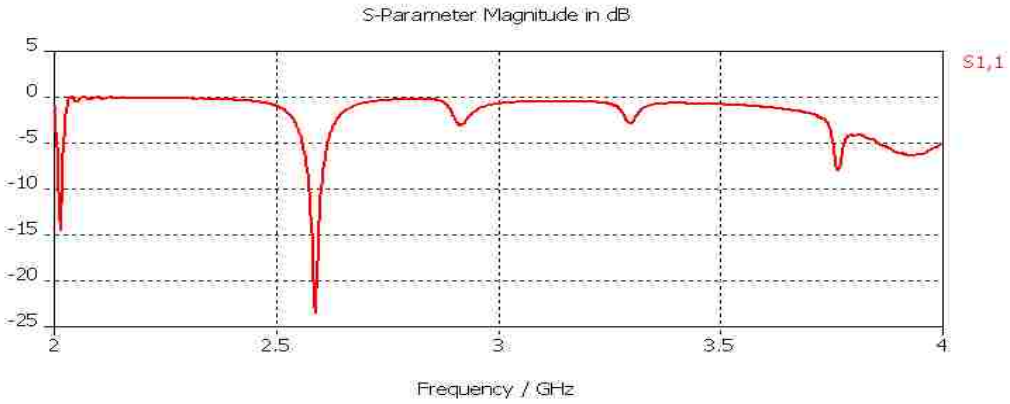

Figure B.1: Simulated reflection coefficient curve for stacked MSA with top layer of $\varepsilon_r = 1.1$.

- For $\varepsilon_r = 1.2$

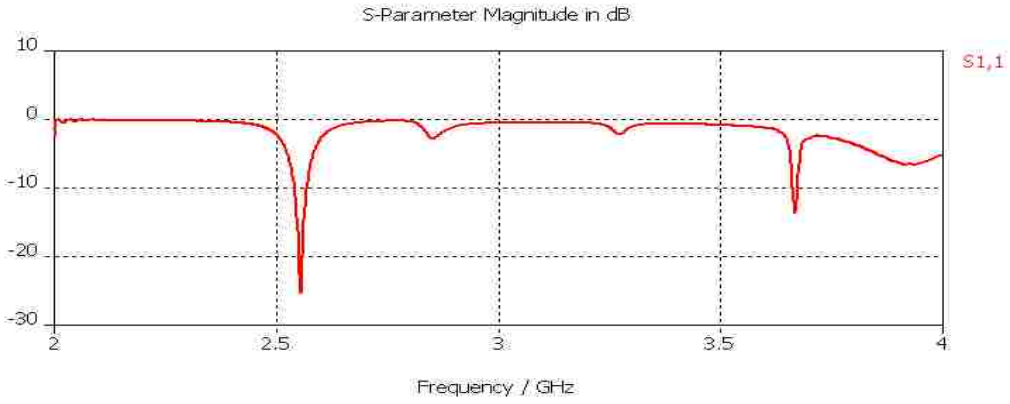

Figure B.2: Simulated reflection coefficient curve for stacked MSA with top layer of $\varepsilon_r = 1.2$.

- For $\varepsilon_r = 1.3$

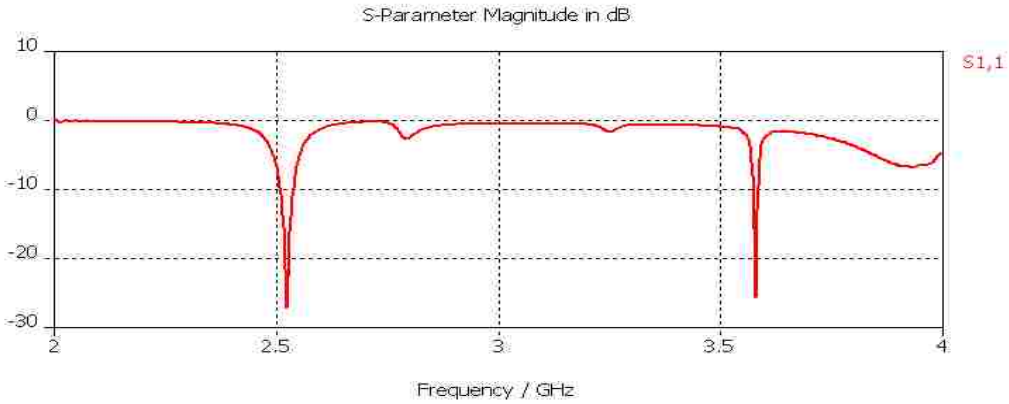

Figure B.3: Simulated reflection coefficient curve for stacked MSA with top layer of $\varepsilon_r = 1.3$.

- For $\varepsilon_r = 1.4$

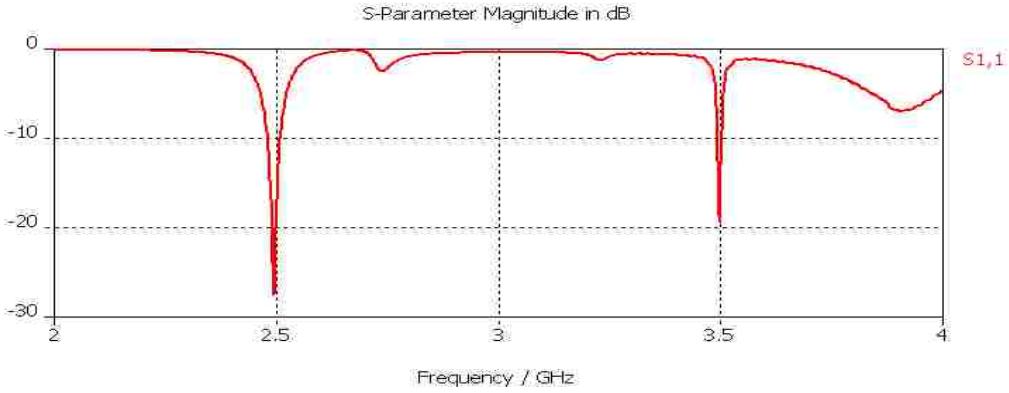

Figure B.4: Simulated reflection coefficient curve for stacked MSA with top layer of $\varepsilon_r = 1.4$.

- For $\varepsilon_r = 1.5$

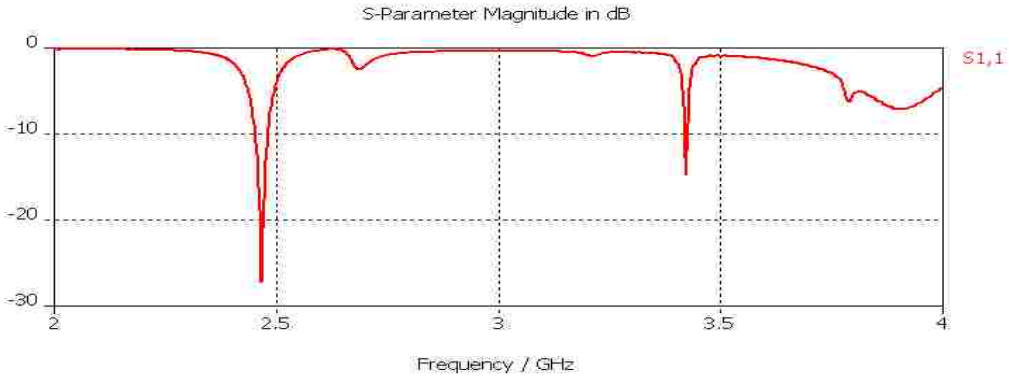

Figure B.5: Simulated reflection coefficient curve for stacked MSA with top layer of $\varepsilon_r = 1.5$.

- For $\varepsilon_r = 1.55$

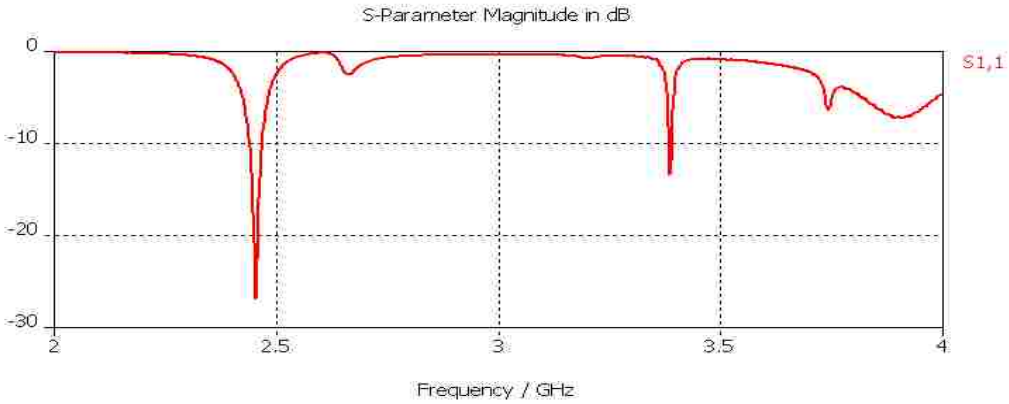

Figure B.6: Simulated reflection coefficient curve for stacked MSA with top layer of $\varepsilon_r = 1.55$.

- For $\varepsilon_r = 1.6$

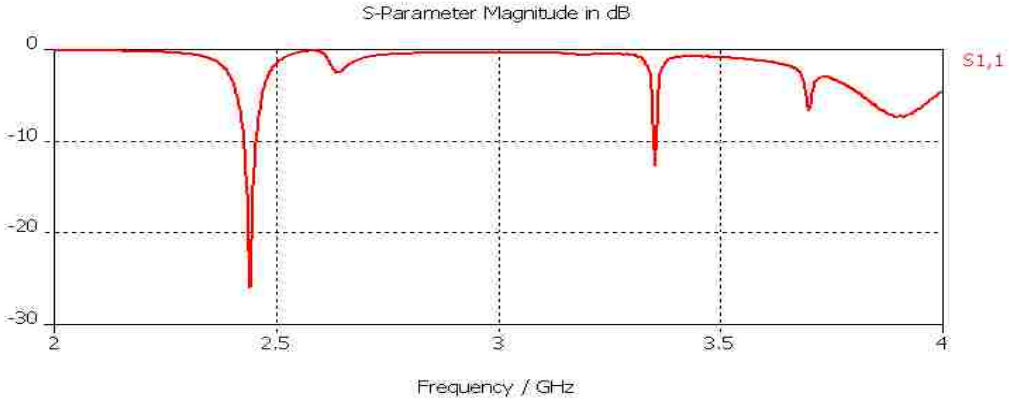

Figure B.7: Simulated reflection coefficient curve for stacked MSA with top layer of $\varepsilon_r = 1.6$.

- For $\varepsilon_r = 1.7$

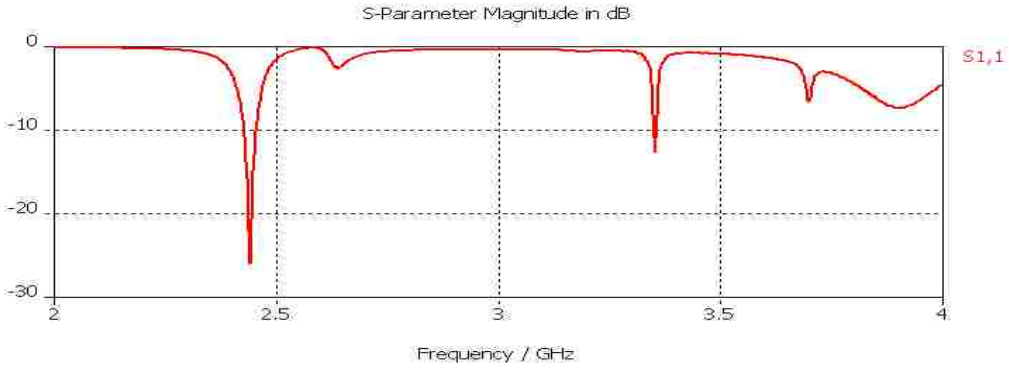

Figure B.8: Simulated reflection coefficient curve for stacked MSA with top layer of $\varepsilon_r = 1.7$.

- For $\varepsilon_r = 1.8$

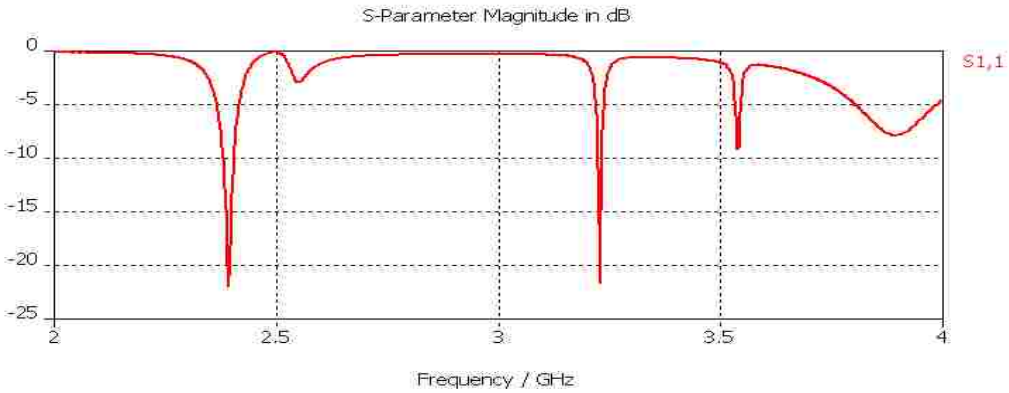

Figure B.9: Simulated reflection coefficient curve for stacked MSA with top layer of $\varepsilon_r = 1.8$.

- For $\varepsilon_r = 1.9$

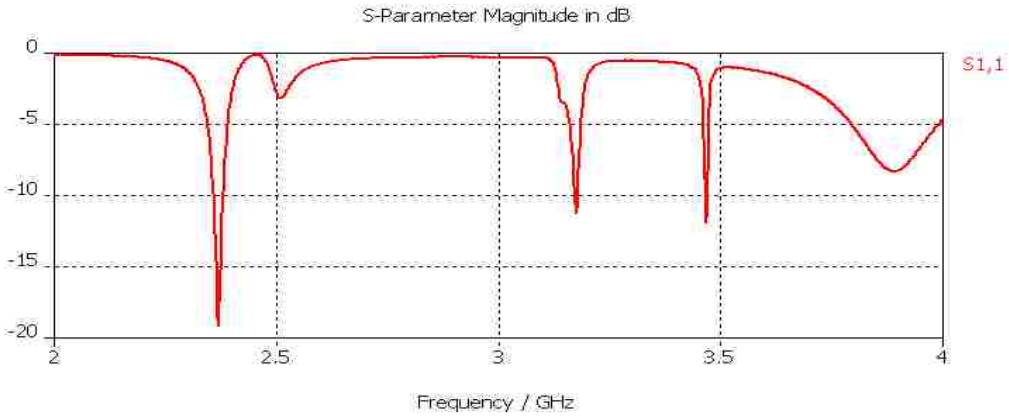

Figure B.10: Simulated reflection coefficient curve for stacked MSA with top layer of $\varepsilon_r = 1.9$.

- For $\varepsilon_r = 2$

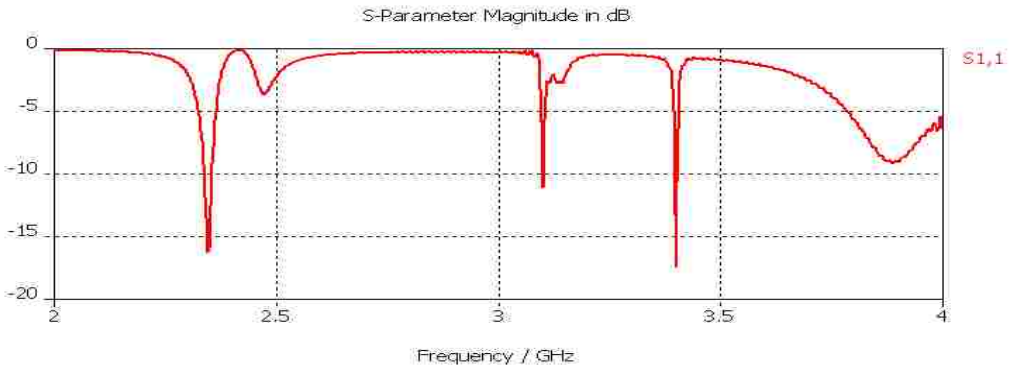

Figure B.11: Simulated reflection coefficient curve for stacked MSA with top layer of $\varepsilon_r = 2$.

• For $\varepsilon_r = 2.1$

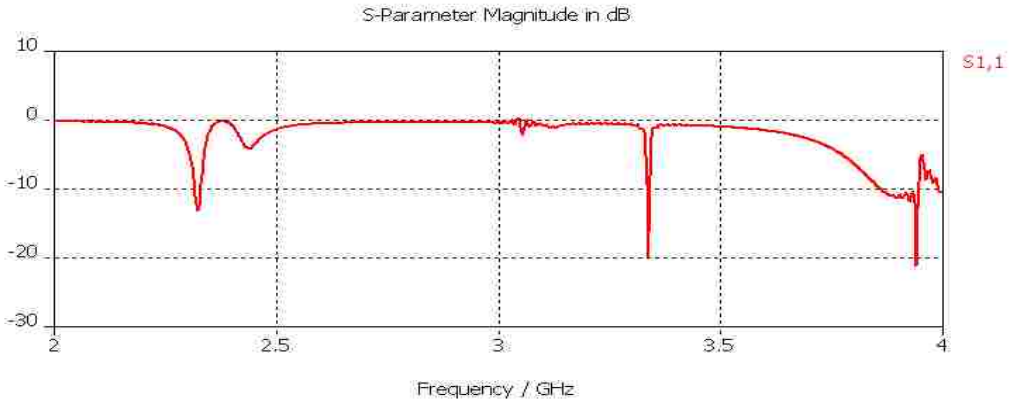

Figure B.12: Simulated reflection coefficient curve for stacked MSA with top layer of $\varepsilon_r = 2.1$.

• For $\varepsilon_r = 2.2$

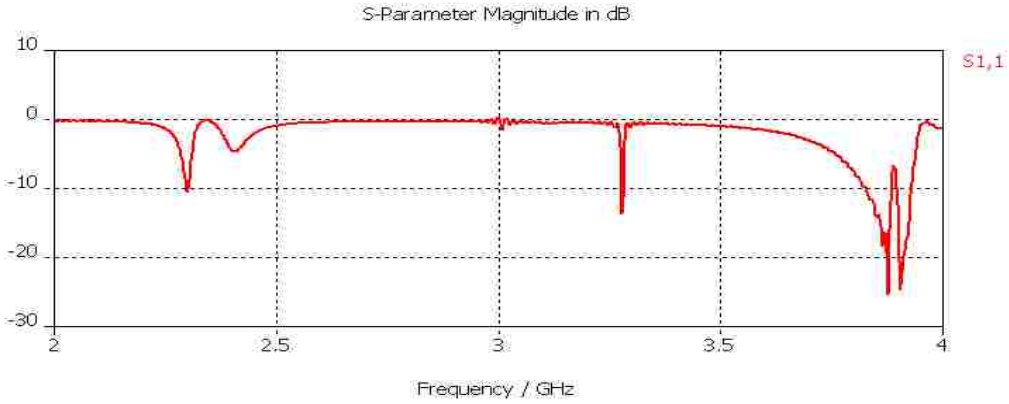

Figure B.13: Simulated reflection coefficient curve for stacked MSA with top layer of $\varepsilon_r = 2.2$.

• For $\varepsilon_r = 2.3$

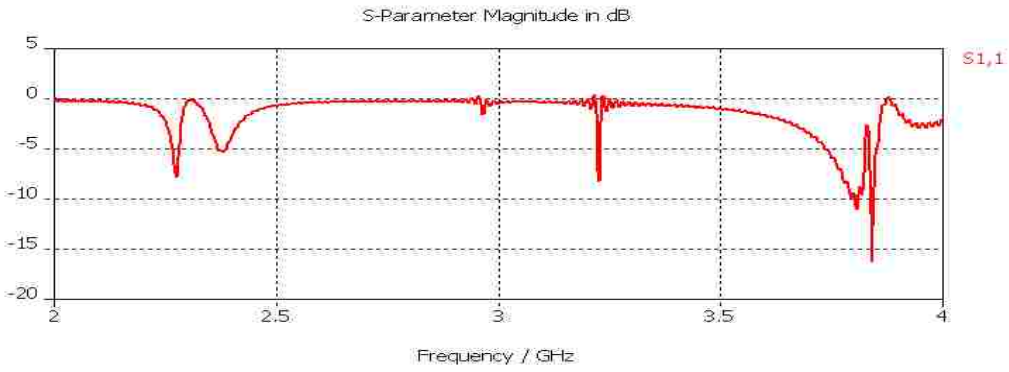

Figure B.14: Simulated reflection coefficient curve for stacked MSA with top layer of $\varepsilon_r = 2.3$.

• For $\varepsilon_r = 2.4$

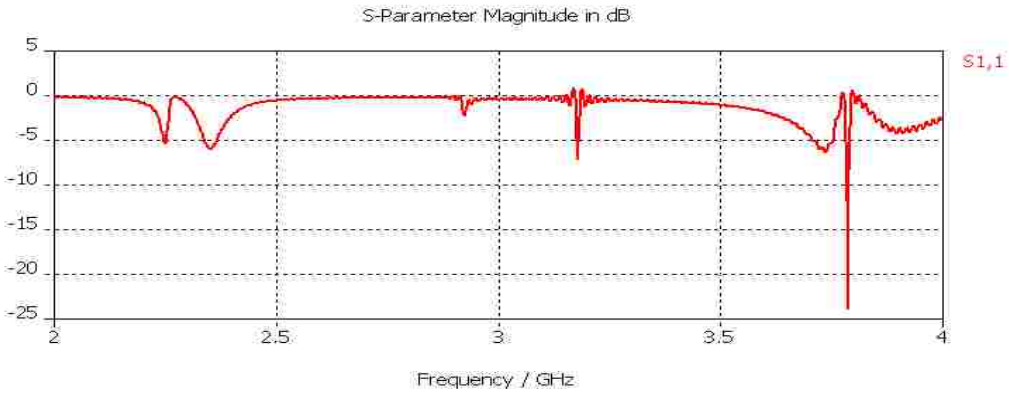

Figure B.15: Simulated reflection coefficient curve for stacked MSA with top layer of $\varepsilon_r = 2.4$.

• For $\varepsilon_r = 2.5$

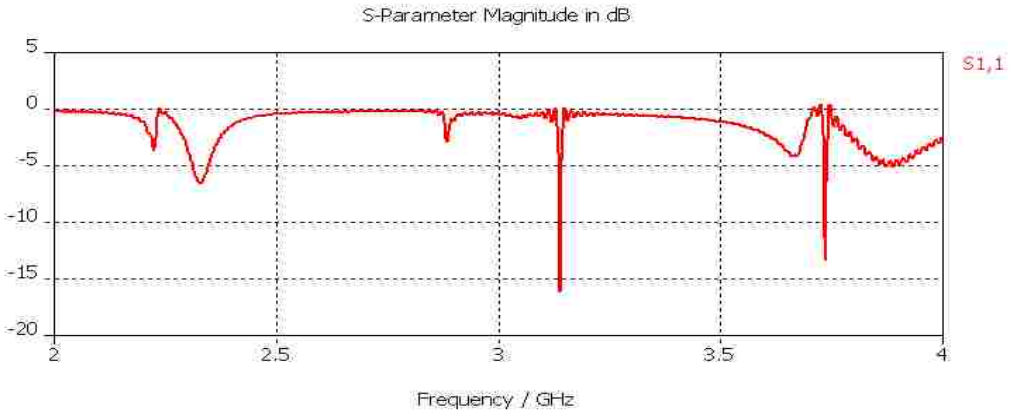

Figure B.16: Simulated reflection coefficient curve for stacked MSA with top layer of $\varepsilon_r = 2.5$.

• For $\varepsilon_r = 2.6$

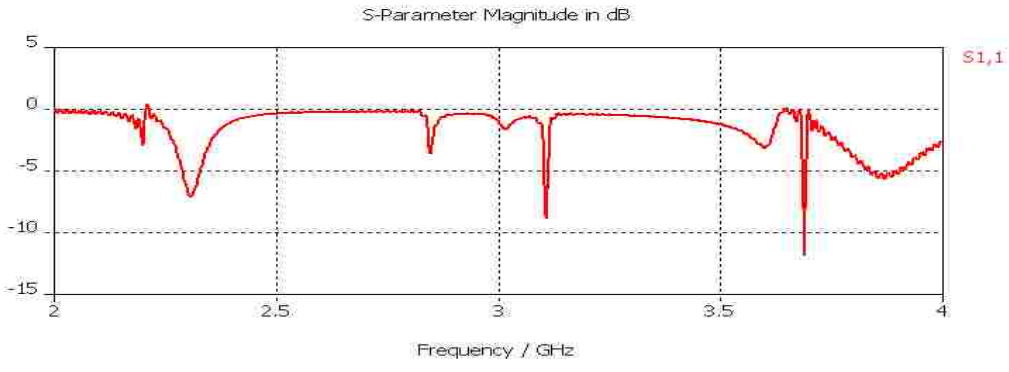

Figure B.17: Simulated reflection coefficient curve for stacked MSA with top layer of $\varepsilon_r = 2.6$.

• For $\varepsilon_r = 2.7$

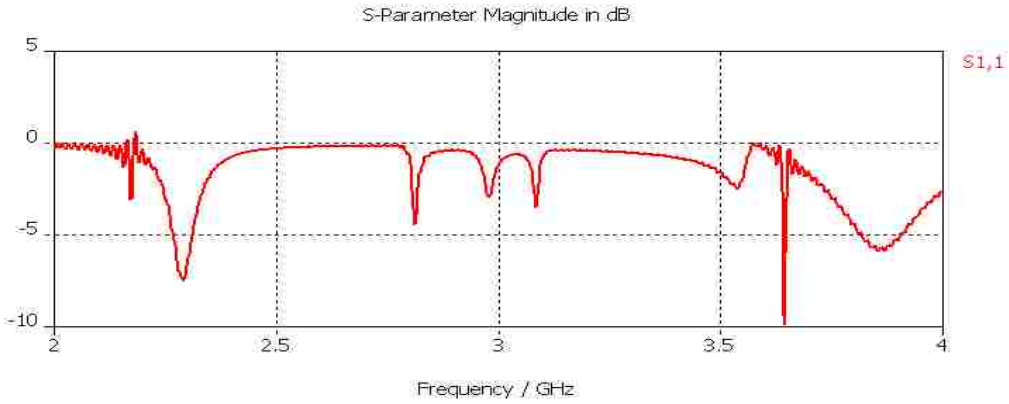

Figure B.18: Simulated reflection coefficient curve for stacked MSA with top layer of $\varepsilon_r = 2.7$.

• For $\varepsilon_r = 2.8$

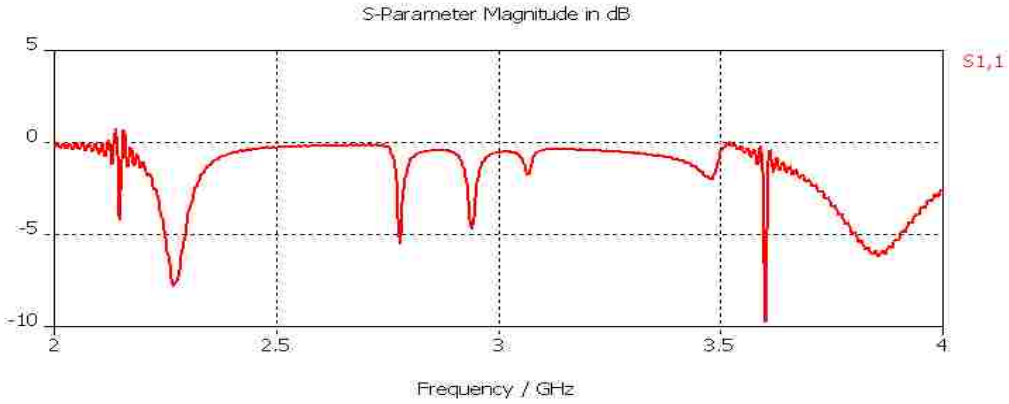

Figure B.19: Simulated reflection coefficient curve for stacked MSA with top layer of $\varepsilon_r = 2.8$.

• For $\varepsilon_r = 2.9$

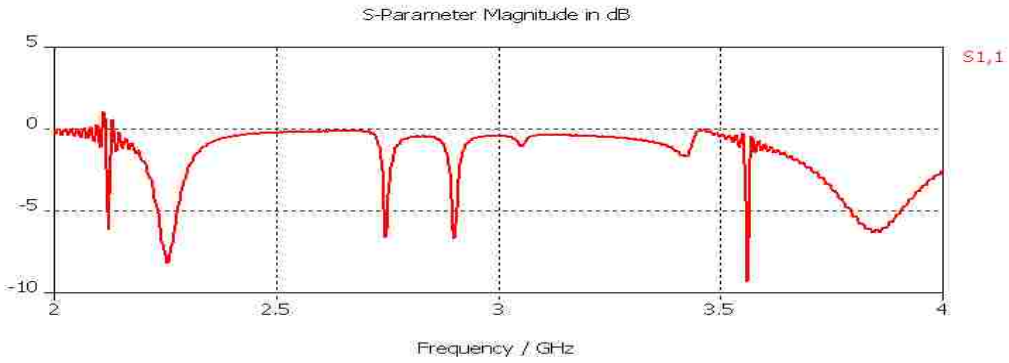

Figure B.20: Simulated reflection coefficient curve for stacked MSA with top layer of $\varepsilon_r = 2.9$.

• For $\varepsilon_r = 3$

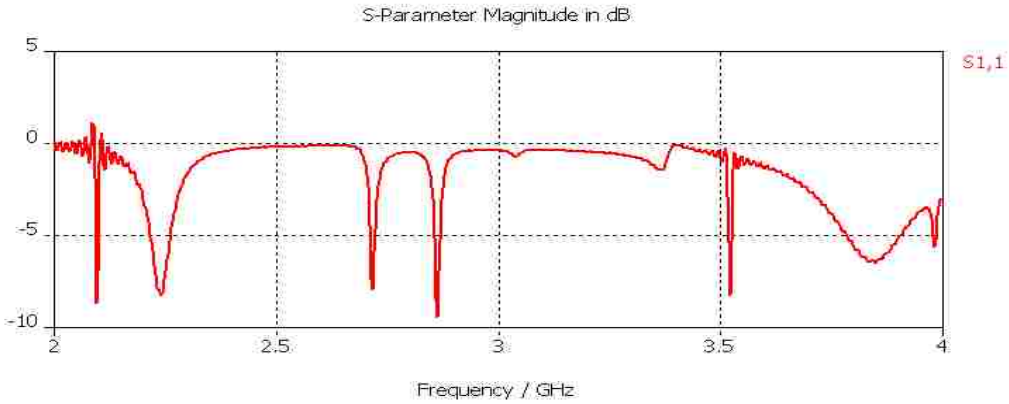

Figure B.21: Simulated reflection coefficient curve for stacked MSA with top layer of $\varepsilon_r = 3$.

• For $\varepsilon_r = 3.1$

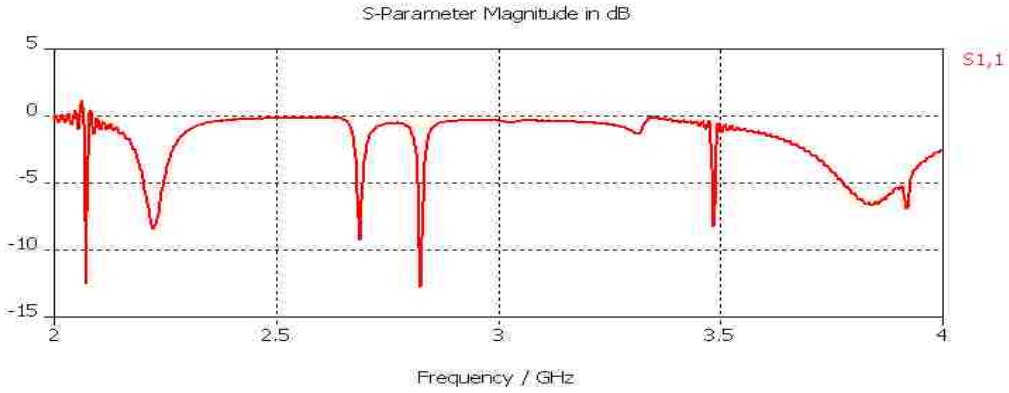

Figure B.22: Simulated reflection coefficient curve for stacked MSA with top layer of $\varepsilon_r = 3.1$.

• For $\varepsilon_r = 3.2$

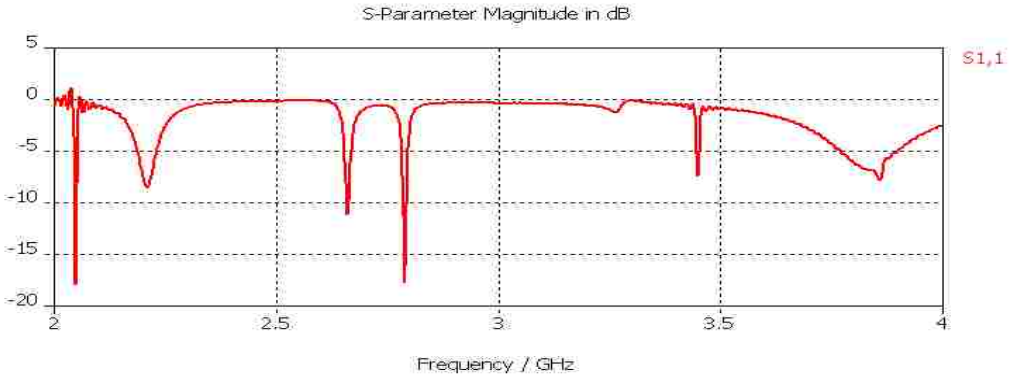

Figure B.23: Simulated reflection coefficient curve for stacked MSA with top layer of $\varepsilon_r = 3.2$.

- For $\varepsilon_r = 3.3$

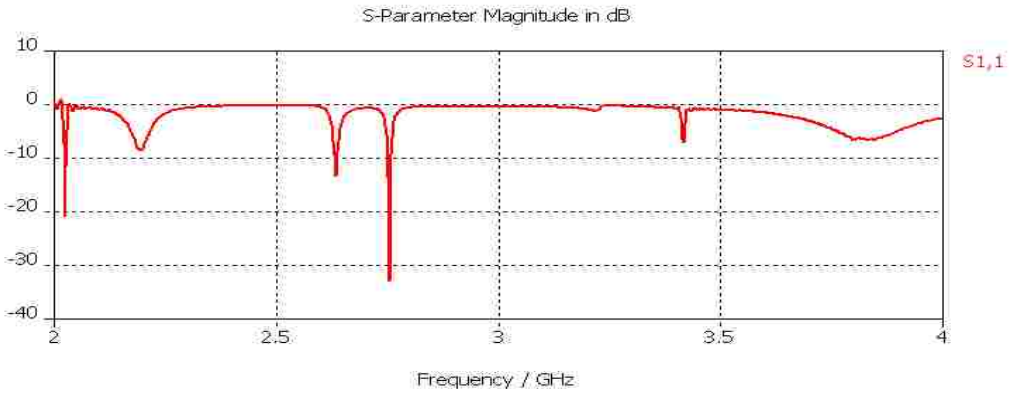

Figure B.24: Simulated reflection coefficient curve for stacked MSA with top layer of $\varepsilon_r = 3.3$.

- For $\varepsilon_r = 3.35$

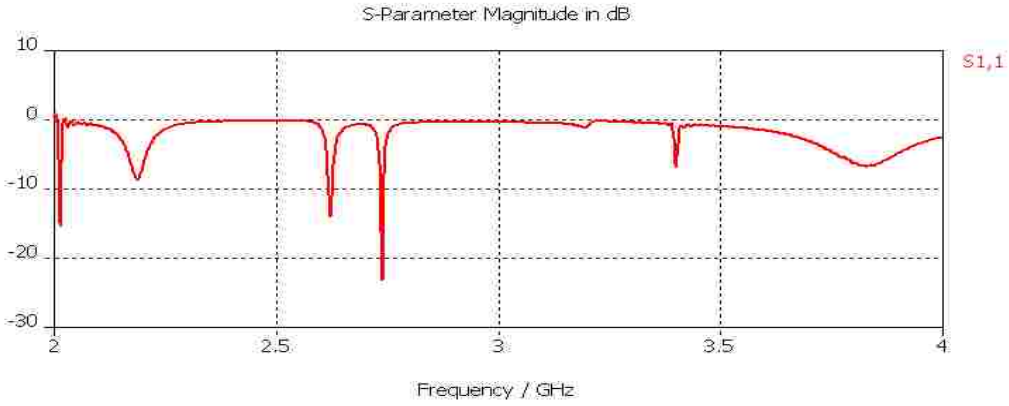

Figure B.25: Simulated reflection coefficient curve for stacked MSA with top layer of $\varepsilon_r = 3.35$.

- For $\varepsilon_r = 3.4$

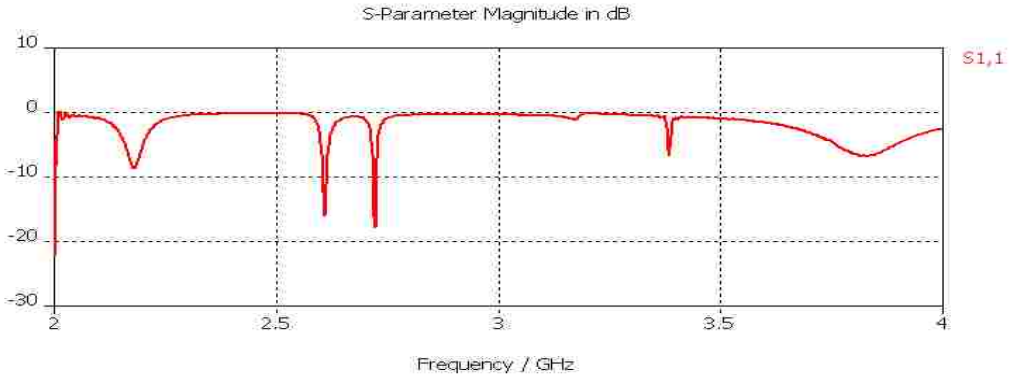

Figure B.26: Simulated reflection coefficient curve for stacked MSA with top layer of $\varepsilon_r = 3.4$.

- For $\varepsilon_r = 3.5$

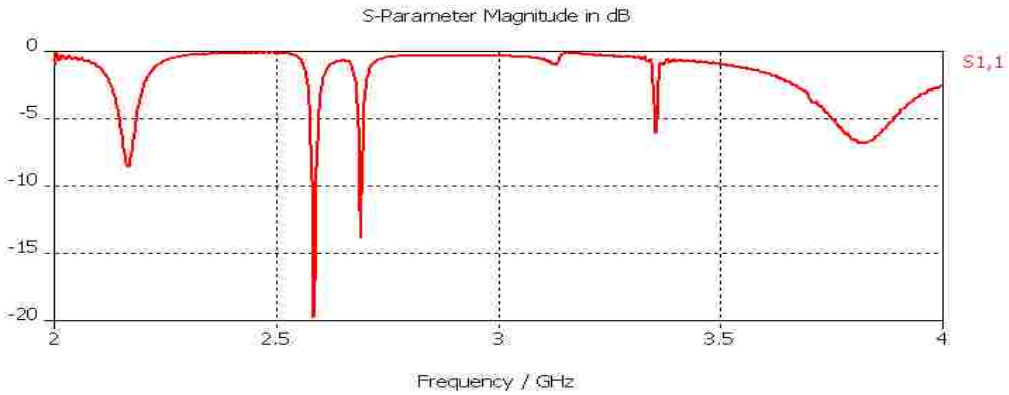

Figure B.27: Simulated reflection coefficient curve for stacked MSA with top layer of $\varepsilon_r = 3.5$.

- For $\varepsilon_r = 4$

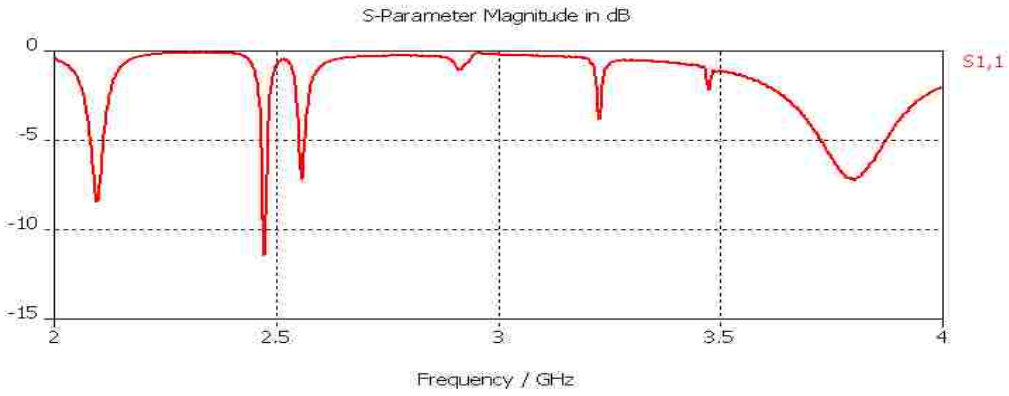

Figure B.28: Simulated reflection coefficient curve for stacked MSA with top layer of $\varepsilon_r = 4$.

Appendix C

For stacked MSA with top substrate (layer) of 1.588 mm height and top patch dimensions of 45×55.
Reflection coefficient curves for stacked MSA with top layer of ε_r between (1.4- 4).

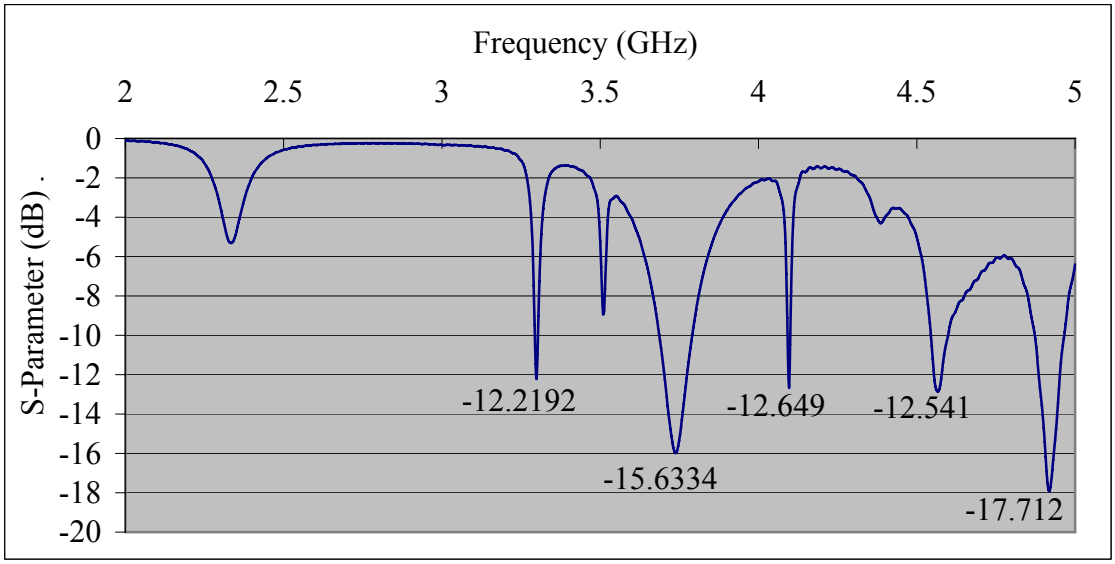

Figure C.1: Simulated reflection coefficient curve for stacked MSA with top layer of ε_r =1.4.

- When ε_r = 1.4, antenna will resonate at the following frequencies; 3.299, 3.746, 4.097,4.574 and 4.922 GHz.

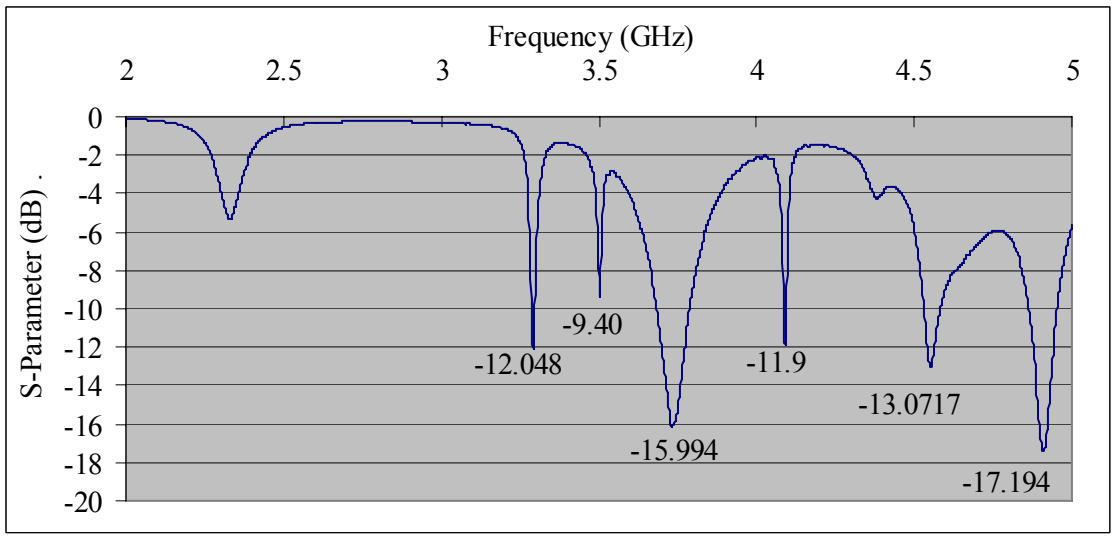

Figure C.2: Simulated reflection coefficient curve for stacked MSA with top layer of ε_r = 1.41.

- When ε_r = 1.41, antenna will resonate at the following frequencies; 3.293, 3.74, 4.019,4.559 and 4.913 GHz. When the frequency equals 3.503 GHz, the return loss will be –9.4 dB, so this is not counted as a resonant frequency.

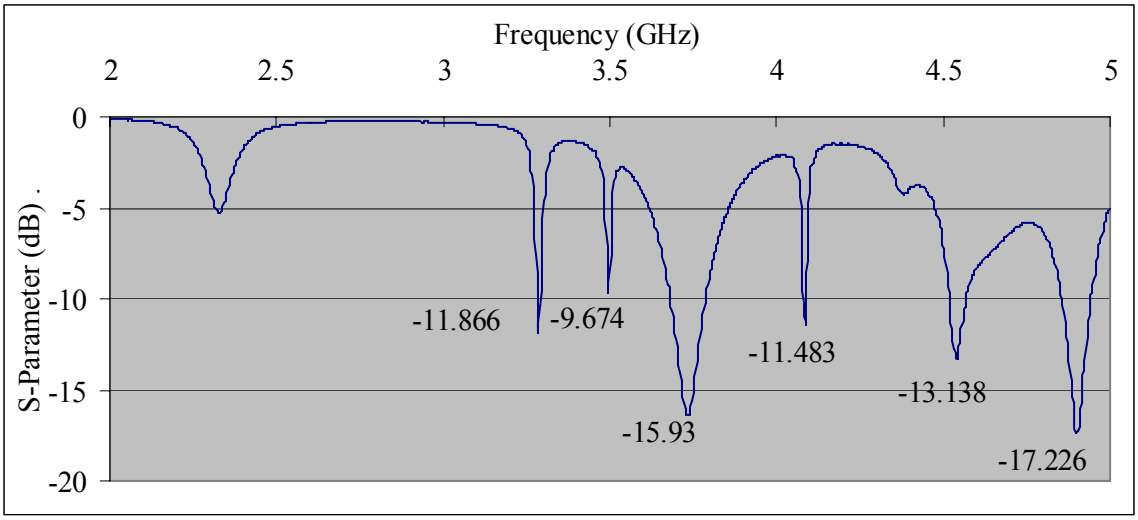

Figure C.3: Simulated reflection coefficient curve for stacked MSA with top layer of ε_r = 1.42.

- When ε_r = 1.42, antenna will resonate at the following frequencies; 3.287, 3.74, 4.085, 4.547 and 4.905 GHz. When the frequency equals 3.497 GHz, the return loss will be –9.674 dB, so this is counted as a resonant frequency in some practical cases.

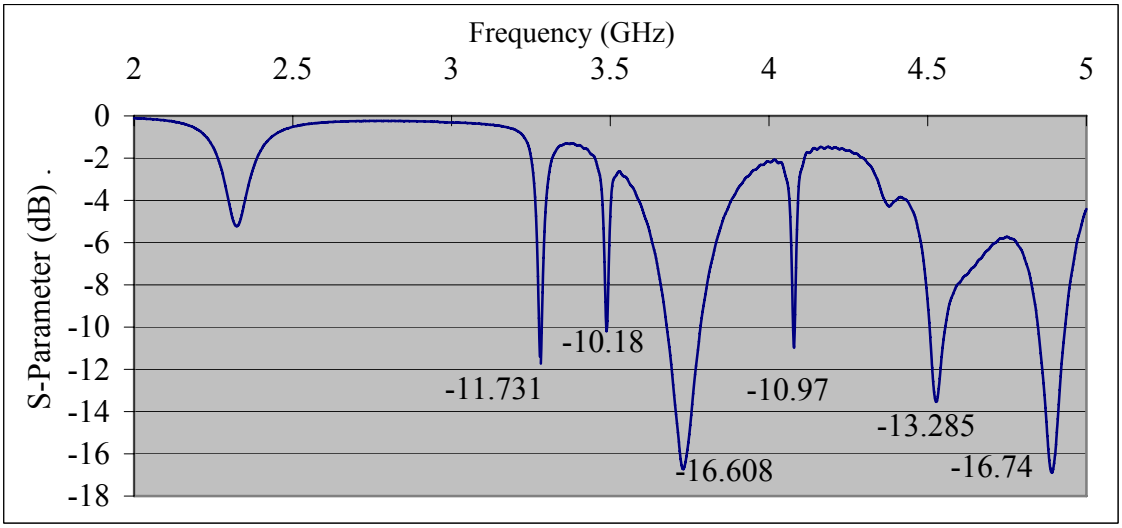

Figure C.4: Simulated reflection coefficient curve for stacked MSA with top layer of ε_r = 1.43.

- When ε_r = 1.43, antenna will resonate at the following frequencies; 3.281, 3.488, 3.737, 4.079,4.532 and 4.895 GHz.

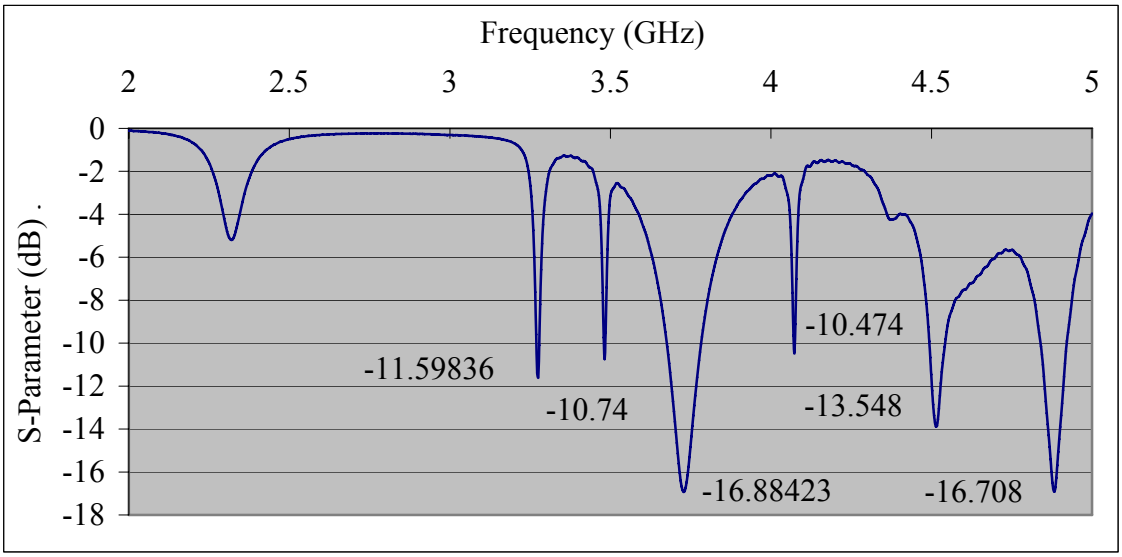

Figure C.5: Simulated reflection coefficient curve for stacked MSA with top layer of ε_r = 1.44.

- When ε_r = 1.44, antenna will resonate at the following frequencies; 3.275, 3.482, 3.734, 4.073,4.52 and 4.886 GHz.

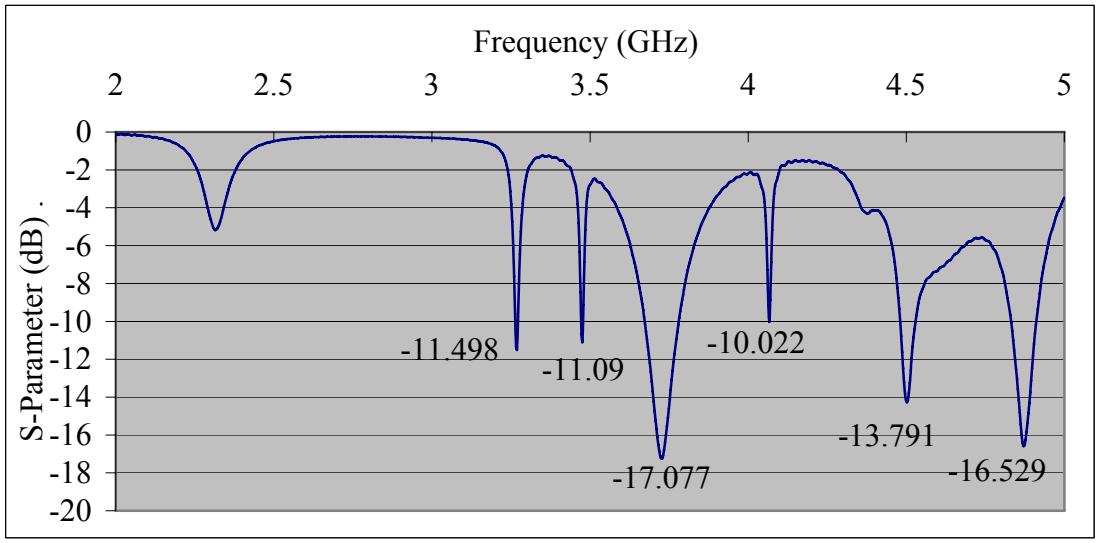

Figure C.6: Simulated reflection coefficient curve for stacked MSA with top layer of ε_r = 1.45.

- When ε_r = 1.45, antenna will resonate at the following frequencies; 3.269, 3.476, 3.731, 4.065,4.508 and 4.874 GHz.

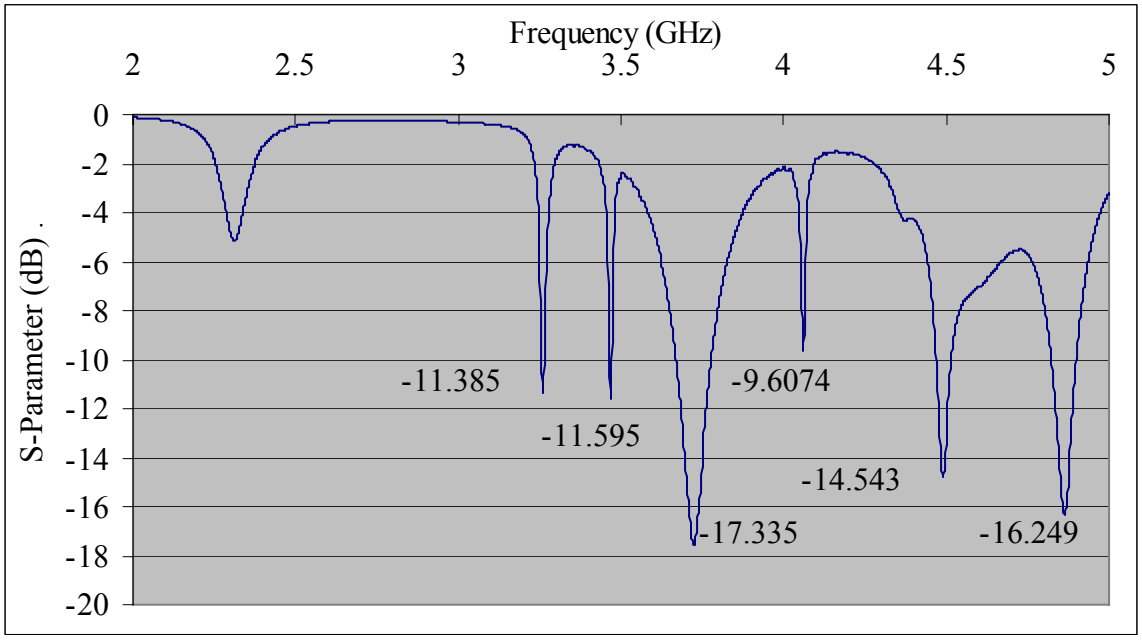

Figure C.7: Simulated reflection coefficient curve for stacked MSA with top layer of ε_r = 1.46.

- When ε_r = 1.46, antenna will resonate at the following frequencies; 3.263, 3.47, 3.722, 4.493 and 4.865 GHz.

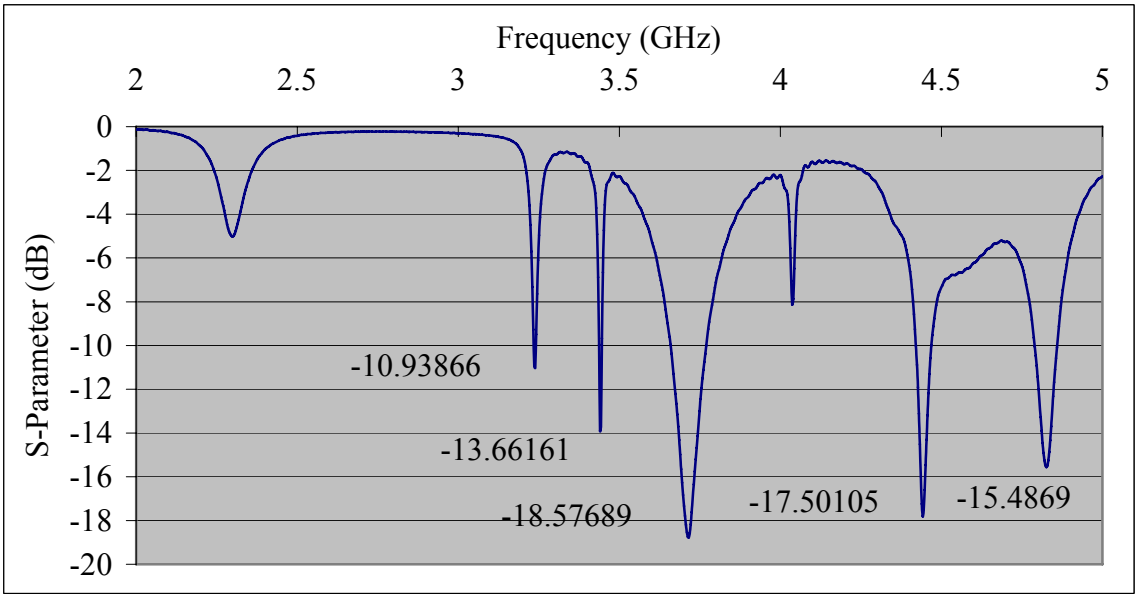

Figure C.8: Simulated reflection coefficient curve for stacked MSA with top layer of ε_r = 1.5.

- When ε_r = 1.5, antenna will resonate at the following frequencies; 3.239, 3.443, 3.719, 4.45 and 4.832 GHz.

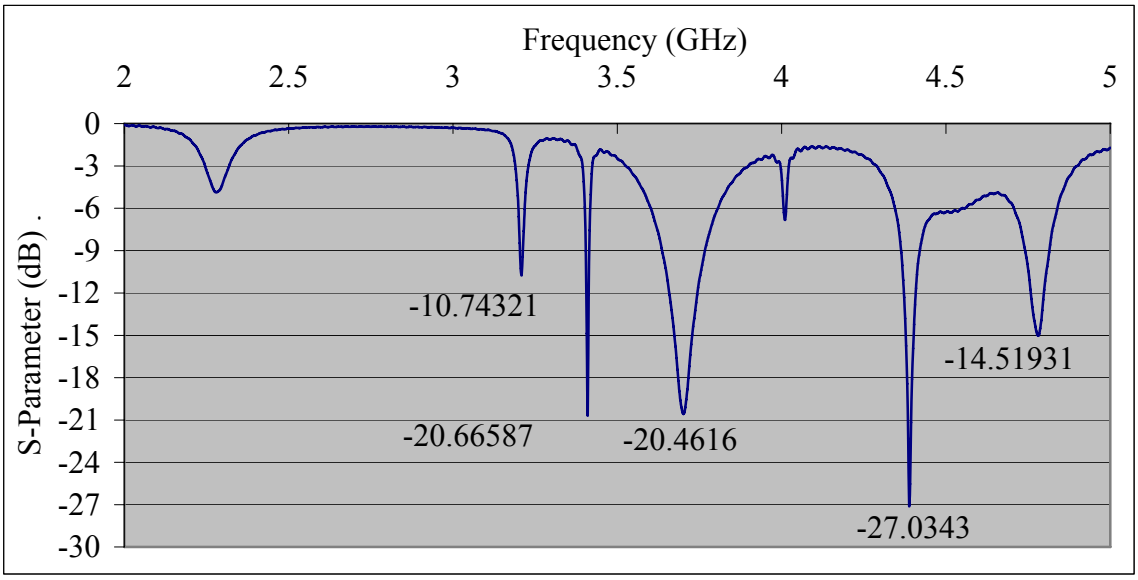

Figure C.9: Simulated reflection coefficient curve for stacked MSA with top layer of ε_r = 1.55.

- When ε_r = 1.55, antenna will resonate at the following frequencies; 3.209, 3.41, 3.704, 4.388 and 4.787 GHz.

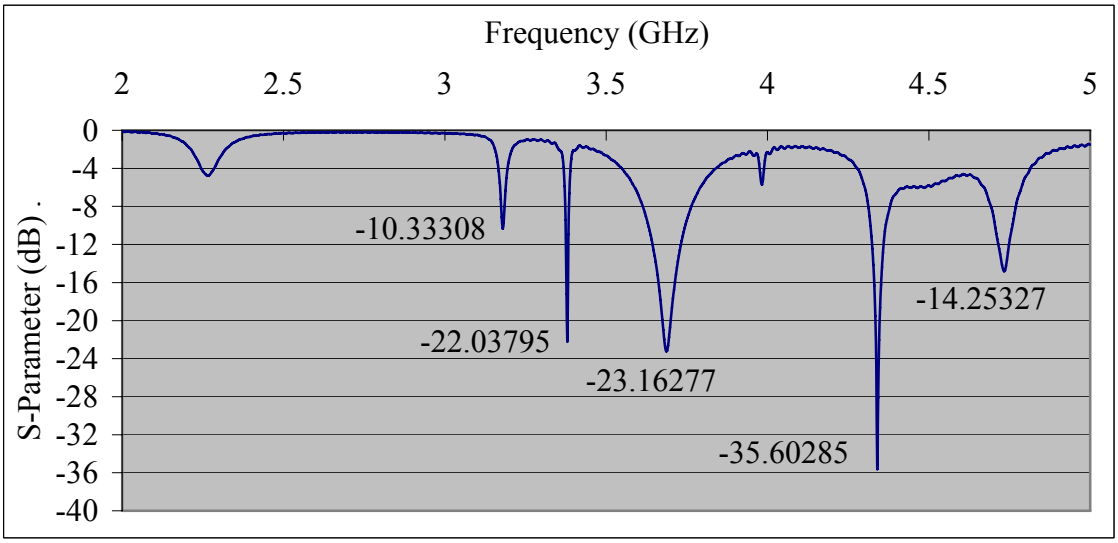

Figure C.10: Simulated reflection coefficient curve for stacked MSA with top layer of ε_r = 1.6.

- When ε_r = 1.6, antenna will resonate at the following frequencies; 3.179, 3.38, 3.689, 4.34 and 4.739 GHz.

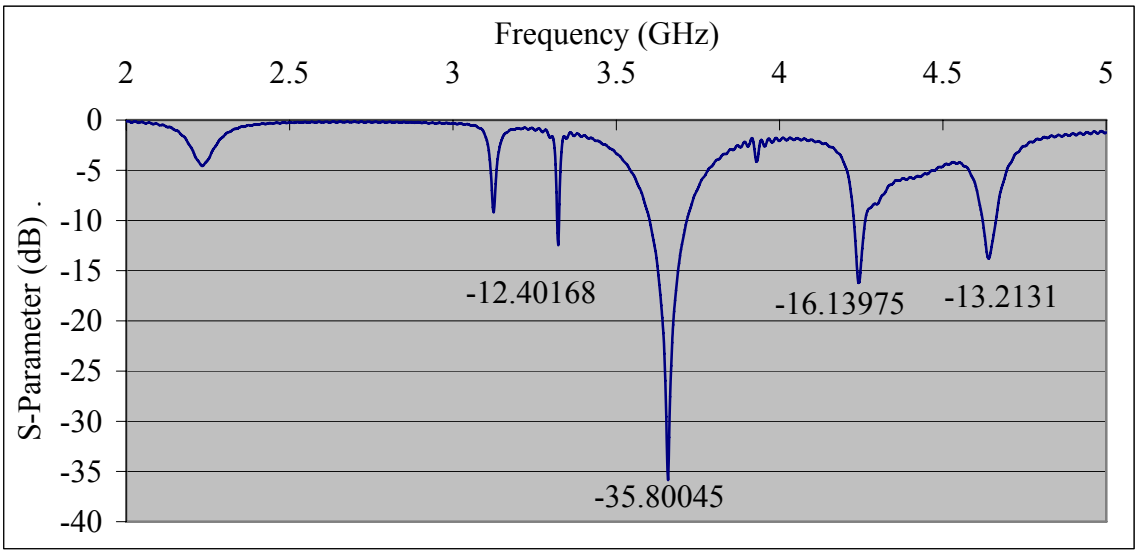

Figure C.11: Simulated reflection coefficient curve for stacked MSA with top layer of ε_r = 1.7.

- When ε_r = 1.7, antenna will resonate at the following frequencies; 3.41, 3.704, 4.388 and 4.787 GHz.

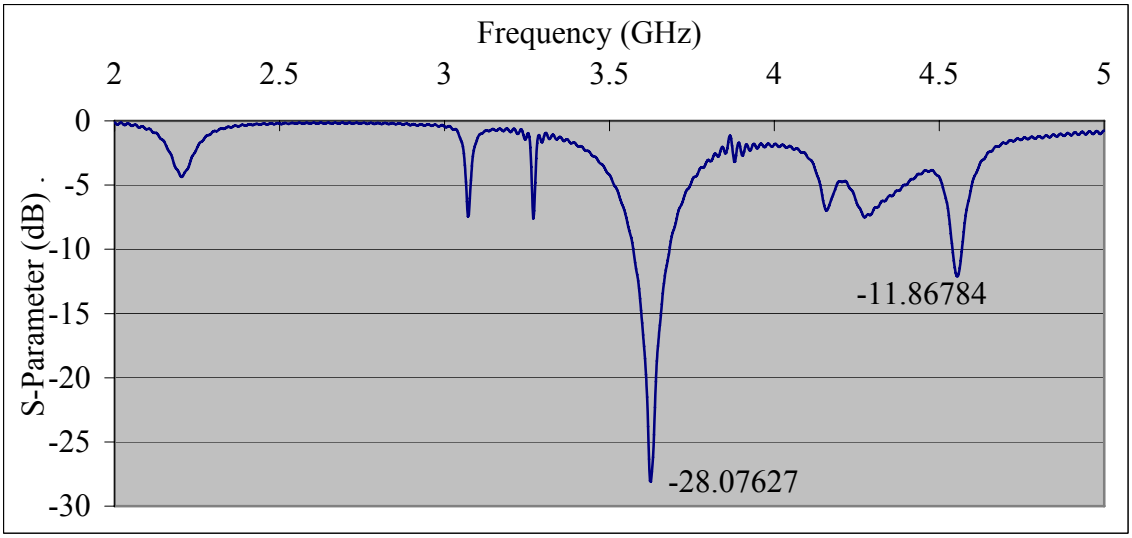

Figure C.12: Simulated reflection coefficient curve for stacked MSA with top layer of ε_r = 1.8.

- When ε_r = 1.8, antenna will resonate at the following frequencies; 3.626 and 4.559 GHz. OFF, OFF.

Appendix D

For stacked MSA with top substrate (layer) of 1.588 mm height and top patch dimensions of 45×55.
Reflection coefficient curves for stacked MSA with top layer of ε_r between (1-2).

- For $\varepsilon_r = 1$

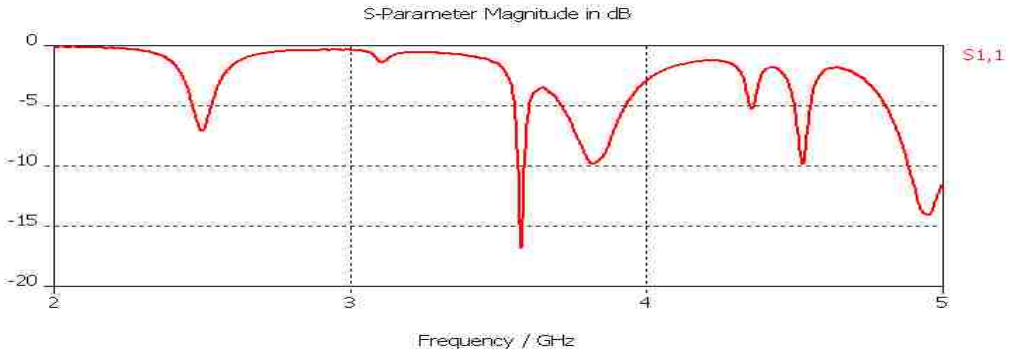

Figure D.1: Simulated reflection coefficient curve for stacked MSA with top layer of $\varepsilon_r = 1$.

- For $\varepsilon_r = 1.05$

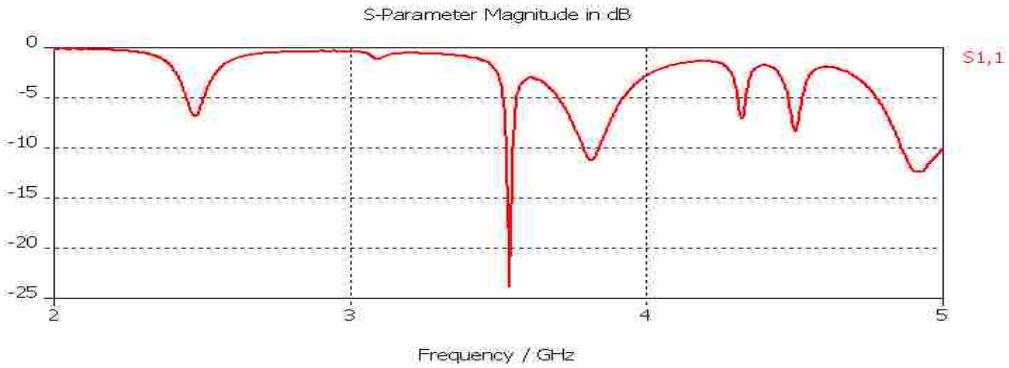

Figure D.2: Simulated reflection coefficient curve for stacked MSA with top layer of ε_r =1.05.

- For $\varepsilon_r = 1.1$

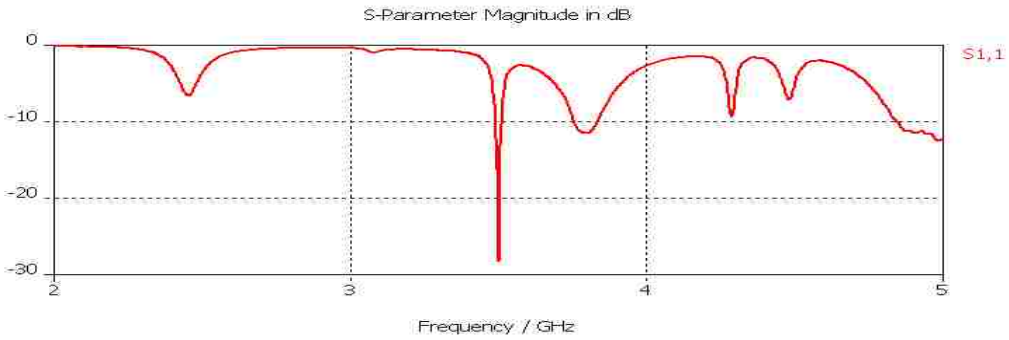

Figure D.3: Simulated reflection coefficient curve for stacked MSA with top layer of $\varepsilon_r = 1.1$.

- For $\varepsilon_r = 1.15$

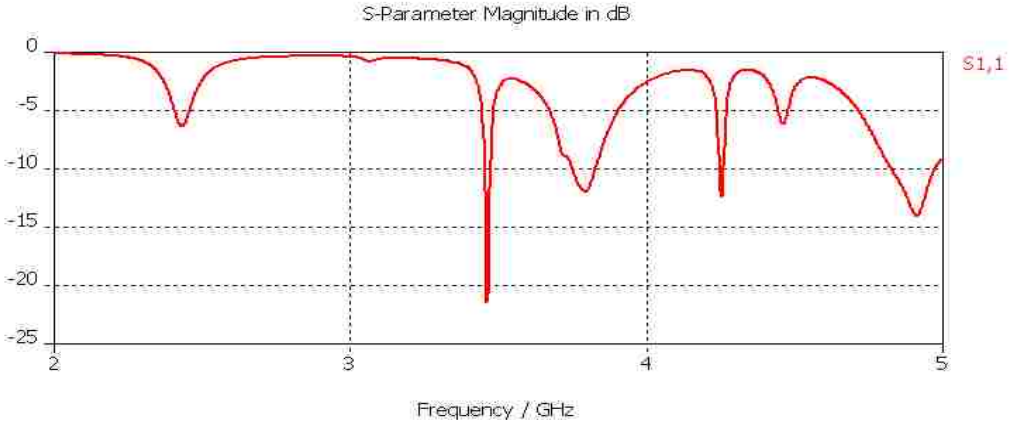

Figure D.4: Simulated reflection coefficient curve for stacked MSA with top layer of $\varepsilon_r = 1.15$.

- For $\varepsilon_r = 1.2$

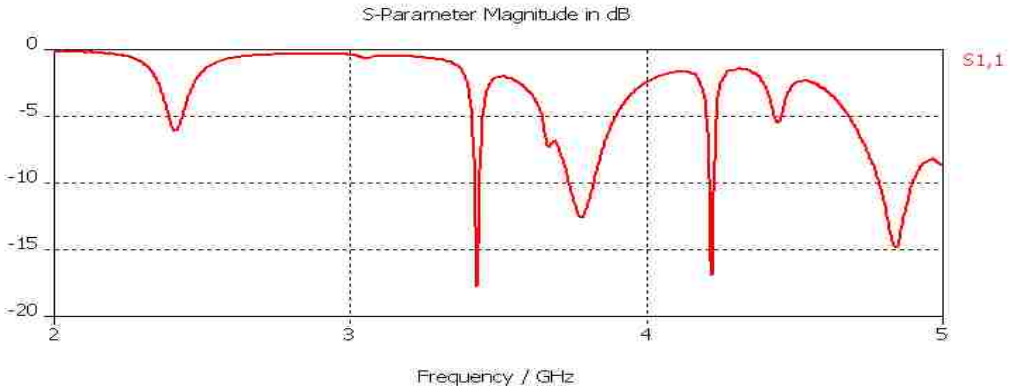

Figure D.5: Simulated reflection coefficient curve for stacked MSA with top layer of $\varepsilon_r = 1.2$.

- For $\varepsilon_r = 1.25$

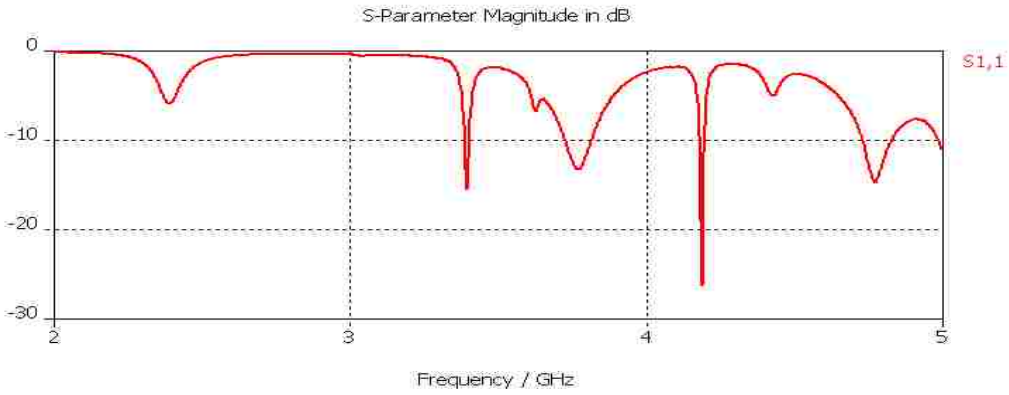

Figure D.6: Simulated reflection coefficient curve for stacked MSA with top layer of $\varepsilon_r = 1.25$.

- For $\varepsilon_r = 1.30$

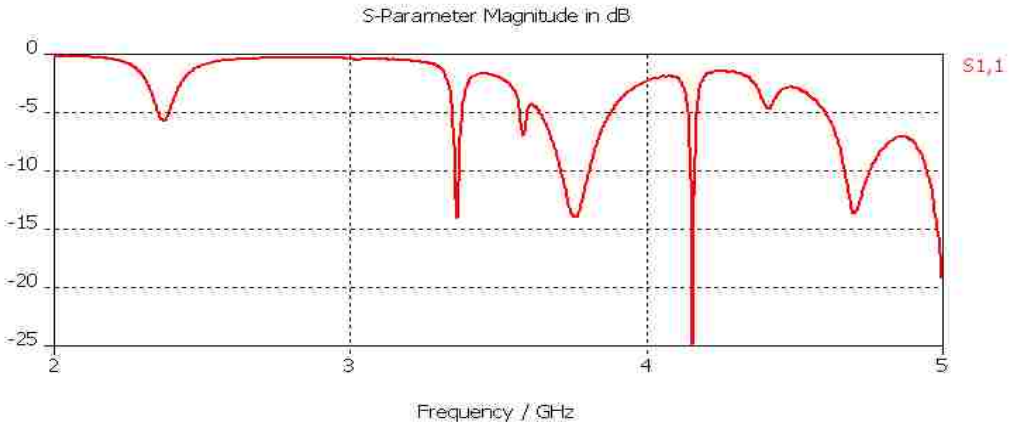

Figure D.7: Simulated reflection coefficient curve for stacked MSA with top layer of $\varepsilon_r = 1.3$.

- For $\varepsilon_r = 1.35$

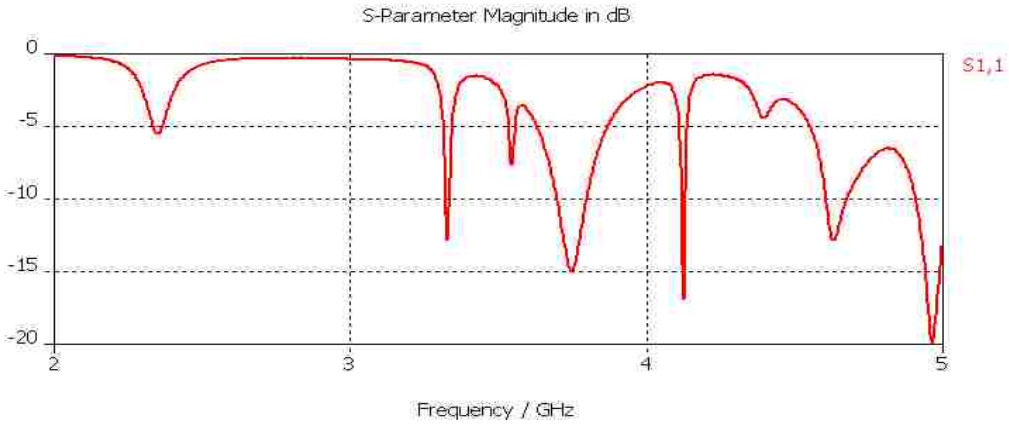

Figure D.8: Simulated reflection coefficient curve for stacked MSA with top layer of $\varepsilon_r = 1.35$.

- For $\varepsilon_r = 1.9$

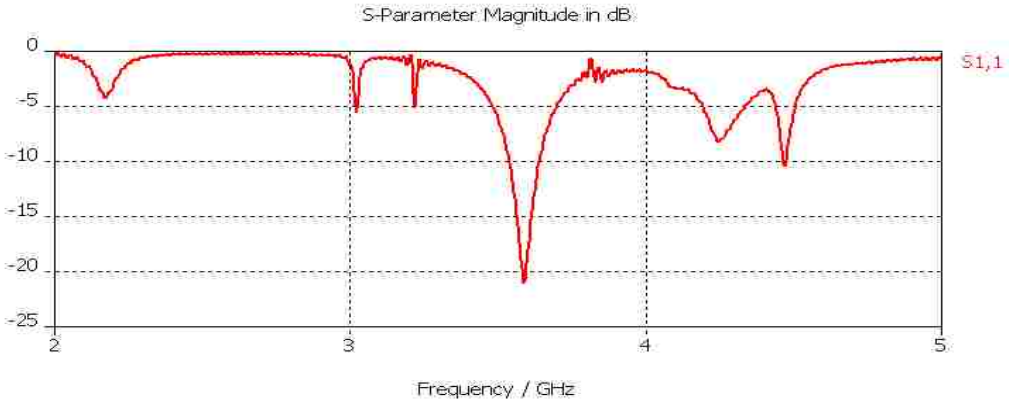

Figure D.9: Simulated reflection coefficient curve for stacked MSA with top layer of $\varepsilon_r = 1.9$.

- For $\varepsilon_r = 2$

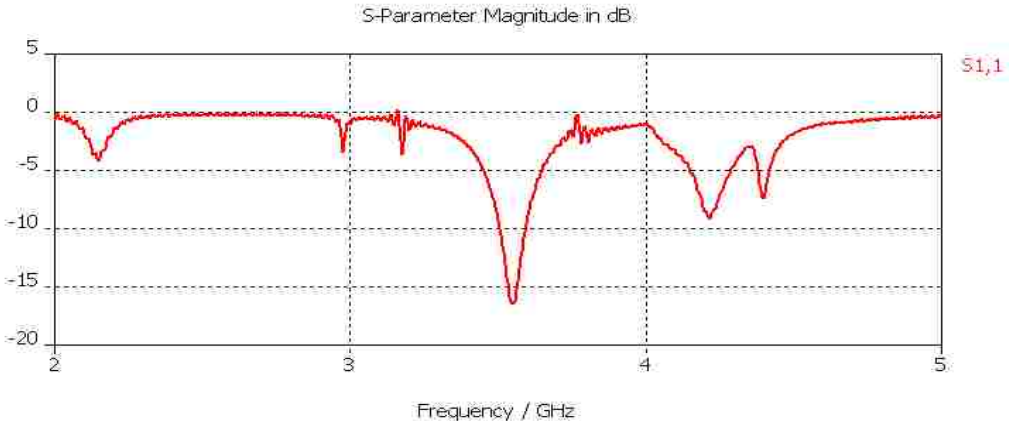

Figure D.10: Simulated reflection coefficient curve for stacked MSA with top layer of $\varepsilon_r = 2$.

References

[1] K. Chung, Y. Nam, T. Yun, and J. Choi, "Reconfigurable Microstrip Patch Antenna with Switchable Polarization", *ETRI Journal*, Volume 28, Number 3, June 2006

[2] S. Xiao, B. Z. Wang, and X. S. Yang, "A Novel Frequency Reconfigurable Patch Antenna," *Microwave Opt. and Technol.Lett.,* 36, Feb. 2003, pp. 295-297.

[3] Broadband Microstrip Antennas, 1st edition, Girish Kumar and K.P.Ray, Artech House Publisher, Norwood, 2003.

[4] Microstrip Antenna Design Handbook, 1st edition, R. Garg, P. Bhartia, I.Bahl and A. Ittipiboon, Artech House Publisher, Norwood, 2001

[5] Antenna Theory Analysis and Design, 3ed edition, Constantine A. Balanis, John Wiley & Sons, New York, 1997.

[6] D. M. Pozar and D. H. Schaubert, Microstrip antennas: the analysis and design of microstrip antennas and arrays, IEEE Press, 1995.

[7] F. Yang and Y. Rahmat-Samii, "Patch Antenna with Switchable Slot (PASS): Dual-Frequency Operation," *Microwave Opt. And Technol. Lett.,* 31, Nov. 2001, pp. 165-168.

[8] F. Yang and Y. Rahmat-Samii, "Switchable Dual-Band Circularly Polarized Patch Antenna with Single Feed," *Electron. Lett.*, vol.37, no. 16, Aug. 2001, pp. 1002-1003.

[9] F. Yang and Y. Rahmat-Samii, "A Reconfigurable Patch Antenna Using Switchable Slots for Circular Polarization Diversity," *IEEE Microwave Wireless Compon. Lett*., vol. 12, no. 3, Mar. 2002,pp.96-98.

[10] M. K. Fries, M. Grani, and R. Vahldieck, "A Reconfigurable Slot Antenna with Switchable Polarization," *IEEE Microwave Wireless Compon. Lett*., vol. 13, no. 11, Nov. 2003, pp.490-492.

[11] Y. J. Sung, T. U. Jang, and Y. S. Kim, "A Reconfigurable Microstrip Antenna for Switchable Polarization," *IEEE Microwave Wireless Compon. Lett*., vol. 14, no. 11, Nov. 2004, pp.534-536.

[12] W. S. Chen, C. K. Wu, and K. L. Wong, "Novel Compact Circularly Polarized Square Microstrip Antenna," *IEEE Trans. Antennas Propagat.,* vol. 49, Mar. 2001, pp. 340-342.

[13] F. Yang and Y. Rahmat-Samii, "A compact Dual Band circularly Polarized Antenna Design for Mars Rover Mission, *IEEE Microwave Wireless Compon. Lett*., vol. 1, June. 2003,pp.858-861.

[14] F. Yang and Y. Rahmat-Samii, "Patch Antenna with Switchable Slots (PASS): Reconfigurable Design for Wireless Communications, *IEEE Microwave Wireless Compon. Lett*., vol. 1, June. 2002,pp.462-465.

[15] R. B. Waterhouse, S. D. Targonski, , and D. M. Kokotoff , "Design and Performance of Small Printed Antennas," *IEEE Trans on Ant. and Prop.,* Vol. 46, Issue. 11, Nov. 1998, pp. 1629 -1633.

[16] D. H. Schaubert, F. G. Farrar, A. Sindoris, and S. T. Hayes, "Microstrip antenna with frequency agility and polarization diversity," *IEEE Trans. Antennas Propagat.*, vol. AP-29, pp. 118–123, Jan. 1981.

[17] C. Delaveaud, P. Leveque, and B. Jecko, "New kind of microstrip antenna: The monopolar wire-patch antenna," *Electron. Lett.*, vol. 30,pp. 1–2, Jan. 1994.

[18] K. Araki, H. Ueda and M. Takahashi, 'Numerical Analysis of Circular Disk Microstrip Antenna with Parasitic Elements," *IEEE Trans. of Antennas and Propagat.,* vol.AP-34, no.12, pp.1390-1394, Dec. 1986.

[19] N. Hasebe, R. Hiramatsu and N. Masuda, "A disk coupled resonant antenna excited by a circular patch," in I985 *Int. IEEEIAP-SSymp. Dig.,* 122-5, 1985.

[20] H. Y. Yang and H. G. Alexopoulous, "Gain enhancement methods for printed circuit antennas through multiple superstrates," *IEEE Trans. of Antennas and Propaget.,* vol.AP-35, pp.860-863, 1987.

[21] R. Q. Lee and K. F. Lee, "Experimental Study of Two-layer Electromagnetically Coupled Rectangular Patch Antenna," *IEEE Trans. ofAntennas andPropagat.,* vol.AP-38, no.8, pp.1298-1302, Aug. 1990.

[22] E. Nishiyama, M. Aikawa and S. Egashira, "Three-Element Stacked Microstrip Antenna with Wide-Band and High-Gain Perdomances," 2003 *Int. IEEE/AP-S Symp. Dig.,* v01.2, pp.900-903, June. 2003.

[23] R. B. Waterhouse, "Small microstrip patch antenna," *Electron. Letters*, vol. 31, pp. 604–605, Apr. 1995.

[24] M. Sanad, "Effect of the shorting posts on short circuit microstrip antennas," in *Proc. IEEE Antennas Propagat. Symp.*, Seattle, WA, June 1994, pp. 794–797.

[25] I. Park and R. Mittra, "Aperture-coupled small microstrip antenna," *Electron. Lett.*, vol. 32, pp. 1741–1742, Sept. 1996.

[26] Practical Microstrip Design and Applications, 1st edition, Gùnter Kompa, Artech House, Boston, 2005.

[27] Design of a compact microstrip antenna at 2.4 GHz by Nurulrodziah Bt Abdul Ghafar, University of Technology Malaysia, November 2005.

[28] Analysis and design of microstrip antenna for a smart-antenna test-bed by Arvind Venugopal, North Carolina State, July 2001.

[29] Microstrip Antennas, The Analysis and Design of a Microstrip Antennas and Arrays, 1st edition, David Pozar, Daniel Schaubert, IEEE Press, New York, 1995.

[30] Bahl, I.j and Bhartia, P., *Microstrip Antennas*, Artech House, 1980 2nd printing 1982,pp.46

[31] H. K. Kan and R. B. Waterhouse, "Size reduction technique for shorted patches, *Electronics Letters,* Vol. 35, pp. 948 - 949, Jun. 1999.

[32] M. Sanad, " Microstrip antennas on very small ground planes for portable communication systems," *Antennas and Propagation Society International Symposium, 1994. AP-S. Digest,* Vol. 2, 1994, pp. 810 -813.

[33] N. G Alexopoulous and D.R Jackson "Fundamental superstate (cover) effects on printed circuit antenna," *IEEE trans. Antennas and Prop*. Vol. AP –32, pp.807-816, Aug 1984.

[34] See http://www.orbanmicrowave.com/The_Basics_Of_Patch_Antennas.pdf

[35] Planar Antenna for Wireless Communications, 1st edition, Kin-Lu Wong, John Wiley and Sons, New Jersey, 2003.

[36] James, J. R., and P. S. Hall, *Handbook of Microstrip Antennas,* Vol. 1, London: Peter Peregrinus, Ltd., 1989.

[37] Gupta, K. C, and A. Bennella, *Microstrip Antennas Theory and Design,* Norwood, MA: Artech House, 1988.

[38] Sainati, R. A., *CAD of Microstrip Antennas for Wireless Applications,* Norwood, MA: Artech House, 1996.

[39] Lee, H. F., and W. Chen, *Advances in Microstrip and Printed Antennas,* New York: John Wiley & Sons, Inc., 1997.

[40] Damiano, J. P., J. Bennegueouche, and A. Papiernik, ''Study of Multilayer Antennas with Radiating Elements of Various Geometry,'' *Proc. IEE, Microwaves, Antennas Propagation,* Pt. H, Vol. 137, No. 3, 1990, pp. 163–170.

[41] Sabban, A., ‘‘A New Broadband Stacked Two Layer Microstrip Antenna,’’ *IEEE AP-SInt. Symp. Digest,* June 1983, pp. 63–66.

[42] See http://www.cst.com/Content/Products/MWS/Overview.aspx.

[43] See http://www.lpkfusa.com/RapidPCB/CircuitboardPlotters/s62.htm.

[44] See http://www.lpkfusa.com/datasheets/prototyping/s62.pdf.